TÉCNICO LISBOA

Optimal Sizing of Solar/Wind–to–Hydrogen Systems in a Suitable Site Selection Geospatial Framework

— The case of Italy and Portugal —

Leonardo Afonso Vidas

Thesis to obtain the Master of Science Degree in

Energy Engineering and Management

Supervisors: Prof. Rui Manuel Gameiro de Castro
Prof. Alessandro Bosisio

Examination Committee

Chairperson: Prof. Luís Filipe Moreira Mendes
Supervisor: Prof. Rui Manuel Gameiro de Castro
Member of the Committee: Prof. Armando José Pinheiro Marques Pires

November 2022

Declaration of Honor

I declare that this document is an original work of my own authorship and that it fulfills all the requirements of the Code of Conduct and Good Practices of the Universidade de Lisboa.

Leonardo Afonso Vidas

Citation

Leonardo Afonso Vidas.
Optimal Sizing of Solar/Wind–to–Hydrogen Systems in a Suitable Site Selection Geospatial Framework: The case of Italy and Portugal. MSc Thesis, Instituto Superior Técnico, Lisbon. November 2022.
For further information or to provide feedback, please contact **leonardo.vidas@tecnico.ulisboa.pt**

Dedicated to Ana, my dear aunt, for she was
the first to discover the little scientist in me.
I miss you.

The noblest pleasure is the joy of understanding.

— Leonardo da Vinci

Acknowledgments

To Professor Rui Castro, who for the past two years has been my teacher, mentor, co–author and above all, my friend. His dedication and commitment always inspired me to be more disciplined and make better judgments about my work. Without his knowledge and permanent availability, I would not have been able to obtain such satisfactory results. His expertise was essential in elevating this manuscript to a level that would have been impossible just by myself.

To Professor Alessandro Bosisio, for first kindly receiving me with open arms in Milan. His helpfulness and goodwill were what enabled me to get into this adventure in the first place. His meticulous analyses of my work and consistent asking of pertinent questions were essential to producing a work of excellence.

To Francesca Limonta, Gabriel Lau, Gonçalo Calado and all others that, in one way or the other, took a bit of their time to help clear the mist in times of need.

To my alma mater, Instituto Superior Técnico, and to Politecnico di Milano, for teaching me what I know today. The value of its contribution does not entirely lie in techno–scientific knowledge but instead in shaping a whole individual into a skilful, qualified and competent person, ready to leave a mark on the world.

To my family, without whom none of this would have been possible. Their constant, enduring support at all levels has been at the root of all my successes so far. I feel absolutely privileged to have such a strong relationship with all my loved ones.

To Mágui Lage, last but not least, for being my life partner. The challenges we have overcome, sometimes alone but always together, have shaped us into what we are today—a couple united by unbreakable bonds of friendship, trust and love.

Abstract

The growing global deployment of renewables has triggered an energy transformation with profound geopolitical implications. As an energy carrier, hydrogen is at the heart of this transformation, enabling international trade and facilitating decarbonisation. This research project aims to find the eligible locations to install renewable systems dedicated to producing green hydrogen. These locations are restricted to onshore and offshore regions of Italy and Portugal. Moreover, the research focuses on identifying the optimal configurations of such systems that minimise the cost of producing hydrogen. The multi–criteria geographical model is built through standard–level procedures, with data collected from several prominent sources, while the optimisation algorithm expands from the detailed computation of the classic levelised cost of hydrogen. Key findings of this study include the acknowledgement that although having only a small percentage of their territory available, both countries have the potential to produce millions of tons of hydrogen every year. Furthermore, the optimal configurations obtained by the algorithm offer reductions in costs to the order of 70%, depending on location in the countries; this can translate to millions of euros in annual savings. Such findings represent unprecedented achievements for both Italy and Portugal and can act as an essential asset to economic analyses performed on this subject by municipalities and even the central governments. Additionally, these results validate the initial premise of the optimisation model, significantly improving the credibility of this study by constructively challenging the standard way of assessing large–scale green hydrogen projects.

Keywords: hydrogen, renewable energies, GIS, economical analysis, LCOH, optimisation

Resumo

O crescimento acelerado das energias renováveis desencadeou uma transformação energética global com profundas implicações geopolíticas. Como vetor de energia, o hidrogénio está no centro dessa transformação, viabilizando o comércio energético internacional e facilitando a descarbonização de setores–chave. Este trabalho de pesquisa visa obter os locais elegíveis para a instalação de sistemas de energias renováveis dedicados à produção de hidrogénio verde, nos territórios *onshore* e *offshore* de Itália e Portugal. Este estudo procura também identificar as configurações ótimas destes sistemas que minimizem o custo de produção de hidrogénio. O modelo geográfico multi–critério é construído tendo por base procedimentos padronizados na literatura internacional, através de dados recolhidos de várias fontes proeminentes. O algoritmo de optimização desenvolve-se detalhadamente a partir do cálculo clássico do custo nivelado de hidrogénio. As principais conclusões deste estudo incluem o reconhecimento de que, embora tenham apenas uma pequena percentagem do território disponível, ambos os países têm capacidade para produzir milhões de toneladas de hidrogénio anualmente. Além disso, as configurações ótimas obtidas pelo algoritmo oferecem reduções de custos até 70%, dependendo da localização nos países considerados—podendo traduzir-se em milhões de euros poupados anualmente. Estes resultados representam um trabalho inédito para Itália e Portugal, e servem como um importante dado para análises económicas realizadas pelos municípios e até mesmo pelos governos centrais. Estes resultados validam ainda a premissa inicial do modelo de otimização, melhorando significativamente a credibilidade deste estudo, ao testar construtivamente o processo clássico de avaliação de projetos de hidrogénio verde de larga–escala.

Palavras-chave: hidrogénio, energias renováveis, GIS, análise económica, LCOH, optimização

Contents

Acknowledgements ix
Abstract xi
Resumo xiii
List of Figures xix
List of Tables xxi
List of Algorithms xxiii
Glossary xxv
Abbreviations xxvii
Nomenclature xxix

1 Introduction **1**
1.1 Motivation 1
1.2 Topic Overview 1
1.3 Objectives and Novel Contributions 2
1.4 Thesis Outline 2

2 State of the Art **3**
2.1 Literature Review 3
2.2 Research Gaps 6

3 Theoretical Framework **7**
3.1 Renewable Energy Sources 8
3.1.1 Solar Photovoltaic Parks 8
3.1.2 Onshore Wind Farms 10
3.1.3 Offshore Fixed Wind Farms 12
3.1.4 Offshore Floating Wind Farms 14
3.2 Hydrogen Production Taxonomy 17
3.2.1 Alkaline Electrolysis 18
3.2.2 Proton Exchange Membrane Electrolysis 19
3.2.3 Other Technologies 21

4 Geographical Model Design **23**
4.1 Study Area . . . 23
4.1.1 Italy . . . 23
4.1.2 Portugal . . . 24
4.2 Data Collection and Handling . . . 25
4.3 Data Exclusion . . . 26
4.3.1 Environmental Criteria . . . 27
4.3.2 Legislative Criteria . . . 28
4.3.3 Safety Criteria . . . 29
4.3.4 Technical Criteria . . . 30
4.4 Data Evaluation . . . 31
4.4.1 Ground Elevation . . . 31
4.4.2 Terrain Slope . . . 32
4.4.3 Air Temperature . . . 33
4.4.4 Seafloor Bathymetry . . . 34
4.4.5 Wind Speed . . . 35
4.5 Eligible Locations . . . 36

5 Numerical Model Layout **39**
5.1 Hydrogen Economic Fairways . . . 39
5.1.1 Levelised Cost of Hydrogen . . . 40
5.1.2 Levelised Cost of Electricity . . . 46
5.2 Simplified General Model . . . 47
5.2.1 RES Maximum Allowed Capacity . . . 47
5.2.2 Localised LCOH Computation . . . 50
5.3 Optimised General Model . . . 52
5.3.1 Problem Setting and Notation . . . 52
5.3.2 Mathematical Formulation . . . 55
5.3.3 Validation Check . . . 58

6 Results and Discussion **59**
6.1 Electricity Generation Potential . . . 59
6.2 Hydrogen Production Potential . . . 62
6.3 Sensitivity Analysis . . . 70

7 Conclusions **75**
7.1 Achievements . . . 75
7.2 Future Work . . . 77

References **79**

A Published Articles **A.1**

B Chart of Citations **B.1**

C RES Systems Cost Breakdown **C.1**

C.1 Solar Photovoltaic C.1

C.2 Onshore Wind C.3

C.3 Fixed Offshore Wind C.4

C.4 Floating Offshore Wind C.6

D QGIS Functions Summary **D.1**

E Density of Shipping Routes **E.1**

List of Figures

3.1 Cost analysis: overview of RES capital and operational expenditures. . . . 8
3.2 Cost analysis: solar photovoltaic capital and operational expenditures. . . . 9
3.3 Cost analysis: onshore wind capital and operational expenditures. . . . 11
3.4 Cost analysis: offshore fixed foundations capital and operational expenditures. . . . 13
3.5 Cost analysis: offshore floating structure capital and operational expenditures. . . . 15
3.6 Hydrogen color–code spectrum. . . . 17
3.7 Illustration of an alkaline electrolyser. . . . 18
3.8 Illustration of a PEM electrolyser. . . . 19
3.9 Cost analysis: PEM electrolyser capital and operational expenditures. . . . 20
3.10 Illustration of a solid oxide electrolyser. . . . 21
3.11 Illustration of an AEM electrolyser. . . . 22
3.12 Illustration of a capillary–fed electrolyser. . . . 22

4.1 Study areas: country overview. . . . 24
4.2 Exclusion analysis: environmental constraints. . . . 27
4.3 Exclusion analysis: legislative constraints. . . . 28
4.4 Exclusion analysis: safety constraints. . . . 29
4.5 Exclusion analysis: technical constraints. . . . 30
4.6 Evaluation analysis: elevation criteria. . . . 31
4.7 Evaluation analysis: slope criteria. . . . 32
4.8 Evaluation analysis: air temperature criteria. . . . 33
4.9 Evaluation analysis: seafloor bathymetry criteria. . . . 34
4.10 Evaluation analysis: wind speed criteria. . . . 35
4.11 Country analysis: total eligible locations. . . . 36
4.12 Country analysis: offshore eligible locations. . . . 37

5.1 Installed capacity upper–limit decision flowchart for photovoltaic solar parks. . . . 47
5.2 Shading derate factor as a function of GCR for multiple PV module configurations. . . . 48
5.3 Installed capacity upper–limit decision flowchart for wind farms. . . . 49
5.4 RES–to–Hydrogen direct coupling: the oversimplified solution. . . . 50
5.5 Vestas V112–3.45 power curve interpolation. . . . 54

6.1 Current solar levelised cost of electricity in eligible locations of selected countries. 60
6.2 Current wind levelised cost of electricity in eligible locations of selected countries. 60
6.3 Distribution of onshore RES technologies based on the cheapest levelised cost of electricity. . . 61
6.4 Current levelised cost of electricity in eligible locations of selected countries. 61
6.5 Oversize factor as function of RES technology. 63
6.6 Oversize factor as function of RES full load hours. 63
6.7 Current solar levelised cost of hydrogen in eligible locations of selected countries. 64
6.8 Current wind levelised cost of hydrogen in eligible locations of selected countries. 65
6.9 Distribution of onshore RES technologies based on the cheapest levelised cost of hydrogen. . . 65
6.10 Current levelised cost of hydrogen in eligible locations of selected countries. 66
6.11 Yearly average solar capacity factor in onshore eligible locations of selected countries. 67
6.12 Yearly average wind capacity factor in eligible locations of selected countries. 67
6.13 Onshore hybrid optimisation. 69
6.14 Sensitivity analysis: onshore solar. 70
6.15 Sensitivity analysis: onshore wind. 71
6.16 Sensitivity analysis: offshore fixed. 72
6.17 Sensitivity analysis: offshore floating. 72
6.18 Sensitivity analysis: electrolyser efficiency and production rate. 73

B.1 Citation chart for references 1—40 . . . . . B.1
B.2 Citation chart for references 41—100 . . . . . B.2
B.3 Citation chart for references 101—155 . . . . . B.3

D.1 GIS procedure flowchart: from new vector layer to buffered layer. D.2

E.1 Density of total shipping routes in 2021. . . . . E.1
E.2 Density of shipping routes around Portugal, in 2021. . . . . E.2
E.3 Density of shipping routes around Italy, in 2021. . . . . E.3

List of Tables

3.1 Currency conversions. . . . 7
3.2 Alkaline electrolyser: summary of features. . . . 18
3.3 Proton exchange membrane electrolyser: summary of features. . . . 19
3.4 Solid oxide electrolyser: summary of features. . . . 21
3.5 Anion exchange membrane electrolyser: summary of features. . . . 22
3.6 Capillary fed electrolyser: summary of features. . . . 22

4.1 Coordinate reference system of each study area. . . . 25
4.2 Data collection: source and format of the data layers. . . . 26
4.3 Summary of environmental constraints. . . . 27
4.4 Summary of legislative constraints. . . . 28
4.5 Summary of safety constraints. . . . 29
4.6 Summary of safety constraints. . . . 30
4.7 Outline of elevation data evaluation. . . . 31
4.8 Outline of slope data evaluation. . . . 32
4.9 Outline of temperature data evaluation. . . . 33
4.10 Outline of bathymetry data evaluation. . . . 34
4.11 Outline of wind speed data evaluation. . . . 35
4.12 Summary of the results for eligible locations. . . . 36

5.1 Summary of the LCOH components for every RES formulation. . . . 45
5.2 Summary of components in the computation of the maximum allowed solar installed capacity. 48
5.3 Summary of components in the computation of the maximum allowed wind installed capacity. 49
5.4 Summary of variables in the optimised general model. . . . 54
5.5 Algorithm outcomes using Octeract Engine. . . . 58

6.1 Summary of project expenses for every renewable energy source. . . . 59
6.2 Summary of results: optimisation algorithm. . . . 62
6.3 Summary of results: hybrid optimisation. . . . 68

C.1 Solar PV system's CapEx categories breakdown structure. . . . C.1
C.2 Solar PV system's OpEx categories breakdown structure. . . . C.2

C.3 Onshore wind system's CapEx categories breakdown structure. C.3
C.4 Onshore wind system's OpEx categories breakdown structure. C.4
C.5 Fixed offshore wind system's CapEx categories breakdown structure. C.4
C.6 Fixed offshore wind system's OpEx categories breakdown structure. C.6
C.7 Floating offshore wind system's CapEx categories breakdown structure. C.6
C.8 Floating offshore wind system's OpEx categories breakdown structure. C.7

D.1 Summary description of QGIS functions. D.1

List of Algorithms

1 Simplified General Model algorithm 51
2 Optimised General Model algorithm 57

Glossary

Glossary of Concepts

Capacity factor	Unitless ratio of a system's annual energy production to the theoretical maximum energy production (if run at the rated power all year); ranges from 0 to 1.
Capital expenditure (CapEx)	Costs spent on all activities up until the project's construction completion date, when it is turned online.
Full load hours	Number of hours a power plant would have to operate at nominal power to generate the same amount of energy as it generates within a year; ranges from 0 to 8760. Same as *utilisation factor*.
Levelised cost of hydrogen (LCOH)	Commonly used measure for the production cost of hydrogen. In general, it represents the cost of producing one unit of hydrogen during the lifetime of the system; it is also defined as the revenue required to earn a rate of return on investment equal to the WACC over the lifetime of the hydrogen project.
Nominal power	Designed maximum power output from a piece of equipment, e.g. photovoltaic module, wind turbine or electrolyser. The equipment is limited to this power output but typically functions at a fraction of this value. Same as *rated power*.
Operational expenditure (OpEx)	Costs spend on all activities from the construction completion date until the decommissioning of the facilities. Includes operation and maintenance, services and other (un)scheduled expenditures.
Oversize Factor	Ratio of the renewable energy source installed capacity to the electrolyser's nominal power. It is an estimation obtained through an optimisation algorithm to apply to extensive geographical analyses.
Weighted average cost of capital	Weighted average rate of return that a power plant owner expects to compensate its internal and external investors over the lifetime of a project. Functions as a proxy for the discount rate.

Glossary of Software

Inkscape v0.92.0	Free and open–source vector graphics editor. Allows the render of primitive vector shapes, which may be filled and their borders stroked; created shapes can be further manipulated with transformations. Used to design and/or edit most of the figures in the document, including charts.
MATLAB R2020a v9.8.0	Proprietary multi–paradigm programming language and numeric computing environment developed by MathWorks. Allows matrix manipulations, plotting of functions and data, and implementation of algorithms. Used to create a proto–program of the optimisation problem.
Microsoft Excel v2203 16.0	Calculation spreadsheet developed by Microsoft. Features computation capabilities, graphing tools, and an integrated macro programming language. Used here to manage the geodata exported from QGIS, estimate energy yields, and calculate capital/operation expenditures.
Octeract Engine v4.3.0	Free proprietary parallel deterministic global optimization solver for general mixed–integer nonlinear programs. It is the only commercial optimisation solver with native support for distributed parallel branch–and–bound. Used to run the multiple simulations of the optimisation model.
Overleaf v3.0.1	Cloud–based TeX editor. Online, real–time collaborative editor for papers, thesis, technical reports and other scientific documents written in the LaTeX markup language. Used for writing and editing the dissertation document.
Pyomo v6.2	Python–based, open–source software package that supports a diverse set of optimisation capabilities to formulate and analyse optimisation models. Used to implement the algorithm of the levelised cost of hydrogen.
QGIS v3.22.5 Białowieża	Open–source, cross–platform desktop geographic information system application. Allows spatial information analysis and operation, supporting raster, vector and mesh layers, and enabling composing and exporting graphical maps. Used to view, edit, and manipulate all geospatial data.

Abbreviations

AlkEl	**alk**aline **el**ectrolyser
AEMEl	**a**nion **e**xchange **m**embrane **el**ectrolyser
BOS	**b**alance **o**f **s**ystem
CapEx	**cap**ital **ex**penditures
CFEl	**c**apillary–**f**ed **el**ectrolyser
CRS	**c**oordinate **r**eference **s**ystem
DecEx	**dec**ommission **ex**penditures
DEM	**d**igital **e**levation **m**odel
EEZ	**e**xclusive **e**conomic **z**one
EU	**E**uropean **U**nion
EUR	**Eur**o
EPSG	**E**uropean **P**etroleum **S**urvey **G**roup
FLH	**f**ull **l**oad **h**ours
GBP	**G**reat **B**ritain **P**ound
GCR	**g**round **c**over **r**atio
GIS	**g**eographic **i**nformation **s**ystem
IEA	**I**nternational **E**nergy **A**gency
IRENA	**I**nternational **R**enewable **En**ergy **A**gency
LCOE	**l**evelised **c**ost **o**f **e**lectricity
LCOH	**l**evelised **c**ost **o**f **h**ydrogen
NPV	**n**et **p**resent **v**alue
NREL	**N**ational **R**enewable **E**nergy **L**aboratory
OGM	**o**ptimised **g**eneral **m**odel
O&M	**o**perations and **m**aintenance
OpEx	**op**erational **ex**penditures
PEMEl	**p**roton **e**xchange **m**embrane **el**ectrolyser
PV	**p**hoto**v**oltaic
ReplEx	**repl**acement **ex**penditures
RES	**r**enewable **e**nergy **s**ources
RC	**r**oughness **c**lass
SGM	**s**implified **g**eneral **m**odel
SOEl	**s**olid **o**xyde **el**ectrolyser
USD	**U**nited **S**tates **D**ollar
UTM	**U**niversal **T**ransverse **M**ercator
VAT	**v**alue **a**dded **t**ax
WACC	**w**eighted **a**verage **c**ost of **c**apital
WGS 84	**W**orld **G**eodetic **S**ystem 19**84**
yr	**yea**r

Nomenclature

Blackboard bold typefaces

$\mathbb{C}$	*set of* Capacity factors
$\mathbb{H}$	*set of* Hours in one year
$\mathbb{L}$	*set of* Eligible location points

Calligraphic typefaces

$\mathcal{D}$	Virtual hydrogen demand, in kg
$\mathcal{F}$	Oversize factor, dimensionless

Greek symbols

Δ	Decommission value of the system, in EUR/kW
δ	Power degradation of the system, in percentage
η	All–round electric efficiency, in percentage
ρ	Net production rate of the electrolyser, in kg/h/kW
υ	Annual utilization factor, in kWh/kW

Roman symbols

$\mathtt{A}$	Area, in square meters
$\mathtt{CF}$	Capacity factor, in percentage
$\mathtt{D}$	Diameter, in meters
$\mathtt{GCR}$	Ground cover ratio, dimensionless
$\mathtt{I}$	Total capital expenditure of the system, in EUR/kW
$\mathtt{i}$	Inflation rate, in percentage
$\mathtt{j}$	Replacement number, equal to 1 or 2
$\mathtt{K}$	Overall cost structure, in EUR

LCOE	Levelised cost of electricity, in EUR/kWh
LCOH	Levelised cost of hydrogen, in EUR/kg
L	Length, in meters
N	Economic lifetime of the system, in years
n	Year number, ranging from 1 to N
O	All–in annual operational expenditures of the system, in EUR/kW/yr
P	Nominal power, in watt
RSD	Rotor safe distance, in meters
R	Electrolyser replacement cost, in EUR/kW
r	Roughness length, in meters
S	Spread factor, dimensionless
u	Wind speed, in m/s
W	Width, in meters
w	Weighted average cost of capital, in percentage
Y	Global hydrogen yield, in kilograms
Z	Virtual support variable, dimensionless
z	Height, in meters

Subscripts

0	*rel* Initial value
ft	Offshore floating wind farms
fx	Offshore fixed wind farms
H_2	*rel* Electrolyser
h	*rel* Hourly value
K	*rel* Cost
max	Maximum allowed
m	*rel* Solar module
nom	Nominal
out	Output

`pv` Solar photovoltaic

`px` *rel* Pixel

`ref` Reference

`RES` Renewable energy source

`r` Real

`t` *rel* Turbine

`v` Virtual

`wd` Onshore wind

`Y` *rel* Yield

Superscripts

(`ft`) *rel* Offshore floating wind farms

(`fx`) *rel* Offshore fixed wind farms

(`pv`) *rel* Solar photovoltaic

(`wd`) *rel* Onshore wind farms

$\odot$ Optimal solution

1 Introduction

'I believe that water will one day be employed as fuel, that hydrogen and oxygen which constitute it, used singly or together, will furnish an inexhaustible source of heat and light, of an intensity of which coal is not capable.'

Jules Verne, *The Mysterious Island*, 1874

1.1 Motivation

The world is changing. The expanding deployment of renewables has put in motion a global energy revolution with profound geopolitical implications. The coming of a new energy age will transform relationships between nations and communities and create a new world of power security, energy independence and human prosperity. Unlike fossil fuels, whose reserves are concentrated in specific regions, renewable energy sources (RES) are available in every country. Renewable energy can be produced everywhere and thus has the potential to significantly change how energy is traded [1]. Nonetheless, in recent times, no sustainable and cost–effective way has been developed to transport renewable electricity over long distances. The use of green–hydrogen could be an answer. As an energy carrier, hydrogen enables renewable energy to be traded across regional and continental borders, also facilitating the decarbonisation of harder–to–abate sectors (like the steel and cement heavy industries). Hence, hydrogen has been recognised as a leading study subject, driven by unprecedented policy focus and put on the spotlight to investors and other market players [2].
Stemming from and subsequent of this recent surge in interest, academia has seen a growing body of research being published containing hydrogen–related keywords. This thesis intends to contribute to said groundwork by exploring the feasible linkages of hydrogen systems directly coupled to RES.

1.2 Topic Overview

Hydrogen technologies have gone through many cycles of expectation over the last decades. Although the vast majority of hydrogen produced to date has come from steam methane reforming, the production through green electrolysis has grown considerably—mostly driven by hydrogen road–maps enacted by governments around the globe [3]. Efforts exist to ramp the up–scaling of electrolysers for high–purity hydrogen production, supported by recommendations by the International Energy Agency (IEA); some suggest that it is not beneficial to connect all this capacity to the electric grid, which is facing enough of a challenge keeping up with the increase in demand for electrification [4]. A solution could come from systems with increasing shares of variable renewable energy sources, where low–cost surplus electricity may be available.

Even so, relying solely on occasional curtailed electricity to produce hydrogen implies electrolysers having very low utilisation factors (and, ultimately, very high unit costs). Hereupon emerges the relevant argument for extensive, dedicated hydrogen projects directly coupled to renewable energy sources. As will be seen, these systems can be located onshore or offshore, and have single or hybrid RES–to–Hydrogen configurations [5].

1.3 Objectives and Novel Contributions

This thesis is then rooted on the central purpose of contributing to the study of these important matters, with an article to be published hereafter. More clearly, the two–part question to be answered in this thesis is:

> **Which locations are available to install renewable energy systems dedicated to the production of green hydrogen, and which configuration results in the lowest hydrogen production cost?**

To answer this question, a series of three objectives have been explicitly established, which constitute the set of expected deliverables of this work. The following list details said objectives, also disclosing the novel contributions associated with each one.

- Create a map of the eligible locations on which to install renewable systems dedicated to the production of green hydrogen. These maps are restricted to Italy and Portugal, and represent an unprecedented achievement for these two countries.
- Obtain a ratio of the RES installed capacity to the electrolyser's nominal power, to apply on these extensive, country–wide systems. This innovative method may be used by the academia in subsequent research papers published on this topic, as a means to make estimations that better resemble reality.
- Develop an algorithm to compute the optimal size of pairs of renewable energy systems and electrolysers, in specific locations, considering single offshore and hybrid onshore configurations. A model with such characteristics has not been found in the literature.

Aside from these novel contributions, in the preparatory work for this thesis, two articles were published in scientific journals: *Recent Developments on Hydrogen Production Technologies: State–of–the–Art Review with a Focus on Green–Electrolysis* in MDPI's Applied Sciences, and *A Review of the Impact of Hydrogen Integration in Natural Gas Distribution Networks and Electric Smart Grids* in MDPI's Energies. A link to each article and their respective first–page covers are provided in Appendix A.

1.4 Thesis Outline

This Introduction began by indicating the rationale of the manuscript, followed by an overview of the topic, and the objectives and novelties of this thesis. The remainder of the document is as follows: Chapter 2 offers a comprehensive review of recent publications on said matters, and the identification of research gaps in the literature. Chapter 3 further expands this review and clarifies the underlying concepts of the theoretical framework in study. Chapter 4 introduces the methods of investigation, elaborating on the different stages of designing the geographical model. The methodology extends to Chapter 5, where the numerical formulation of the economic models is described in detail. The discussion of results takes place in Chapter 6, and Chapter 7 provides the overall findings of this work, with its achievements and recommendations for future work.

2 State of the Art

Nowadays it is extraordinarily uncommon to study a subject completely unknown to the scientific community. On the contrary, most discoveries are increasingly achieved through joint efforts and supported by iterative research on the same matters. The topic of this thesis abides to that, and so this chapter aims to present the body of knowledge published so far related to it. Section 2.1 provides a broad overview of such issued works, while Section 2.2 addresses potential research gaps and the respective solutions hypothesised in this thesis.

2.1 Literature Review

Some past Masters' endeavours have produced remarkable pieces of work concerning hydrogen technologies.

B. Franco [6] carries out a techno–economic analysis of hydrogen offloading systems for offshore wind farms, by studying the competitiveness of different pathways of producing and exporting hydrogen. Among other factors, the economic analysis includes the production costs and net–present value of the projects, with and without implementation of selected European Union's policies for hydrogen deployment. A major finding of this work is the improved economic viability of the projects when the market value of oxygen is considered (as a byproduct). A sensitivity analysis at the end also shows how the cost of hydrogen is mainly influenced by the costs of electricity and the electrolyser.

K. Narayan [7] instead focus on exploring hydrogen as a potential element to power long–distance, heavy duty transport. The viability of switching different modes of transportation to green hydrogen is first addressed, through a cost study that includes capital and operational expenses, net–present value and the levelised cost of hydrogen (LCOH). A similar conclusion to the previous case is reached here, in the sense that selling byproduct oxygen guarantees the economic viability of the projects. Furthermore, the sensitivity analysis also confirms that the cost of hydrogen is mainly dependent on capital costs and the cost of electricity.

C. Groenewegen [8] conducts a geospatial techno–economic analysis analogous to what is presented in this thesis. In it, the potential for large–scale, low–cost green hydrogen production is assessed, in Europe and in the region of North–Africa. Using geographic information systems, the author builds a visual model depicting suitable areas with high hydrogen potential. The technical hydrogen capacity is associated with the yields of solar and/or wind systems, while the economic readiness is ruled by the levelised cost of hydrogen. Considering it being based on rough, approximate models, this research still gives a first good estimate of the potential for green hydrogen production, ultimately showing that it is more significant in South–Europe and North–Africa.

The aforementioned study touches on two central points that are specifically addressed in the next pages.

Review on geospatial–based economical analysis

Geographic information systems (GIS) have become a main tool around the world, to use in the selection of the most fitting sites for the installation of RES–associated projects.

D. Vagiona and M. Kamilakis [9] present an integrated method to evaluate and prioritise suitable regions for the development of sustainable offshore wind farms. As customarily, the study comprises the application of a few exclusion criteria, in this case based either on the legislative framework or the international literature. The combined use of geographic information systems and multi–criteria decision methods outputs a result that ensures the spatial sustainability of the wind farms, together with better policies for renewable energy resources. The paper found two particular areas of Greece's South Aegean region to be the most suitable to contribute to the European obligations of increasing the RES share in the country to 20%.

Juárez–Casildo et. al [10] explore the concept of hydrogen cities, by proposing the production of hydrogen in urban settlements. Using GIS tools, the monthly potential of solar–hydrogen in metropolitan areas of Mexico is assessed. The requirements of piped and rainfall water are considered, as are estimated the hydrogen needs and carbon dioxide emissions avoided if lightweight transport used hydrogen instead of fossil fuels. The authors conclude that the country's total annual hydrogen demand can be entirely satisfied by just one–month production of certain urban areas, at relative low cost, if large–scale alkaline electrolysers are chosen. Additionally, further conclusions agree with previous observations that metropolitan production of hydrogen has low water requirements, with minimal infrastructure footprint.

B. Raillani et al. [11] aim to make a techno economic–evaluation of a large photovoltaic (PV) power plant dedicated to the production of hydrogen in eastern Morocco. A multivariate non–linear regression model is implemented to obtain a fitting energy production equation, adjusted to provide accurate, high–resolution GIS data. The simulations reveal immense potential for hydrogen production in the region, specifying the locations with best economic conditions with considerable map accuracy.

Pandora G. S. and Theocharis T. [12] incorporate expert's opinions and an extensive survey to local stakeholders into the GIS framework for optimal siting of offshore wind farms. Focused in the island of Crete, the authors offer a particular view into the complexity of installing RES systems in the context of energy independence. Through several rigorous evaluation criteria, including the pressing issue of social acceptance, the study shows an over–potential capacity to cover the annual energy demand of the island with just four wind farms. A recommendation remains for the aesthetic component of the installations to be minutely evaluated.

T. Gunawan and his co–authors [13] develop a techno–economic model of distributed wind–to–hydrogen systems located in Ireland. The systems are not completely off–grid since the grid may provide electricity when needed. The hydrogen in this analysis is produced, compressed, stored temporarily and then transported to be injected on the gas network. Akin to a basic optimisation algorithm, the model uses a correlation–based approach to chose the optimal electrolyser capacity that yields the minimum LCOH, from a set of three different scenarios. The conclusions coincide with the expected, in which the electrolysers must work at full capacity to reach a reasonably low LCOH.

The optimal computation of the levelised cost of hydrogen here referred is another research topic of major importance to this thesis—reason by which it is reviewed below.

Review on optimal computation of hydrogen costs

An inaccuracy present on most studies mentioned so far is the fact that all the energy produced by the dedicated RES is considered to be consumed by the electrolyser—implying that both systems are of the same size. A more careful analysis instead looks at ways to optimise the size of the electrolyser, taking into account the electricity generated by the renewable sources, in order to minimise project costs.

O. Atlam et al. [14] present one of the first methods to optimally size an electrolyser connected directly to a solar photovoltaic system. The method consists in a precise match of linear approximations of the electrolyser polarisation curve and the curve comprising the maximum power points of the PV system (at distinct irradiation levels). For each number of series and parallel strings of modules, an electrolyser size is obtained that optimises power transfer efficiency. The influence of PV temperature is also considered, and found to be inversely correlated with the optimum size of the electrolyser—for the same photovoltaic system.

More recently, the US National Renewable Energy Laboratory (NREL) published a comprehensive technical report on optimising integrated renewable electrolysis systems [15]. The study considers six different RES connections, including an 'islanded' one where no electricity purchases or sales are made to the grid. This configuration avoids market fees but limits the electrolyser to the solar capacity factor, resulting in initial higher unit costs. Through iterative processes, a general optimal electrolyser–PV ratio of 60% is achieved; further increases of the electrolyser size increase hydrogen production, yet also raise electrolyser costs and decrease its utilisation factor.

Y. Jiang et al. [16] perform a size optimisation, techno–economic assessment of a far–offshore wind to hydrogen project. In order to better contribute to investors' decision–making, the wind power output fluctuations and the aging degradation and replacement cost of the electrolyser are taken into account. A chance–constrained programming model is built to establish a benchmark maximum net present value (NPV) of the project, considering the aforestated aspects. Additionally, information–gap decision theory is applied to check acceptable hydrogen price ranges, with the maximum hydrogen cost uncertainty as the upper–layer, and the minimum admissible NPV as the lower–layer objectives. A particle swarm optimisation of stochastic simulation is selected to solve both models. In the end, a case study is used to demonstrate and make comparisons between results, including optimal size, economic viability and hydrogen prices.

M. Scolaro and N. Kittner [17] investigate the cost competitiveness of market ancillary services for offshore wind–based hydrogen production. The size of the electrolyser is determined through two different methods—optimal bidding strategy and optimal sizing of the facilities—and the project feasibility evaluated by metrics such as the NPV and the LCOH. Applying to case of Germany, and making use of empirical data from the European power market, this analysis concludes that these projects need participation in the ancillary service market to yield net positive revenues at present levels of wind generation. Another recommendation to ease cost reduction relates to the possibility of hydrogen producers getting access to subsidies similar to offshore wind farms that only generate electricity.

2.2 Research Gaps

The literature review was purposely divided into the former contents so that an evaluation of each individual research gap is possible.

The fundamental issue with the past MSc theses presented is the oversimplification of the RES–to–Hydrogen connection; the same applies to the subsequent articles. All these works generally consider the electrolyser to have the same nominal capacity as the renewable source they are connected to, which increases the overall cost of the project considerably—besides representing an excessive waste of the electrolyser potential capacity, due to its low utilisation factor.

Regarding the geospatial economical analysis, few consulted papers provide an extensive, multi–criteria assessment of the available locations—and if they do, it is not broadly applied, e.g. to a whole country. In addition, neither of these articles present a true LCOH mapping, comprising the areas previously evaluated. Furthermore, no work has been found in the literature that simultaneously contain both onshore and offshore geographic analysis of the same region.

Concerning LCOH optimisation, many different approaches exist, depending on the desired outcome. Simple linear approximations may be a quick method but lack deep exactitude; particle swarm optimisation commonly require less parameters and have easier constraints, but may produce early convergence, low–quality solutions. Likewise, works such as the ones discussed rarely include map–based optimal economical analysis of hydrogen systems.

With the research gaps identified, the solutions are suggested throughout the material methods of this thesis, in accordance to the objectives and novel contributions presented in Section 1.3.
The methodologies of this work are supported on an extensive body of recent references, which can be visually examined in the chart of citations of Appendix B.

3 Theoretical Framework

Standalone projects designed to produce green hydrogen always comprise two distinct systems. First, a RES system generates renewable electricity through green technologies; the two considered in this work are solar photovoltaic parks and onshore/offshore wind farms. Then, a hydrogen system converts this green electricity into gaseous hydrogen. The conversion is achieved by an electrolyser, that can be of different types—primarily alkaline and proton exchange membranes.

This chapter explores such systems in detail, providing an overview of the underlying theory regarding each topic. Section 3.1 discusses the current status and future outlook of onshore solar and wind technologies, as well as both offshore wind techniques (fixed foundations and floating devices). Section 3.2 reviews the two major electrolyser technologies existing today, and outlines three other currently developing techniques.

The economic analysis undertaken in the following chapters presupposes a standardisation of currencies retrieved from the consulted literature. For this purpose, all monetary values collected from techno–financial reports are converted to Euro (EUR). Table 3.1 provides the average exchange rate used in these conversions, based on the guidelines from the European Central Bank [18].

Table 3.1: Currency conversions. Adapted from [18].

Average Exchange Rate to EURO		EUR_{2019}	EUR_{2020}	EUR_{2021}
Great Britain Pound	GBP_{2019}	**1.1399**		
	GBP_{2020}		**1.1248**	
	GBP_{2021}			**1.1636**
United States Dollar	USD_{2019}	**0.8934**		
	USD_{2020}		**0.8768**	
	USD_{2021}			**0.8614**

To conduct an analysis as updated as possible, a thorough investigation was carried out to collect values of expenses from the last three years only.

Value added tax (VAT) was initially included in the cost study, following the procedure of the International Energy Agency in their Strategic PV Analysis and Outreach Task [19]. However, it ends up being excluded since it represents a quantity ultimately recovered by the companies, during the later selling process.

3.1 Renewable Energy Sources

The competitiveness of renewable energy sources has improved greatly in the last decade, as shown by data from the International Renewable Energy Agency (IRENA) Cost Database [20]. Between 2010 and 2021, reports indicate a decline of 88% in the cost of renewable electricity from utility–scale solar projects, 68% from onshore wind and 60% from offshore wind [21]. These costs are usually divided into capital expenses (CapEx) happening at the beginning of the project, and operational expenses (OpEx) taking place during its lifetime. In this work, CapEx includes hardware installation costs, balance of system (BOS) costs and soft financing costs, while OpEx includes fixed and variable operation costs and costs associated with maintenance and services. This distribution follows the suggestions of IRENA and the US Department of Energy's National Renewable Energy Laboratory [22, 23], which are summed up in Appendix C.

Figure 3.1 presents a summary of up–to–date capital and operational expenditures for each of the four technologies in study. These values are further detailed and explained in the following subsections.

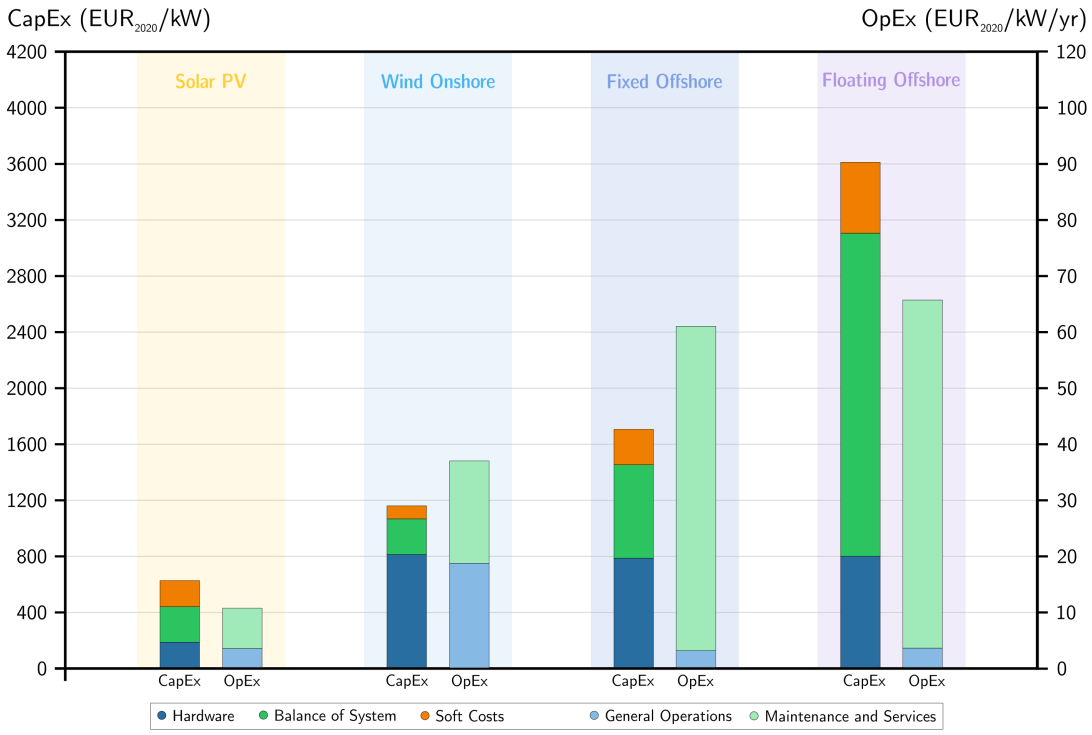

Figure 3.1: Cost analysis: overview of RES capital and operational expenditures.

3.1.1 Solar Photovoltaic Parks

In general, solar energy is defined as the conversion of sunlight into usable energy forms. Solar PV technology harvests light from the sun using mainly crystalline silicon modules, whose price declined up to 95% in the last 11 years [21]. This very high learning rate makes solar PV one of the most well established RES today, dominating the global renewable energy installed capacity [24]. Policy deadlines led to this deployment boom in the recent years, with countries from the United States to China expanding RES installation to achieve the 2030 climate targets. Overall, the world deployed 133 GW of solar PV last year—a new record [25].

Current status

Presently, standalone utility–scale solar PV capital expenditures amount to 630 EUR_{2020}/kWp. This value is deduced from recent reports [22, 26], after a careful reasoning is performed on the choice of each specific component. Since the RES power plant in this analysis is not grid–connected but instead linked to the electrolyser directly, all costs related to the inverter and the connection to the grid are excluded—leading to a reduction in CapEx of around 22%.

Figure 3.2 displays a waterfall chart of the individual contents considered to be part of current solar PV capital expenditures (top). A detailed description of these constituents can be found in Appendix C.1.

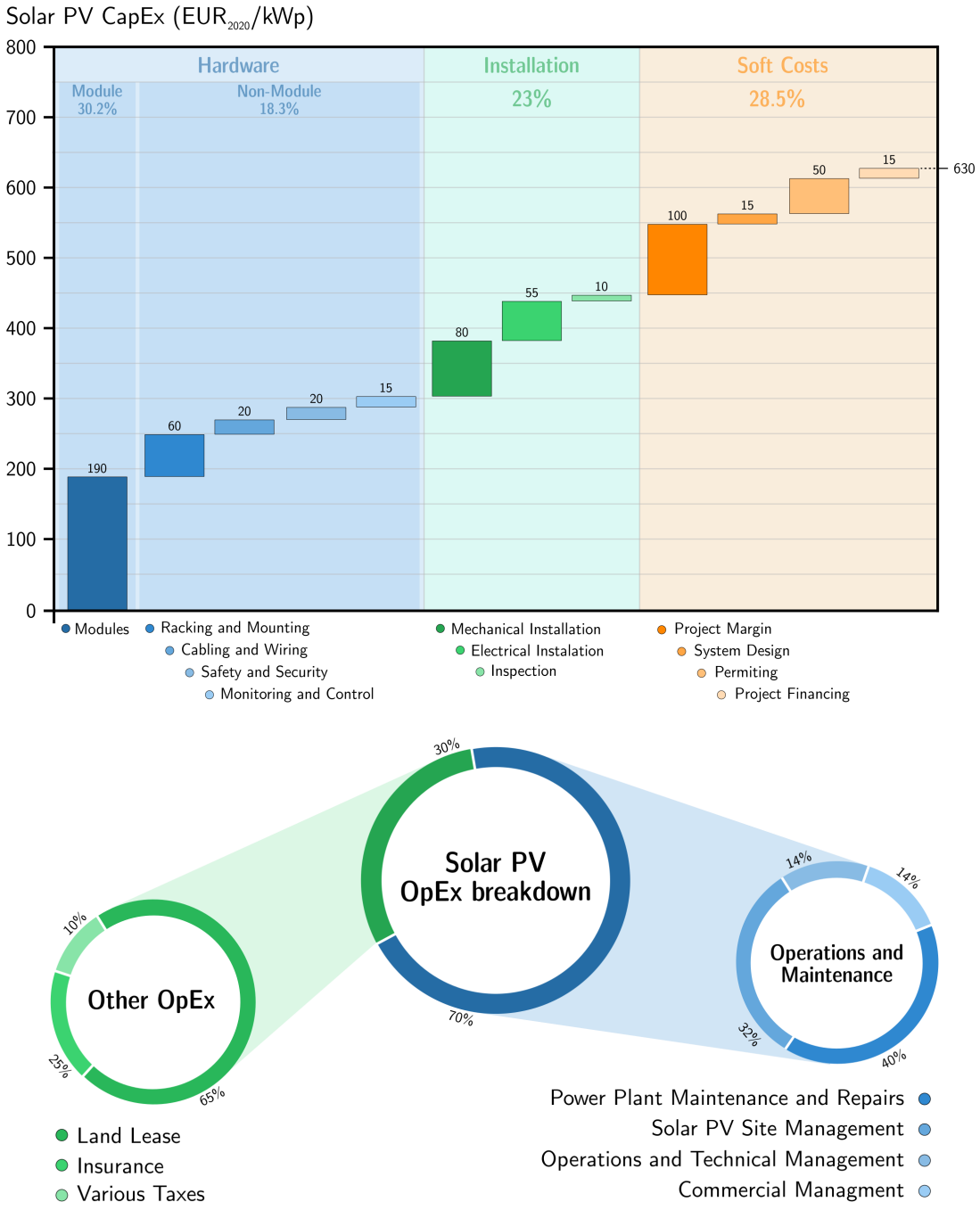

Figure 3.2: Cost analysis: solar photovoltaic capital and operational expenditures.

Operational expenditures are also lower for standalone projects than for grid–connected ones, adding up to just around 11 $EUR_{2020}/kW/yr$. The computation carried out in this analysis follows the main works of reference consulted [27–29]. Note that this analysis contemplates 'all–in OpEx', a metric that accounts for all operational expenditures of the enterprise—these include the traditional operation and maintenance (O&M) costs (scheduled and unscheduled) and other expenses like land lease, insurance, and various taxes. Based on E. Vartiainen et al. [29], the overall O&M is set to be 1% of CapEx and represent 70% of the total OpEx. Figure 3.2 presents a breakdown circular chart of current solar photovoltaic operational expenditures (bottom). Appendix C.1 offers a thorough description of each parcel too.

Future outlook

The competitiveness of solar PV technology is expected to continue increasing in the long-term, based on various distinct factors: the steady improvement of module efficiencies, the optimisation of manufacturing and innovation on the designs. The average crystalline module efficiency increased more than 6% in 10 years, to 20.90% in 2021 [21]. Passivated emitter and rear cell architectures have grown into state–of–the–art module technology, while perovskite solar cells have set the highest power conversion efficiencies to date—23.13%, with the possibility of achieving up to 30% if combined with existing silicon solar cell technology [30].
The development of perovskite solar cells has recently benefited from much of the research directed towards its improvement: 'smart windows' have been unveiled in the last couple of years, where thermochromic photovoltaic modules darken their colour when heated by sunlight to decrease the cooling needs of the building [31]. Although showing great potential for low–cost, high–efficiency solar energy, perovskite solar cells' long–term stability is still holding this technology back from widespread commercial application [32].
Lightweight organic solar cells is another technology making great progress lately. Several manufacturers around the world are printing photovoltaic material on bendable plastic substrate sheets by half the cost of silicon–based modules, while being up to 100 times lighter [33]. One application of this technology can be on agrivoltaics, where PV panels are installed at a height so that plants grow underneath them. Besides shading the crops (meaning less water is needed for irrigation), the panels are also cooled by the 'sweating' of the plants—increasing their efficiency and ultimately maximising land productivity [34].

3.1.2 Onshore Wind Farms

The kinetic energy of air in motion—or wind energy—is described as the process in which wind is used to produce mechanical work, that in turn is converted to electricity. This energy is mostly all captured by tall horizontal–axis turbines, generally using rotors with three blades oriented upwind, attached to a nacelle on top of a tubular tower [21]. Like solar PV, onshore wind turbine technology has progressed considerably over the past ten years. Hub heights have increased 50%, rotor diameters have doubled and the nameplate capacity of the turbine has tripled in some cases. From 2010 to 2020, by reason of greater competitiveness, economies of scale and grown maturity of the sector, total installation costs, turbine costs and O&M costs have fell around 30%, 40% and 50%, respectively [35].
Besides a fifty–fold raise of global wind power generation in the last two decades [36], the IEA predicts onshore wind installed capacity to be almost 25% higher in the next five years than it was during 2015–2020 [24].

Current status

According to the latest financing and investment trends [37], onshore wind turbines not connected to the grid have capital expenditures per kilowatt situated around 1162 EUR_{2020}/kW. This value is obtained after a thorough analysis of the individual categories and sub–categories of the CapEx components, provided by NREL's recent review report [23]. A detailed expenditure breakdown is provided in Appendix C.2, which helps give meaning to the drivers of wind energy costs.

Figure 3.3 (top) presents a waterfall chart of the individual parts that comprise the capital expenses of a standalone wind turbine today.

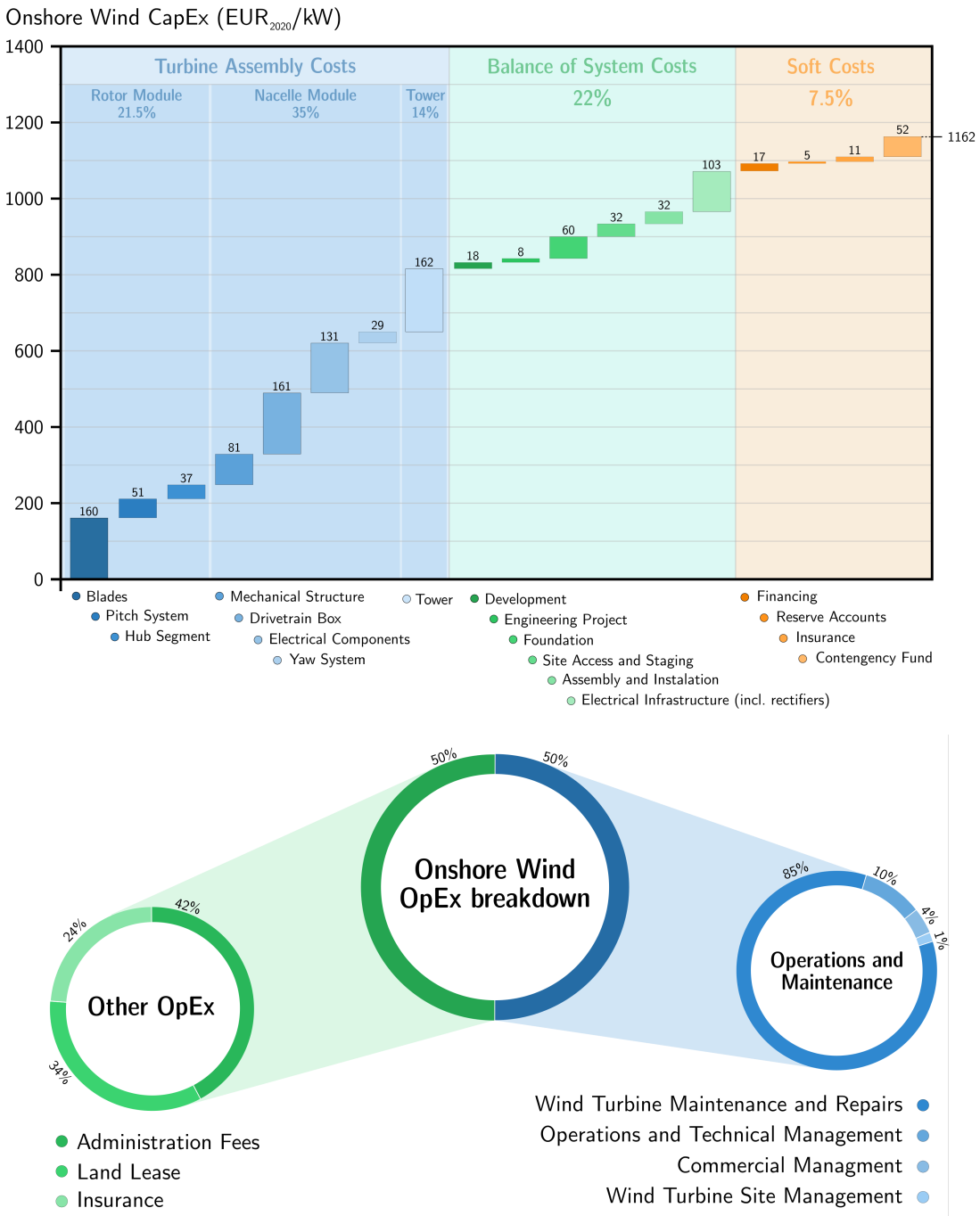

Figure 3.3: Cost analysis: onshore wind capital and operational expenditures.

Based on the latest NREL report on the matter [23], the operational expenditures of a land–based wind turbine in this work is set to 34 $EUR_{2020}/kW/yr$. B. Steffen et al. [28] corroborates the previous suggestion of T. Rubert et al. [38] in which the relation between O&M and other OpEx is set to 50/50. The distribution of the respective sub–components is presented in the circular chart of Figure 3.3 (bottom). Appendix C.2 also provides a comprehensive description of the OpEx breakdown structure.

Future outlook

Onshore wind power is one of the most mature and yet fastest growing, cost–competitive RES technologies today. For these reasons, it will continue to be an essential renewable energy alternative in the forthcoming decades. The Realistic Expectations Scenario of WindEurope's five–year Market Outlook predicts that 2022 will be a record year of new installed capacity, with 22 GW solely in the European Union (EU)—26% more than in 2021 [39]. This trend should continue on average in the next five years, until a cumulative capacity of 225 GW is reached in 2026. Note that this scenario is conditional to the current policies and permitting barriers in the EU.

Regarding global long–term forecasts, IRENA reports a three–fold growth by 2030 in onshore wind total installed capacity, and nearly a ten–fold by 2050, when compared to 2018 values. This prediction is considering a conservative average compound annual growth rate of 7%, well below the average 21% achieved in the past couple of decades. The feasibility and ease of scaling up is thus assured simply by keeping the historical pace of onshore wind installation—still, 5 TW by 2050 is only around 5% of the total wind resource potential, as estimated by a technical committee of the World Wind Energy Association [40].

Improved wind energy yields and lower capital and operational expenditures per unit of installed capacity are expected, supported by further innovations towards continued higher turbines and larger rotor diameters. Major future trends include: technology enhancements in the design of aerodynamic profiles and materials of the blades [41]; optimisation of power electronics' reliability and dimensions, and improvement of forecasting mechanisms to better regulate the turbine's controls and maximise the overall energy output—ultimately cutting down unscheduled operational costs [42]; and the use of distinct sustainable materials alongside low–cost recycling processes in newly manufactured turbine blades, to contribute for the circular economy [43].

3.1.3 Offshore Fixed Wind Farms

The working principle of offshore wind technology is the same as onshore, only the turbines are placed in the sea instead of inland. Offshore turbines are often larger than their onshore counterparts since generally there are higher mean wind power densities seaward, meaning better wind resources [44]. Several factors can impact the site suitability of offshore wind farms, namely the roughness length and the bathymetry of the location. Fixed foundations are the most common type of installation and the most mature offshore technology. These foundations are generally divided into gravity, monopile, tripod and jacket bases, and are consistently installed at depths up to around 40 meters, at up to 80 km from the coast [45].

As projects became sited at greater depths and farther away from shore and used more advanced technology, installation costs peaked. However, with economies of scale and recent increases in developer and manufacturer experience, cost reductions unlocked widespread deployment of fixed offshore wind turbines [21].

Current status

In this work, cost data for offshore technology in general is collected from NREL's 2020 Cost of Wind Energy Review [23] and the Guide to an Offshore Wind Farm published on behalf of The Crown Estate and the Offshore Renewable Energy Catapult [46]. These reports present the most detailed, up–to–date and in–depth description of the costs associated with this technology; regarding fixed foundations, the total capital expenditure value is around 1700 EUR_{2020}/kW. This value is obtained after performing a strict assessment of each individual component since here there is no electricity transmission to onshore substations.
The waterfall chart of Figure 3.4 (top) shows the detailed composition of an offshore wind turbine CapEx. Appendix C.3 provides a thorough breakdown of the structure of these categories.

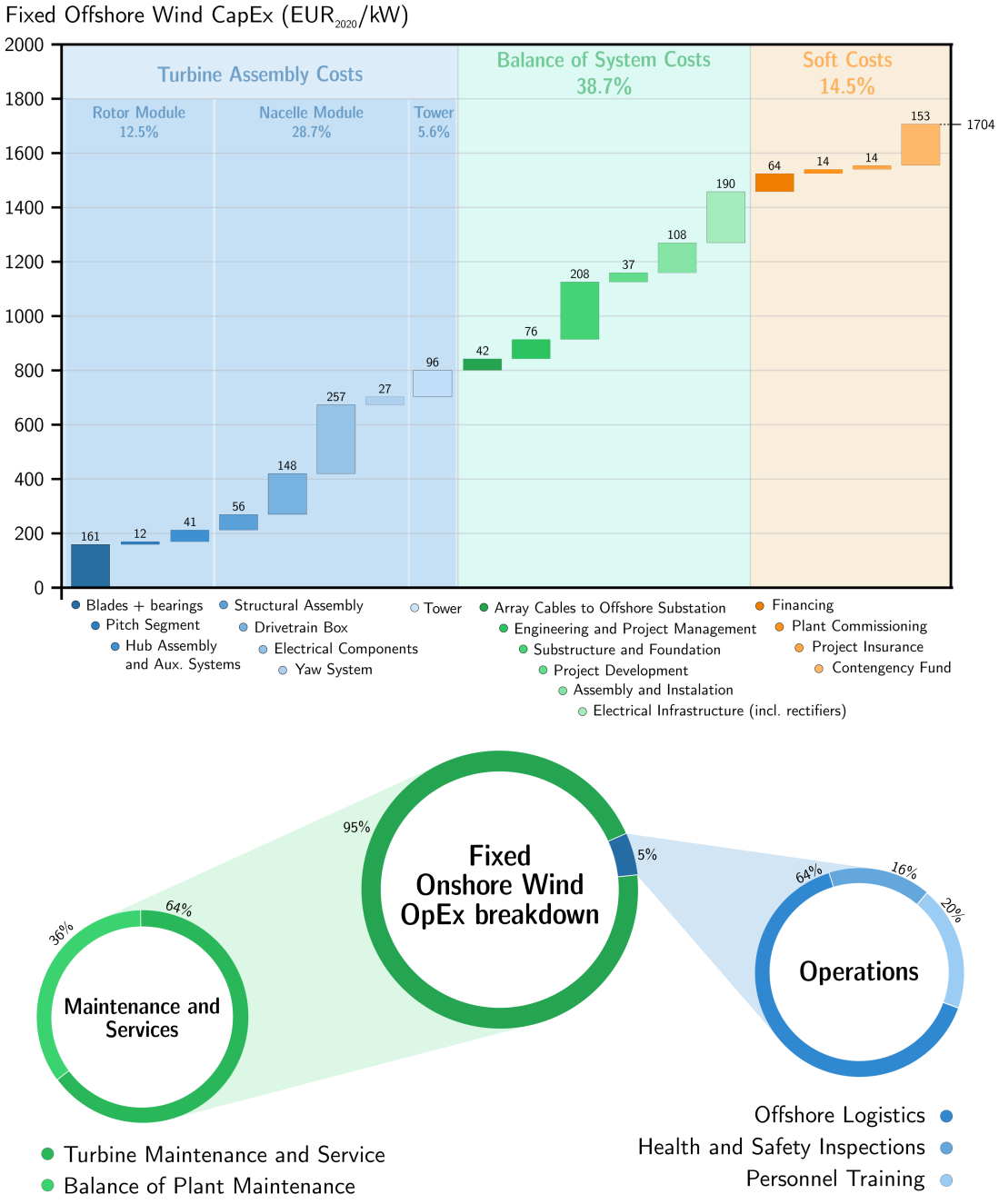

Figure 3.4: Cost analysis: offshore fixed foundations capital and operational expenditures.

Figure 3.4 also shows a circular chart (bottom) of the current weight distribution concerning operational expenditures of offshore wind turbines with fixed foundations. Additional information regarding OpEx is taken from NREL's last year's market report [47], setting this value at 61 $EUR_{2020}/kW/yr$.
The composition of operational expenses in offshore wind technologies is very different from onshore; the vast majority of costs go to maintenance and service of the turbine (and balance of system), which are naturally exposed to harsher conditions at sea. Since this is not as mature a sector as onshore wind, there are also costs associated with personnel training and regular inspections. All these categories are explained in Appendix C.3.

Future outlook

Over the last decade, offshore wind's global cumulative installed capacity grew ten–fold to 34 GW. In that period, total installed costs dropped 32%, rotor diameters rose 46%, and turbine capacities 143% [35]. O&M costs have decreased considerably too, by over 43% between 2015 and 2018 [21].
WindEurope's Realistic Expectations Scenario predicts a 3.5 MW installation growth in 2022 alone, with some countries like Italy seeing their first commercial offshore wind farm deployed; until 2026, Europe will increase its installed capacity by 28 MW [37]. Over the next 30 years, the global offshore market is set to grow substantially, from just 23 GW in 2018 to around 230 GW in 2030 and almost 1000 GW in 2050 [48].
Much of this increase in installed capacity will come from larger turbines. GE Renewable Energy's Vineyard Wind project announced they would be using 13 MW turbines, with blades 107 meters long that can satisfy an average household's daily electricity needs in under seven seconds [49]. Siemens Gamesa has recently launched an even bigger offshore turbine, with a nameplate capacity of 14 MW and a 222–meter rotor diameter [50]. Going even further, The Netherlands–based Tetrahedron has unveiled plans lately to build a prototype crane that can make existing jack–up vessels suitable for installing up to 20 MW turbines at sea [51].
As wind turbines continue to increase in size, new solutions will be developed for different foundations. Manufacturers such as Steelwind Nordenham are already offering ultra–large XXL Monopiles, with lengths of up to 120 meters and weights that reach 2400 tonnes, to support new–generation turbines [52]. J. T. Hansen et al. [53] propose yet another distinct solution, in the form of vertical–axis wind turbines; these turbines, when set in pairs, increase the overall performance by 15%, since they can be placed much closer together.

3.1.4 Offshore Floating Wind Farms

In contrast with fixed foundations, floating wind farms are not limited to close–shore shallow depths. In fact, wind farms are steadily moving further towards deeper waters to larger areas in the sea, where wind conditions are more stable. This departure from shore helps mitigate the visual impact inland and reduces installation activities on the seabed, diminishing the harmful effects on marine life [54].
Floating technologies can be mainly of barge, sensi–submersible, spar, articulated multi–spar or tension–leg platform type, as reported by IRENA [45].
Nowadays, wind farms are already being deployed up to 100 km offshore in waters deeper than 100 meters, with the instalment of new–generation turbines planned much further out [52]. While this tendency benefits from the advantages mentioned above, it also implies an increase in construction and operation costs, as well as technological challenges.

Current status

Current expenses associated with offshore floating turbines are collected from the same sources as offshore fixed ones. This technology is by far the most expensive of the four considered in this work: 3605 EUR_{2020}/kW in capital expenditures and 72 $EUR_{2020}/kW/yr$ in operational expenditures. The costs related to the substructure and foundation of the wind farms are the largest parcel of CapEx, accounting for almost 40% of the total, while the balance of system electrical infrastructure is the second predominant parcel.

Figure 3.5 illustrates the CapEx breakdown cost structure of floating technologies today (waterfall chart on top) and the respective OpEx weight distribution (circular chart on bottom). Appendix C.4 provides a detailed description of each of these categories.

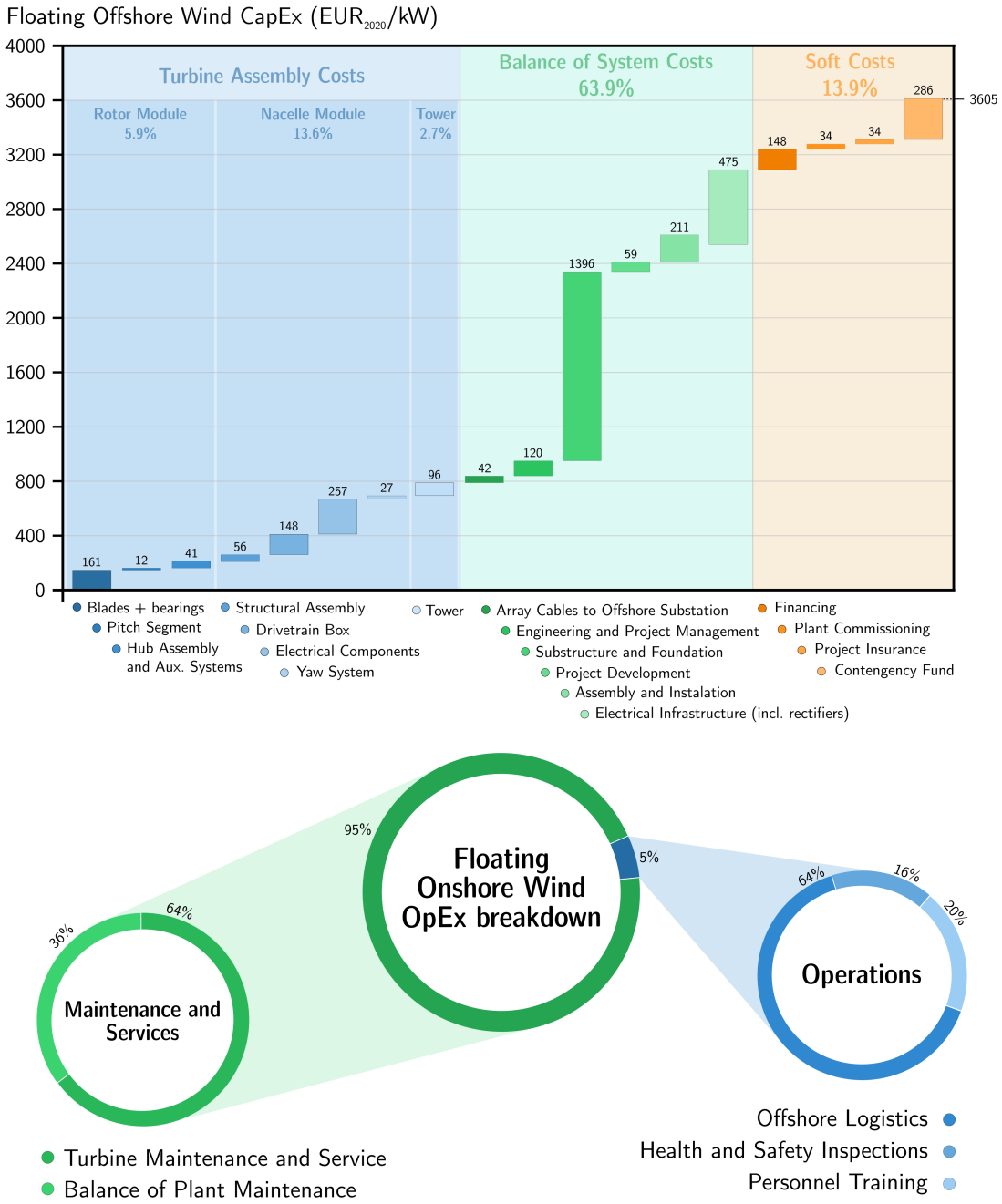

Figure 3.5: Cost analysis: offshore floating structure capital and operational expenditures.

The considerable increase in costs from offshore fixed to offshore floating wind farms is correlated with the sector's maturity and inherent technological differences. In this case, turbines are deployed much further seaward, implying longer shipping journeys to and from the turbine for maintenance purposes. Floating foundations also still impose more significant installation challenges than fixed bases.

Future outlook

Accelerated development of floating wind turbines is to be expected in the near future due to the convenience of this technology for some countries that lack easy access to shallow waters. Also, as more and more countries expand their offshore floating activities globally, economies of scale and falling installation costs will ease the market penetration of this technology and make it accessible for even more countries [45].
In Europe, many countries recently adopted floating foundations, with the 2020 average water depth and offshore distance being respectively 36 meters and 44 km—an increase of 64% and 33% from 2014 [54]. As an example, Portugal's 2020 WindFloat Atlantic deployed a total of 25 MW in the north of the country, a project that uses an innovative moored semi–submersible platform [55].
This rise in installed capacity is expected to continue in the coming years. Industry experts predict offshore floating cumulative installations to grow up to 30 GW worldwide by 2030 [56]. At this pace, IRENA estimates floating wind farms to cover around 15% of the global offshore wind installed capacity by 2050 [40].

Further expansion of floating devices will benefit from layout optimisation and repowering of sites. Advancements in software tools to characterise wind resources, aerodynamic wake effects, oceanic meteorology and bathymetry conditions allow more informed and complete layouts of offshore wind farms. A standardisation of installation methods may also spur widespread deployment of these technologies in the future [40]. Since offshore O&M spending is expected to grow 17% annually worldwide [42], Condition Monitoring Systems—an O&M tool to help operators monitor the status of wind turbine components—could predict any possible issues in advance and thus boost the efficiency of maintenance activities.

Finally, there is also a rising interest in coupling these technologies with green hydrogen production, mainly attributed to the following three factors [45]:

- Offshore wind (especially floating devices) has, on average, the highest capacity factor among all RES. This correlates with higher electrolyser full load hours (FLH) and thus a decrease in overall costs.

- Localisation advantage near demand centres. Since industrial clusters are usually located in areas close to shore, they can be the primary users of the hydrogen produced offshore.

- Elimination of land eligibility constraints with improved system flexibility. Implementation of large–scale green hydrogen projects onshore requires notably more land resources than offshore projects.

The cost structure of current leading electrolyser technologies and other developing methods is described in the next section.

3.2 Hydrogen Production Taxonomy

The hydrogen feedstock industry is well established nowadays, having decades of experience in distinct sectors, from the production of ammonia to iron, steel, glass and electronics. Yet, the market is set to continue growing significantly in the coming years [57].

The large majority of hydrogen today is produced based on fossil–fuels, whether coal or gas. While efforts have been made to produce 'blue' hydrogen with carbon capture and storage (CCS) techniques, the hydrogen industry is still mostly polluting. However, the use of water electrolysis to produce 'green' hydrogen has been on the rise lately. Generally, hydrogen colour codes are used to express the main feedstocks, energy sources and production processes, in this way differentiating between types of hydrogen [58]. Figure 3.6 illustrates the updated hydrogen colour spectrum.

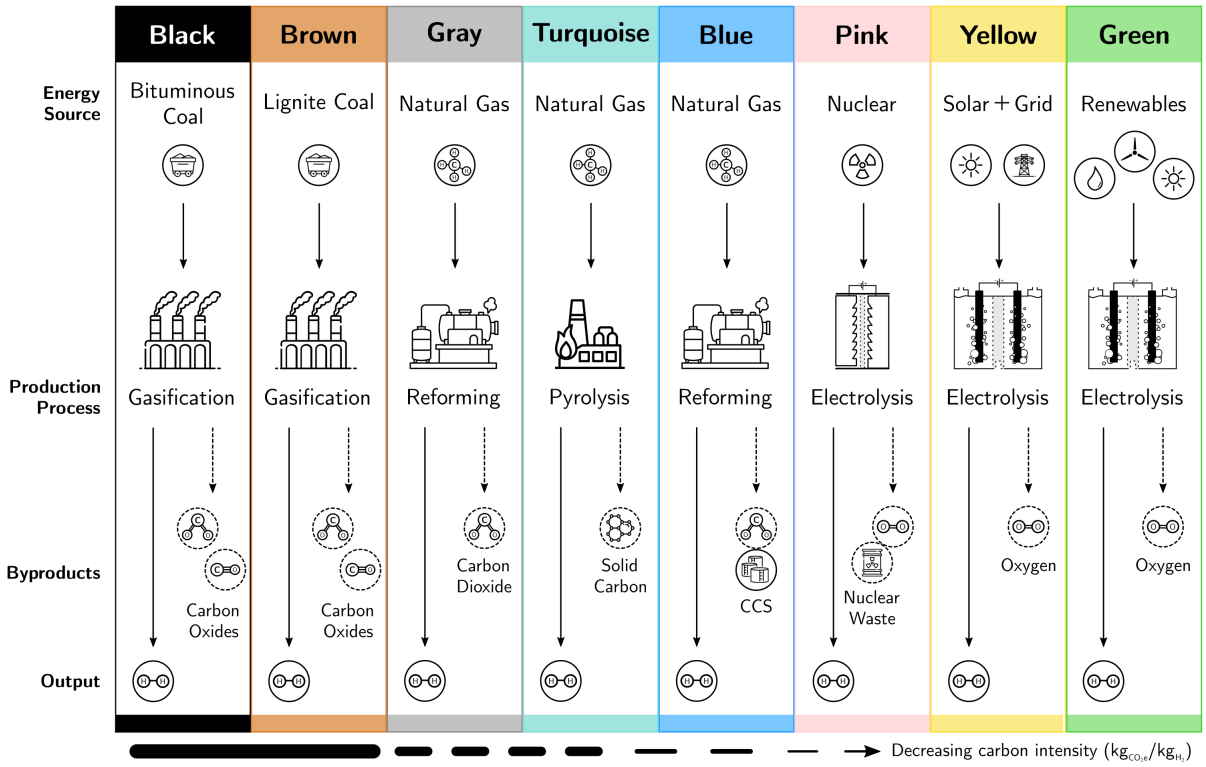

Figure 3.6: Hydrogen color–code spectrum. Designed using resources from [59].

Nowadays, most of the research has been focused on developing and improving electrolysis techniques. This production process is the one with the least life–cycle carbon intensity (measured in kilograms of carbon dioxide equivalent per kilogram of hydrogen), thus being the most sustainably alluring [58].

This section presents a technology–viewpoint overview of electrolysis, related to the specific features, current status and future outlook of the most developed electrolysers, and some new developing techniques.

After establishing the electrolyser technology for the methodological analysis, the geographical model design is presented in the next chapter.

3.2.1 Alkaline Electrolysis

Alkaline water electrolysis was introduced in the late 18th century, being now a well–established commercial technology. Today's alkaline electrolysers (AlkEl) are characterised by two electrodes placed within a liquid electrolyte solution, generally, potassium hydroxide mixed with water [60]. These electrodes are isolated by a separator, through which occurs the transfer of hydroxide ions (OH^-). Figure 3.7 offers a schematic illustration of an alkaline electrolyser, and Table 3.2 summarises their present and future features.

Current status

Alkaline electrolysers have been commercially mature since the mid–twentieth century, thus having a relatively low CapEx today compared to other types of electrolysers [61]. They also benefit from not having precious metals in their composition, which would increase their cost. In the last 15 years, capital expenditures fell 61%, from as high as 1858 EUR_{2005}/kW to as low as 290 EUR_{2020}/kW [35]. AlkEl projects prevail essentially in the low–MW range, with the electrolyser stack being responsible for about 50% of CapEx [4]. Reliability and stack lifetimes are among the highest in the sector, whereas a slow load–following prevents this technology from being coupled directly with RES [60].

Future outlook

As electrolysers get larger, economies of scale in the manufacturing process will come into play. Combining multiple electrolyser stacks increases the overall system capacity, enabling costs to decrease 20% [4]. New enterprises have been expanding installed capacities to about 30 MW, with some representative quotes going up to 300 MW [35]. The operational cell pressure is set to increase to avoid using an output compressor; IRENA predicts stack lifetimes to double as a 2050 target, further reducing unit costs [62].

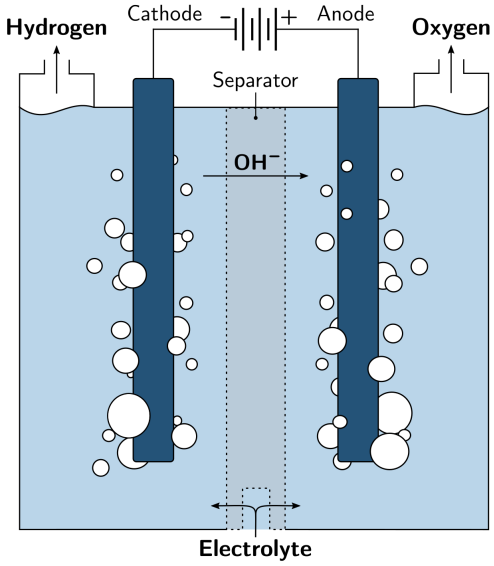

Figure 3.7: Illustration of an alkaline electrolyser.

Table 3.2: Alkaline electrolyser: summary of features.

AlkEl Features	2020	2050	Ref
Operational parameters			
Temperature (°C)	40–90	>90	[60, 62]
Pressure (bar)	1–30	>70	[4, 62]
Nominal attributes			
Production rate (Nm^3/h)	≈ 3140	≈ 3140	[63]
Load range (%rnl)	10–110	5–300	[4, 62]
System characteristics			
Consumption (kWh/m^3)	≈ 4.10	<3.77	[62, 63]
Efficiency (%LHV)	63–70	≈ 80	[4]
Stack Lifetime (kh)	60–90	100–150	[4]
Cold start (min)	<50	<30	[62]

Note: features whose predictions for 2050 are not found in the literature remain the same as 2020. Nevertheless, improvement in the coming decades is always expected. rnl = relative to nominal load; LHV = lower heating value; kh = thousands of hours.

3.2.2 Proton Exchange Membrane Electrolysis

The first proton–exchange membrane electrolysers (PEMEl) were developed and commercialised in the 1960s, almost 200 years after the first AlkEls [60]. PEMEls introduced some fundamental changes to overcome the drawbacks of alkaline electrolysers, offering a simpler and more compact system design and leading to fewer costs and maintenance [62]. PEM electrolysers use a solid polysulfated membrane as the electrolyte, working like a proton conductor through which the hydrogen atoms (H^+) move during electrolysis. Figure 3.8 shows a simplified illustration of a proton–exchange membrane water electrolyser.

These membranes can operate at high differential pressures and ambient temperatures, enabling the production of highly pure hydrogen with low environmental impact. Other promising advantages include high net production rates, sizeable operating load ranges and fast response times—making this technology ideal to couple directly with renewable energy sources and produce green hydrogen in a flexible way [57]. Table 3.3 presents a summary of the abovementioned features.

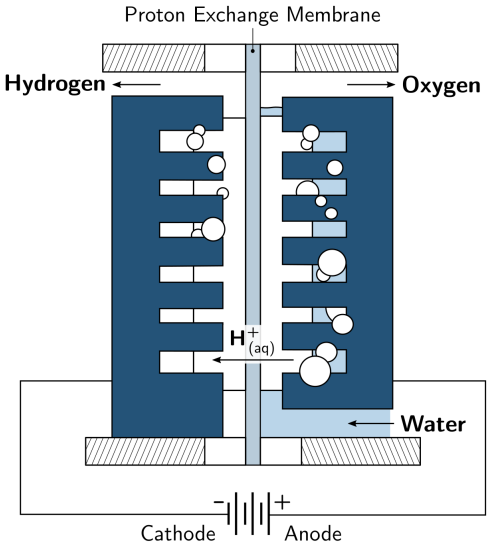

Figure 3.8: Illustration of a PEM electrolyser.

Table 3.3: PEM electrolyser: summary of features.

PEMEl Features	2020	2050	Ref
Operational parameters			
Temperature (°C)	20–100	80	[60, 62]
Pressure (bar)	30–80	>70	[4, 62]
Nominal attributes			
Production rate (Nm^3/h)	≈ 5000	≈ 5000	[64]
Load range (%rnl)	0–160	5–300	[4, 62]
System characteristics			
Consumption (kWh/m^3)	≈ 4.60	<4.04	[62, 64]
Efficiency (%LHV)	56–60	>80	[4, 62]
Stack Lifetime (kh)	30–90	100–150	[4]
Cold start (min)	<20	<5	[62]

Note: features whose predictions for 2050 are not found in the literature remain the same as 2020. Nevertheless, improvement in the coming decades is always expected. rnl = relative to nominal load; LHV = lower heating value; kh = thousands of hours.

Current status

PEMEl costs have fallen over time, following progressive learning rates. Concerning this topic, numerous recent articles and reports [65–67] have published different values based on different assumptions. A meticulous reasoning is performed upon consulting the literature to ensure the credibility and validity of results. Data is first gathered from IRENA [62] to draw a detailed cost breakdown of a 1 MW PEM electrolyser (assumed to be the same for larger stacks). Further research from issued papers [68, 69] and technical reports [5, 70, 71] put current PEMEl capital expenditures at 1136 EUR_{2021}/kW and operational expenditures at 38 $EUR_{2021}/kW/yr$. Here, OpEx is mainly defined by fixed and variable water consumption costs. These typically vary across the country's regions since each administrative division refers to its own water company; for the sake of generality, an average value is used from the Italian company ABC, following the procedure of M. Minutillo et al. [72].

Figure 3.9 (top) displays a waterfall chart of the individual components comprising the capital expenditures of a proton exchange membrane electrolyser. The circular chart on the bottom gives the distribution of each specific element of the operational expenses.

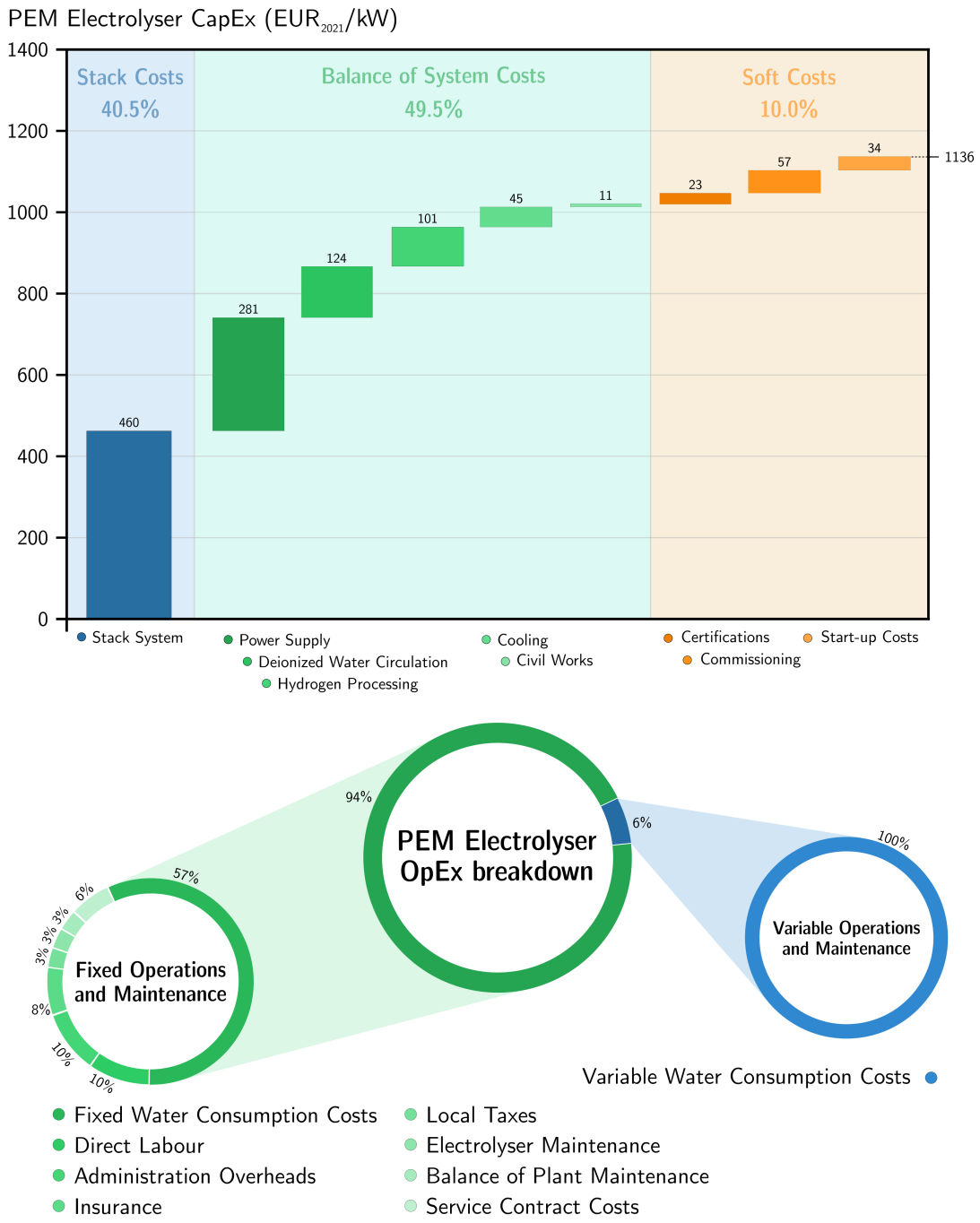

Figure 3.9: Cost analysis: PEM electrolyser capital and operational expenditures.

Future outlook

Cost reductions in the future will be determined by technological innovations, such as cheaper electrodes and thinner membranes. Research and development focus should be primarily on system design and the catalysts used, since the need for expensive platinum and iridium metals greatly raises PEMEl capital expenses [62]. The development of larger multi–stack electrolysers can also bring down CapEx values up to 40% [4].

3.2.3 Other Technologies

Although AlkEls and PEMEls are the two most mature technologies, other alternatives have been developed recently, hoping to further diversify the ways to produce green hydrogen through water electrolysis. Current research is directed at improving the lifetime, stack and system electrical efficiency, power density and technology scale–up while reducing costs and manufacturing times [58].

Solide Oxyde Electrolysis

Solid oxide electrolysers (SOEl) use ceramic membranes to transfer oxygen ions at very–high temperatures, splitting superheated steam into hydrogen and oxygen. Figure 3.10 illustrates the process described with a schematic SOEl. The electrical efficiency offered by this technology is usually much higher than other methods—and unlike AlkEls and PEMEls, reverse–mode operation as a fuel cell is attainable. This particular characteristic enables the electrolyser to have higher utilisation factors, ultimately reducing costs [4].
Of the three in this section, solid oxide technology is the most developed, although still in early market commercialisation [58]. Table 3.4 outlines the main features of SOEls.

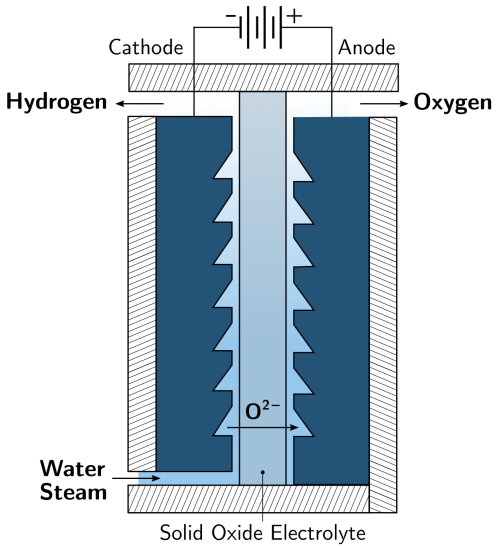

Figure 3.10: Illustration of a solid oxide electrolyser.

Table 3.4: SOEL electrolyser: summary of features.

SOEl Features	2020	2050	Ref
Operational parameters			
Temperature (°C)	<1000	<600	[60, 62]
Pressure (bar)	1	>20	[62]
Nominal attributes			
Production rate (Nm^3/h)	≈ 2884	≈ 2884	[73]
Load range (%rnl)	20–100	0–200	[4, 62]
System characteristics			
Consumption (kWh/m^3)	≈ 3.60	<3.33	[62, 73]
Efficiency (%LHV)	74–81	77 – 90	[4]
Stack Lifetime (kh)	10–30	75–100	[4]
Cold start (min)	>600	<300	[62]

Note: features whose predictions for 2050 are not found in the literature remain the same as 2020. Nevertheless, improvement in the coming decades is always expected. rnl = relative to nominal load; LHV = lower heating value; kh = thousands of hours.

Anion Exchange Membrane Electrolysis

Anion exchange membrane electrolysers (AEMEl) are a fairly recent technology with minimal market deployment. Its potential lies in combining a less harsh environment than AlkEls with the simplicity of PEMEls, thus helping improve electrolysis efficiency and reducing cold start times [60]. Table 3.5 provides a summary of the features of this technology. At the cell level, the water–electrolyte breaks apart within the membrane, transferring hydroxide ions back to the anode half–cell and releasing hydrogen atoms. Figure 3.11 shows a schematic illustration of an AEM electrolyser.

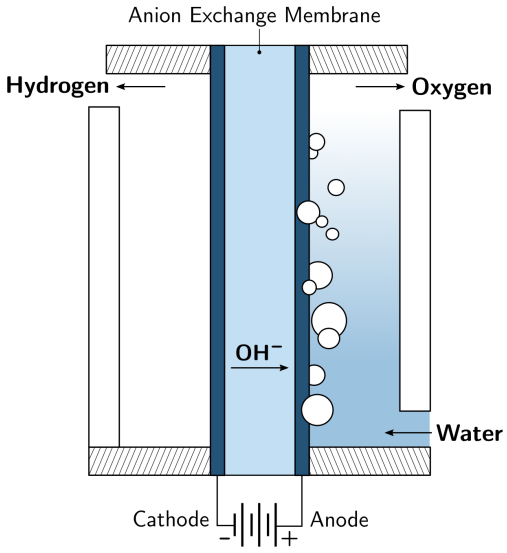

Figure 3.11: Illustration of an AEM electrolyser.

Table 3.5: AEM electrolyser: summary of features.

AEMEl Features	2020	2050	Ref
Operational parameters			
Temperature (°C)	40–60	80	[62]
Pressure (bar)	<35	>70	[62]
Nominal attributes			
Production rate (Nm^3/h)	0.5	0.5	[74]
Load range (%rnl)	5–100	5–200	[62]
System characteristics			
Consumption (kWh/m^3)	≈ 6.27	≈ 5.18	[58]
Efficiency (%LHV)	52–67	52 – 67	[58]
Stack Lifetime (kh)	>5	100	[62]
Cold start (min)	<20	<5	[62]

Note: features whose predictions for 2050 are not found in the literature remain the same as 2020. Nevertheless, improvement in the coming decades is always expected. rnl = relative to nominal load; LHV = lower heating value; kh = thousands of hours.

Capillary–fed Electrolysis

As recently as this year, a group of Australian researchers published a paper [75] reporting exceptional performance of a new type of technology: a capillary–fed electrolyser (CFEl). This method delivers water to the electrodes via capillary–induced transport along a porous separator, which leads to an inherently bubble–free operation. Figure 3.12 illustrates the working principle of a CFEl. Table 3.6 summarises the known features of this technology (many still lack verifiable data).

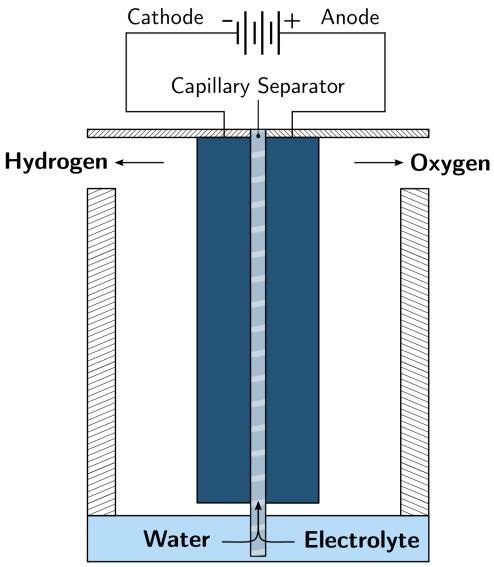

Figure 3.12: Illustration of a capillary–fed electrolyser.

Table 3.6: CF electrolyser: summary of features.

CFEl Features	2020	2050	Ref
Operational parameters			
Temperature (°C)	85	85	[75]
Pressure (bar)	1	1	[75]
Nominal attributes			
Production rate (Nm^3/h)	N/D	N/D	—
Load range (%rnl)	N/D	N/D	—
System characteristics			
Consumption (kWh/m^3)	3.64	3.64	[75]
Efficiency (%HHV)	98%	98%	[75]
Stack Lifetime (kh)	N/D	N/D	—
Cold start (min)	N/D	N/D	—

Note: features whose predictions for 2050 are not found in the literature remain the same as 2020. Nevertheless, improvement in the coming decades is always expected. rnl = relative to nominal load; HHV = higher heating value; kh = thousands of hours.

4 Geographical Model Design

This chapter describes the distinct stages of material work undertaken to design and develop the geographical model. Section 4.1 presents the main characteristics of both study areas and Section 4.2 explains the data collecting and handling. Sections 4.3 and 4.4 present the diverse set of criteria used for the exclusion and evaluation phases, respectively; lastly, Section 4.5 discusses the final eligible locations.

4.1 Study Area

This work focuses on two similar but different countries located in Europe, to enable a comparative analysis of the potential for hydrogen production.

4.1.1 Italy

The Republic of Italy is a country located in the Southern part of Europe between latitudes 35°–47° N and longitudes 6°–19° E. To the North, Italy borders France, Switzerland, Austria, and Slovenia and is delimited by the Alpine watershed; to the South, it consists of the entirety of the Italian Peninsula and the two Mediterranean islands of Sicily and Sardegna, in addition to many smaller islands—as shown in Figure 4.1(a). The sovereign states of San Marino and the Vatican City are enclaves within Italy, while Campione d'Italia is an Italian exclave in Switzerland. The country has a total inland area of 301,230 square kilometres, comprising 21 regions grouped into five major territories, and an exclusive economic zone (EEZ) of 541 915 square kilometres that extends 200 nautical miles (∼370 km) from its shores within the Ligurian and Tyrrhenian seas to the west, the Ionian Sea to the South and the Adriatic Sea to the east [76].

The climate in Italy is influenced by the large body of water of the Mediterranean Seas, which constitute a reservoir of heat and humidity within the Southern temperate zone, determining a particular climate with local differences due to the geomorphology of the territory. Because of the length of the peninsula and the mostly mountainous hinterland, Italy's climate can be highly diverse—in most inland central Northern regions, the climate ranges from humid subtropical to humid continental and oceanic, whilst the coastal areas generally fit the Mediterranean climate stereotype. Annual precipitation naturally varies across regions too, with the South having a reasonably even rainfall pattern and most of the precipitation occurring in the far Northern mountains of Italy—often recording more than 1200 mm; snow is expected in the winter months, although in the Alps snow falls more in autumn and spring. In Italy, the coastal strips of Sardegna, Sicily and Apulia have more than 2600 hours of sunshine per year, averaging more than seven hours per day [77].

4.1.2 Portugal

The Portuguese Republic is a country whose mainland is located on the Iberian Peninsula of Southwestern Europe, between latitudes 36°–42° N and longitudes 9°–6° W. It is bordered to the West and South by the Atlantic Ocean and to the North and East by Spain; its territory also includes the Atlantic archipelagos of the Azores and Madeira, which form two autonomous regions with their regional governments—they are left out of this analysis for this particular reason and the fact that thousands of kilometres separate them from the continent (making it extremely difficult to visualise the results clearly).

The country occupies a total inland area of 92 090 km^2, divided into 18 districts, and a North–Atlantic EEZ of 327 667 km^2, as seen in Figure 4.1(b). Portugal is essentially characterised by a Mediterranean climate, with a temperate maritime climate in the mainland North–western highlands and mountains and a semi–arid climate in certain parts of the Beja district. It is one of the warmest countries in Europe, with the annual average temperatures varying from 10–18 °C, depending on the region. Annual average rainfall in the mainland varies from just over 3200 mm in Vila Real to less than 500 mm in southern parts of Beja. At the same time, snowfalls occur regularly during the winter in the interior North and Centre zones, particularly in the mountains. Finally, continental Portugal has around 2300 to 3200 hours of sunshine a year, averaging up to 10–12 h in the summer, with higher values in the south–east and south–west regions and the coast of Algarve.

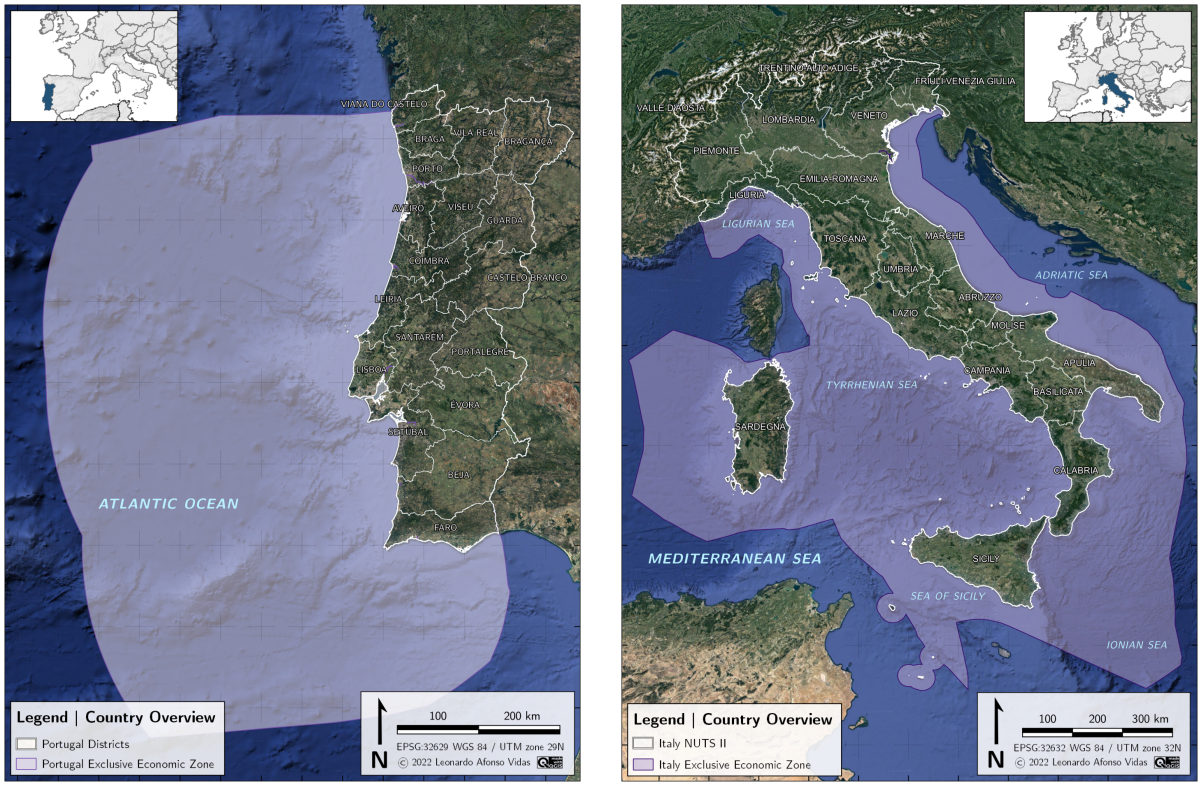

(a) Portugal (b) Italy

Figure 4.1: Study areas: country overview.[1]

[1] Note: in accordance with [78], "This document and any map included herein are without prejudice to the status of or sovereignty over any territory, to the delimitation of international frontiers and boundaries and to the name of any territory, city or area."

Identifying suitable locations for implementing solar parks and wind farms in a given geographic region includes several steps and compromises. Some related works [9, 12, 79] integrate multi–criteria decision–making methods (Analytical Hierarchy/Network Processes, Ordered Weighted Averaging, Technique for Order Preference by Similarity to Ideal Solution, etc.) to access the weight preferences and impacts of such compromises, namely through public surveys and expert interviews. To the contrary, others [80] choose not to and instead consider an equal–weight distribution for all criteria. Since expert elicitation studies and surveys to the public are out of the scope of this thesis, an equal–weight analysis is performed.

The present work methodology is divided into three phases, using a combination of procedures retrieved from the international literature. The first stage is collecting and handling the data, as described in the following section; this comprises creating a specific GIS database serving as a generation tool for distinct theme layers. The second stage consists of excluding incompatible areas according to selected criteria and surface area restrictions; these are identified considering a set of environmental, legislative, safety and technical constraints, elaborated in Section 4.3. The overlapping rejection of such constraints leads to the admissible areas, further evaluated in the third and last stage, detailed in Section 4.4. From the evaluation phase emerges the set of final eligible locations that are used as a mask to get the material values of the simulation, as explained in Section 4.5. This procedure is conducted on QGIS [81], the leading open–source desktop GIS software.

4.2 Data Collection and Handling

A geographical framework begins with establishing its coordinate reference system (CRS). This process is required to avoid angular, length or area distortions on the imported data, enabling precise algebraic computation of acceptable regions and the creation of buffer zones. The native geographic coordinate reference system of QGIS is the World Geodetic System 1984 (commonly referred to as WGS 84). Upon projection to the Universal Transverse Mercator (UTM) CRS, latitudes, longitudes and degrees are respectively converted to northing values, easting values, and distances [82]. Since map projections never represent the sphericity of the Earth exactly, the appropriate UTM zone should be used as CRS for each area of interest to minimise distortion and get correct analysis results. A summary of the aforementioned is presented in Table 4.1.

Table 4.1: Coordinate reference system of each study area.

Study Area	**Geodetic CRS**	**Projected CRS**	**Public Registry**	**Ref.**
Italy	WGS 84	UTM zone 32N	EPSG:32632	[83]
Portugal	WGS 84	UTM zone 29N	EPSG:32629	[84]

Once the coordinate reference system is set up, both raster and vector datasets are imported from a multitude of sources, summarised in Table 4.2. Raster files convey geospatial data as an image, with a specific extent and a pixel resolution; each of these pixels encompasses a unique value that defines a property of its respective location. Vector datasets, on the other hand, supply information as a compilation of features and their related attributes; each feature is given by a geometry that may be a point, a line, or a polygon [85].

Table 4.2: Data collection: source and format of the data layers.

Source	Data layer	Format	Source	Data layer	Format
[86]	Countries in Europe	Polygon vector	[87]	Boundary of Italy	Polygon vector
[88]	Europe hillshade	DEM[1] raster	[89]	Italy regions	
[90]	Countries in Africa	Polygon vector	[91]	Italy EEZ	
[88]	North–Africa hillshade	DEM raster	[92]	Boundary of Portugal	
[93]	Mediterranean Sea	Polygon vector	[89]	Portugal regions	
[94]	Mediterranean bathymetry	DEM raster	[91]	Portugal EEZ	

[1] Digital elevation model.

These create a work structure on which additional datasets are superimposed, enabling the exclusion and evaluation phases of the methodology. Nonetheless, the datasets described in the following sections need refinement to improve the processing time. While some software exists that has this data–handling capability already integrated into its code [95], an intrinsic methodological process was developed for this work.

The proper land–eligibility operation starts with setting the working resolution. Both countries have thousands of square kilometres in area, whilst some polygons of the datasets have just a few square meters; so, even with the data divided into regions, this would mean evaluating several million points each time an operation is made—resulting in extra hours of wasted time. For simplicity's sake, yet without compromising the good accuracy of results, a general resolution was defined as 1 km^2. Higher resolutions were found to bring no benefit to country–scale analysis; furthermore, some of the raster files also do not have higher resolutions, thus eventually leading to wasted computational effort if a more refined mesh was chosen.

All the steps described below are performed in a batch sequence for every dataset, and the respective QGIS functions are described in Appendix D. In general, the first procedure is to add geometry attributes to each layer (area and perimeter of the polygons or length of the lines); then, a minimum threshold is applied, the values below which are selected and deleted—in this case, an area smaller than 1 km^2 or a length less than 1 km. This process eliminates several tiny polygons and lines that would otherwise be requesting computing power unnecessarily, considering they are smaller than the set resolution. Secondly, most holes left within the layers are erased after applying the same area limit. Finally, a merge and dissolve processing tool is used to aggregate all layers that overlap but are not unified. It is often needed to correct some geometries before applying further processing, as well as create spatial indexes that increase the performance of the operations. After these procedures, every exclusion criterion is categorised into its respective group, and an appropriate buffer is applied, following the method described in the next section.

4.3 Data Exclusion

The second stage of the methodology consists of the actual exclusion of unsuitable sites for the installation of RES. This operation starts with setting a buffer over the constraints previously categorised into four main restriction criteria—environmental, legislative, safety and technical. This distribution follows the ones found in literature [80, 85] and comprises restraints related to the conservation of habitats, broad safeguard distance from buildings, airports, roads, railways and shipping routes, as well as pipelines, power lines and other cables.

4.3.1 Environmental Criteria

Any environmental criterion is generally characterised by zones of recognised natural and ecological value and beauty, where the viability and conservation of biodiversity are ensured through legislation. These include, but are not restricted to, forests, parks and beaches, classified as 'Natural Areas', natural or artificial large lakes and glaciers (as 'Bodies of Water'), and residential, commercial or industrial areas and agricultural fields as general 'Land–Use'. Offshore nature conservation sites may include the Natura 2000 Network—Special Protection Areas, Sites of Community Importance and Special Areas of Conservation—, the Common Database on Designated Areas, the *Posidonia Oceanica* meadows and other seabed habitats and biotopes. The aforesaid information is summarised in Table 4.3, while the results are presented in Figure 4.2.

Table 4.3: Summary of environmental constraints.

	Source	Data layer	Format	Buffer (m)	Ref.
Onshore	[96]	Natural Areas	Polygon vector	1000	[85]
	[92]	Bodies of Water		200	
	[97]	Land–Use		0	
Offshore	[98]	Broad–scale Seabed Habitats	Polygon vector	0	[12, 98]
	[99]	Word Database on Protected Areas			[12, 99]
	[98]	*Posidonia Oceanica* meadows			[12, 98]
	[99]	Natura 2000 (SPA, SCI, SAC)			[12, 99]
	[99]	CDDA Protected Areas			[12, 99]

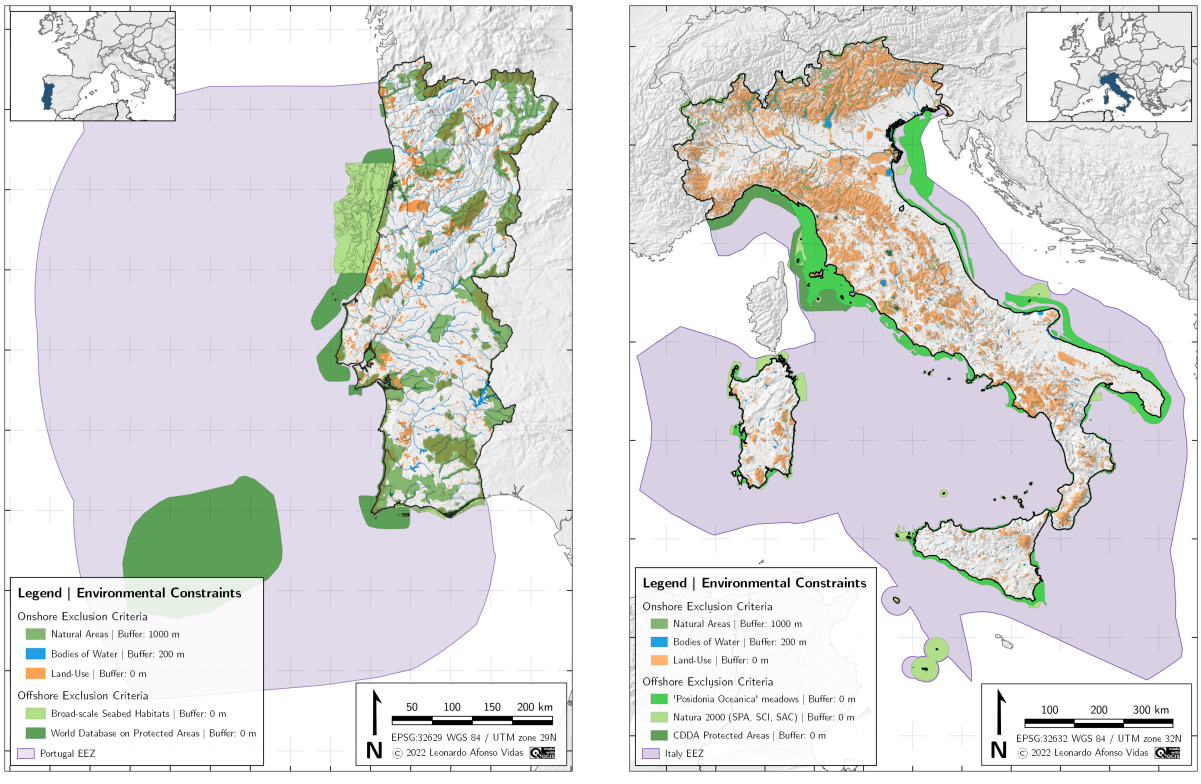

(a) Portugal (b) Italy

Figure 4.2: Exclusion analysis: environmental constraints.

4.3.2 Legislative Criteria

A legislative criterion is provided by law and intends to define acceptable regions through a safe distance from terrestrial and maritime infrastructure. This analysis divides terrestrial infrastructure into 'Transport Facilities' and 'General Buildings'. While the former comprises ferry terminals, train platforms and bus stations, the latter includes all major public infrastructure, residential and commercial buildings, leisure and business establishments, rural areas and places of worship. Regarding offshore locations, the safe distance to 'Fishing Areas' and 'Island Settlements' is typically absorbed by the broad 'Shore' buffer. This distance is the advisable radius to abide by the law and compensate costs, considering the increasing route expenses to and from the offshore location as it moves away from the coast [100].

Table 4.4 summarises this information and Figure 4.3 shows the resulting outcome.

Table 4.4: Summary of legislative constraints.

	Source	Data layer	Format	Buffer (m)	Ref.
Onshore	[97]	Transport Facilities	Polygon vector	5000	[85]
	[97]	General Buildings	Polygon vector	500	[85]
Offshore	—	Shore	Virtual Polygon	*	[100]
	[99]	Fishing Areas	Polygon vector	1852	[12]
	[98]	Island Settlements	Polygon vector	1500	[12]

* Distance to shore below one or above 50 nautical miles.

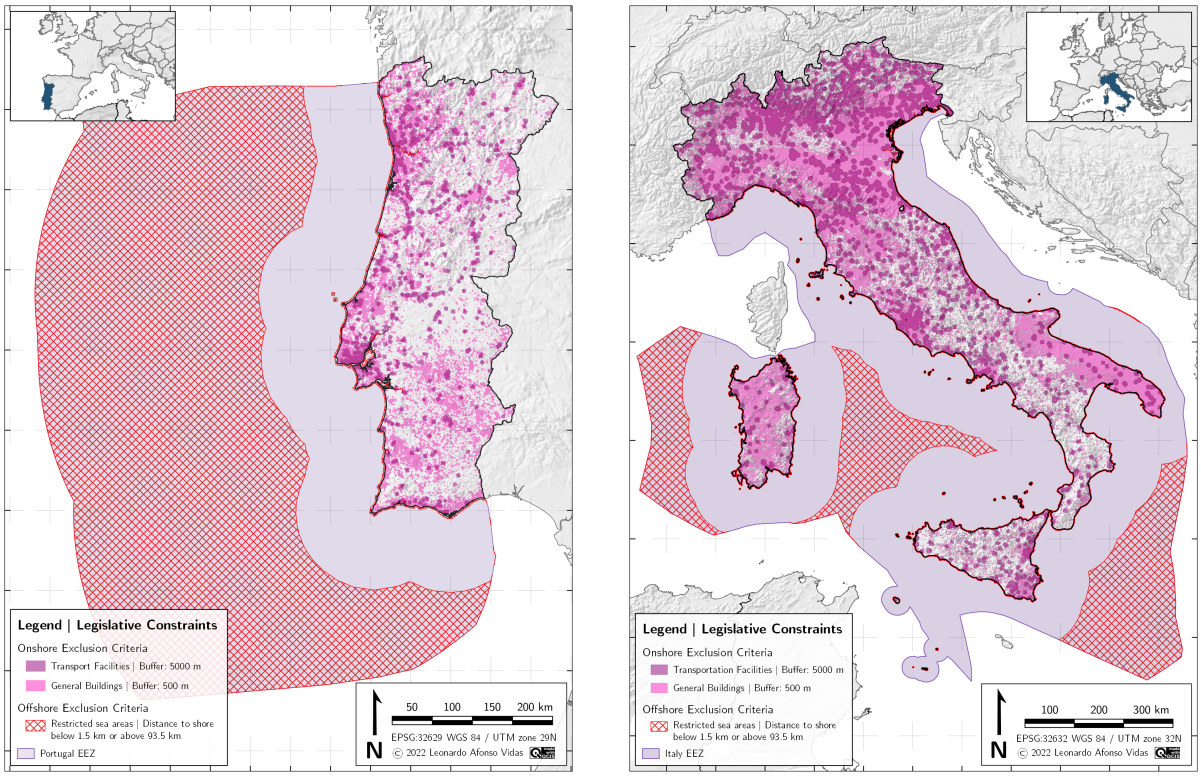

(a) Portugal (b) Italy

Figure 4.3: Exclusion analysis: legislative constraints.

4.3.3 Safety Criteria

Safety criteria encompass those related to the safe operation of transport activities, whether on land (rail or road), air or sea. 'Railways' include operational regular and light tracks for trains, subways and trams, while 'Major Roads' combine highways and primary national roads; these are considered to decrease possible visual and auditory disruptions (such as glare from PV panels and noise from wind turbines). Regarding 'Airports', a buffer zone of 3000 m from all major international airports is selected to avoid potential collisions with aircraft and to reduce the possible interference with radar systems. 'Shipping Routes' comprise a 0.5 nautical miles buffer from cargo, tanker, fishing and passenger routes above 1000 units per square kilometre in one year. The individual route density of each country is presented in Appendix E.

Table 4.5 is a brief review of these constraints—the result of which is shown in Figure 4.4.

Table 4.5: Summary of safety constraints.

	Source	Data layer	Format	Buffer (m)	Ref.
Onshore	[92, 97]	Railways	Line vector	50	[85]
	[92, 97]	Major Roads	Line vector	50	[85]
Offshore	[97]	Airports	Point vector	3000	[12]
	[99]	Shipping Routes	Polygon vector	926	[101]

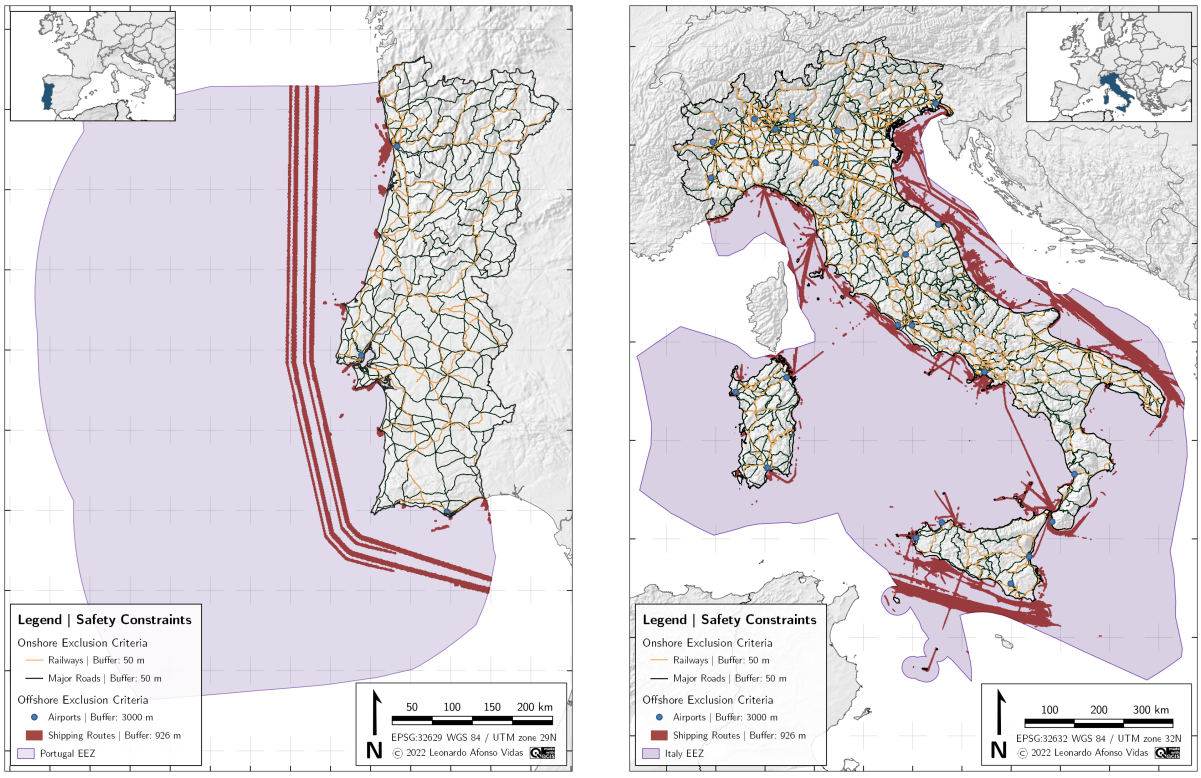

(a) Portugal (b) Italy

Figure 4.4: Exclusion analysis: safety constraints.

4.3.4 Technical Criteria

Finally, a technical criterion regards fixed infrastructure that has already been deployed in a potentially admissible area. For instance, 'Pipelines' include the main oil and gas large–pipe network, underground or above ground. 'Powerlines' consist of the electric transmission grid, from Very–High Voltage to High Voltage (excluding the Medium/Low Voltage distribution grid), and submarine energy interconnections. Concerning offshore exclusions, 'Telecom Cables' and 'SHOM Underwater Cables' (from the French *Service Hydrographique et Océanographique de la Marine*) refer to telecommunication lines and internet optical fibres, while both 'Wind Farms' and 'Oil and Gas Platforms' involve groundwork around which no other activities are permitted. Table 4.6 outlines this information and Figure 4.5 presents the results.

Table 4.6: Summary of safety constraints.

	Source	Data layer	Format	Buffer (m)	Ref.
Onshore	[102, 103]	Pipelines	Line vector	100	[85]
	[102, 104]	Powerlines	Line vector	150	[85]
Offshore	[99]	Existing Wind Farms	Point vector	1000	[105]
	[99]	Oil and Gas Platforms	Polygon vector	500	[106]
	[107]	SHOM Underwater Cables	Line vector	500	[108]
	[107]	Telecom Cables	Line vector	500	[108]

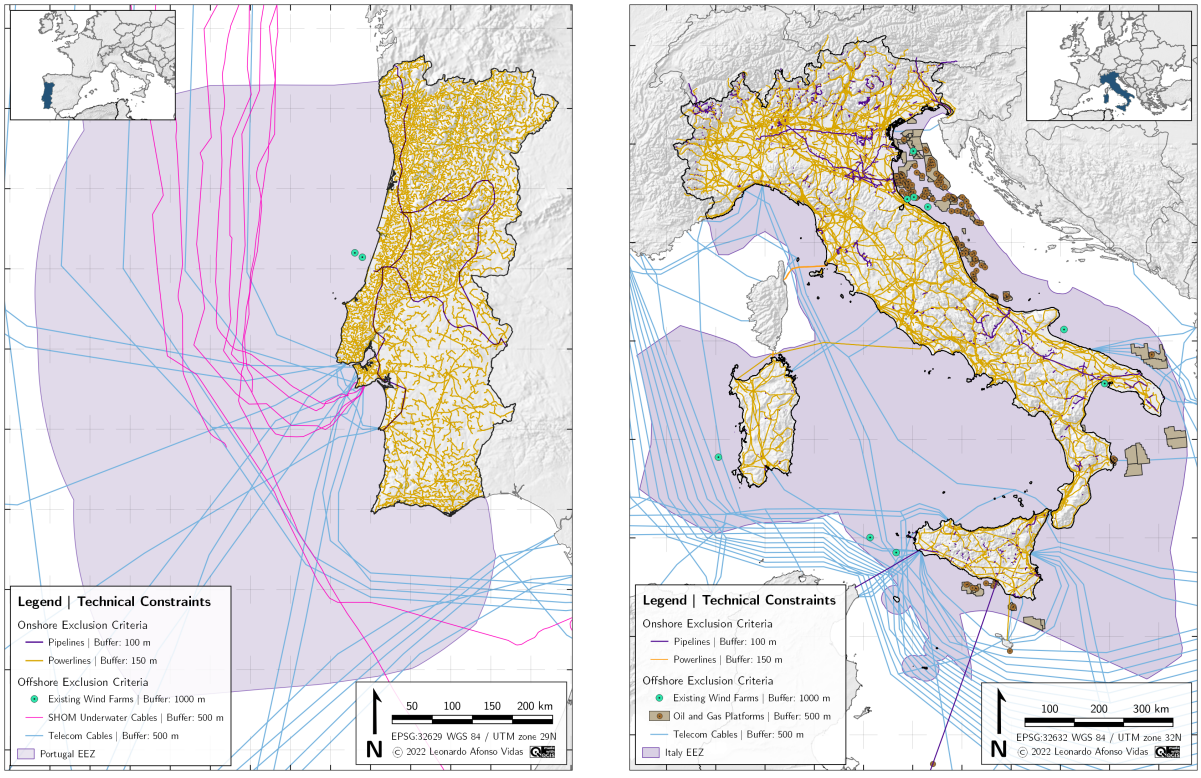

(a) Portugal (b) Italy

Figure 4.5: Exclusion analysis: technical constraints.

4.4 Data Evaluation

Following the creation of acceptable areas through data exclusion, the last step of the methodology consists of their evaluation through characteristic criteria. These parameters concern region–specific physical attributes, on which limits are imposed to maximise energy production. Criteria such as elevation, slope, temperature, bathymetry and wind speed are evaluated to generate new acceptable areas that further overlapped with the previous ones, yielding the eligible locations analysed in the subsequent section.

4.4.1 Ground Elevation

Mean elevation is included in this analysis on the premise that RES suitability decreases at extreme altitudes, mainly due to diminishing resources (like lower air density or increased cloud coverage) and increased inaccessibility, leading to higher installation costs. The exclusion threshold is set to 2000 meters, following the literature review by D. Rayberg [85]. Since the highest peak in continental Portugal is only 1993 meters, no elevation restrictions exist in that country. Table 4.7 outlines the sources of the digital elevation model raster files and Figure 4.6 shows the results.

Table 4.7: Outline of elevation data evaluation.

Source	Data layer	Exclusion threshold	Ref.
[109]	Italy DEM	Above 2000 m	[85]
[96]	Portugal DEM		

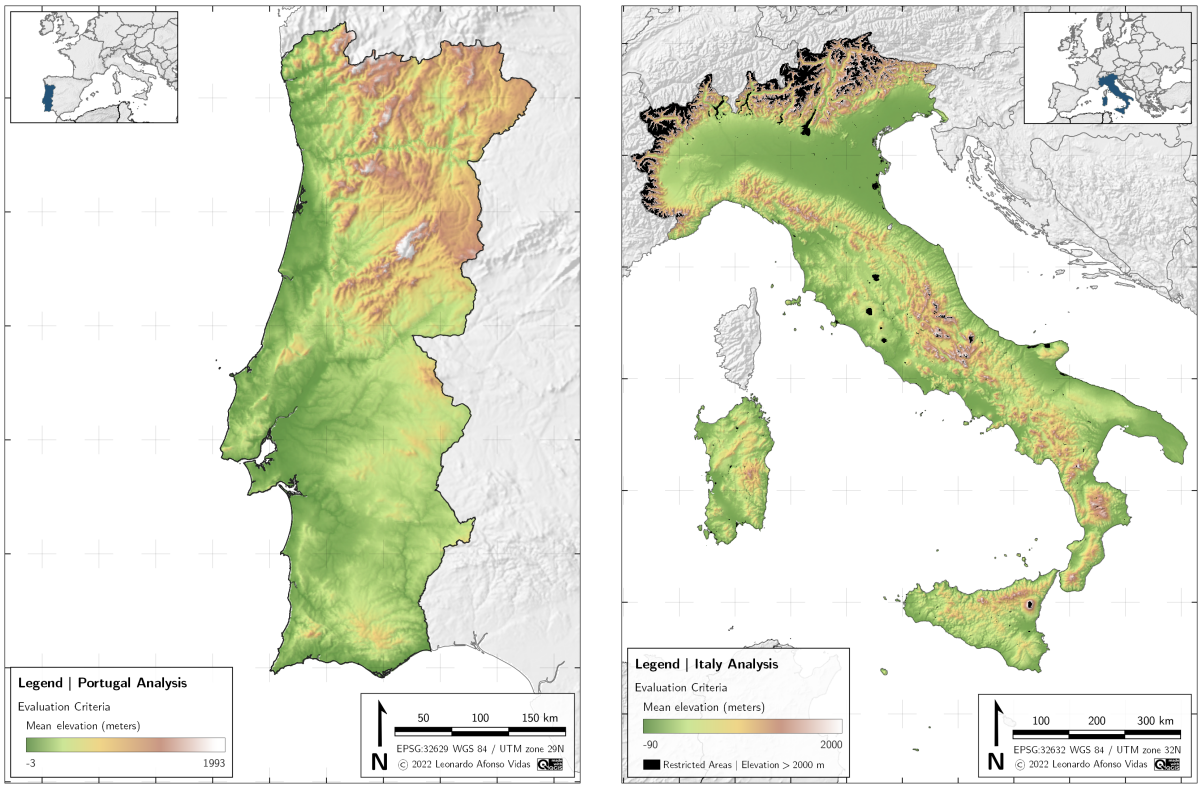

(a) Portugal (b) Italy

Figure 4.6: Evaluation analysis: elevation criteria.

4.4.2 Terrain Slope

The average terrain slope is an essential physical criterion on pair with elevation; in this work, it is used to evaluate the terrain's angle and orientation. Slopes not facing between southwest and southeast can be excluded from photovoltaic siting analysis, although that not being the case here. Most studies in the literature [85] typically set a threshold on average terrain slopes above 10° since steeper topographies are found to cause problematic installation of solar panels and wind turbines. Note that this attribute should not be confused with the tilt of the solar modules; generally, fixed panels are installed with a tilt angle approximately equal to the latitude of the place where they are located. This method is simple and cheap but not the most efficient—new solutions can now continuously track the sun's relative position and optimise the tilt angle accordingly using deep learning (increasing the solar output power up to 10%) [110].

The mean slope dataset and its derived topographic continuous variables are collected based on the works of G. Amatulli et al. [111] and presented in Table 4.8. Figure 4.7 shows the results of this evaluation criteria.

Table 4.8: Outline of slope data evaluation.

Source	Data layer	Exclusion threshold	Ref.
[112]	Italy slope raster	Above 10°	[85]
[96]	Portugal slope raster		

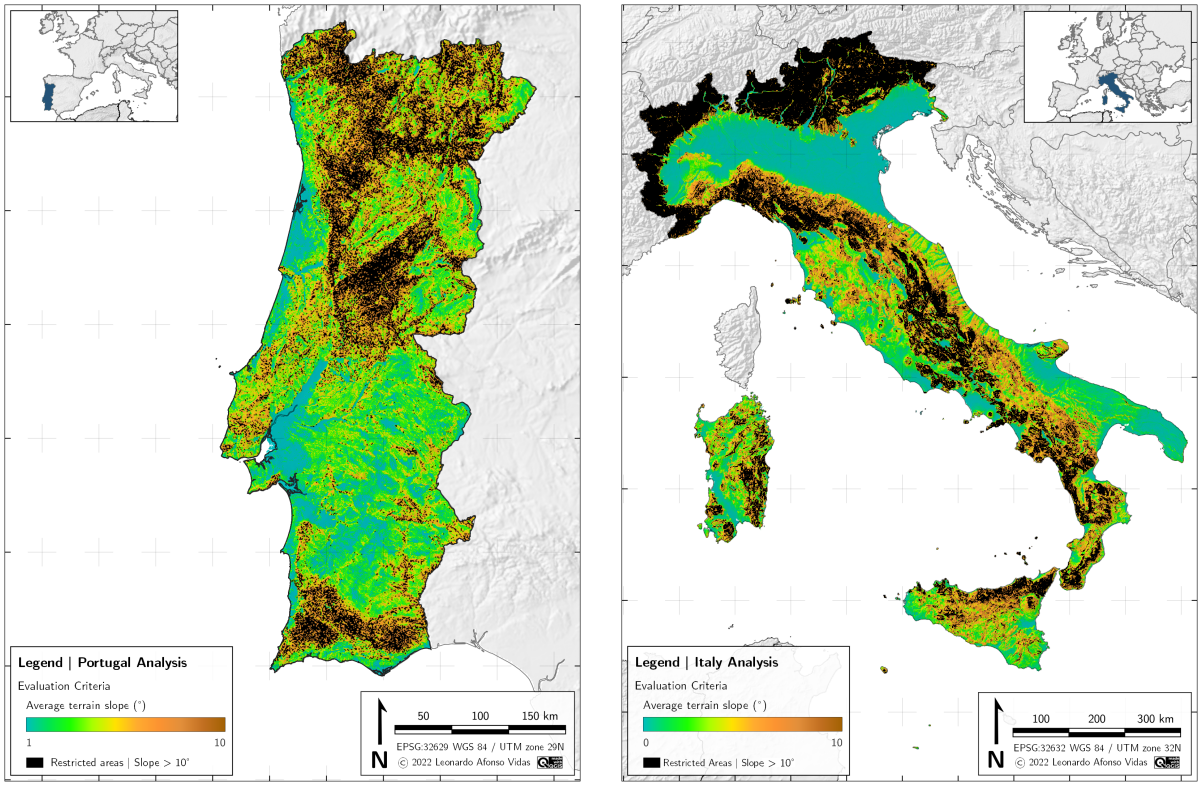

(a) Portugal (b) Italy

Figure 4.7: Evaluation analysis: slope criteria.

4.4.3 Air Temperature

The impact of temperature on the performance of photovoltaic modules is a well–known phenomenon in which increasing air temperature leads to a decrease of the module's voltage output. Typically, manufacturers define the nominal peak power of a solar panel at 25 °C (module temperature), but this temperature can vary significantly during operation. Several simplified relations exist that linearly correlate the module's temperature with air temperature, solar irradiance and the normal operating cell temperature of the module. The panels used in this work require air temperatures between –10 °C and 50 °C for regular operation.

Besides, warmer air is less dense than cold air; so in hotter locations, there is a decrease in the turbine's electricity yield since there is a lower energy extraction from the wind. Consequently, in this analysis, cooler air is always preferred for renewable electricity generation.

Table 4.9 provides the sources and references of the temperature data layers of both countries. Figure 4.8 offers a view of the air temperature at two meters above ground level, as a long–term (diurnal) annual average of the past 25 years [113].

Table 4.9: Outline of temperature data evaluation.

Source	Data layer	Exclusion threshold	Ref.
[114]	Italy temperature raster	$<$–10 °C $\vee$ $>$50 °C	[115]
[116]	Portugal temperature raster		

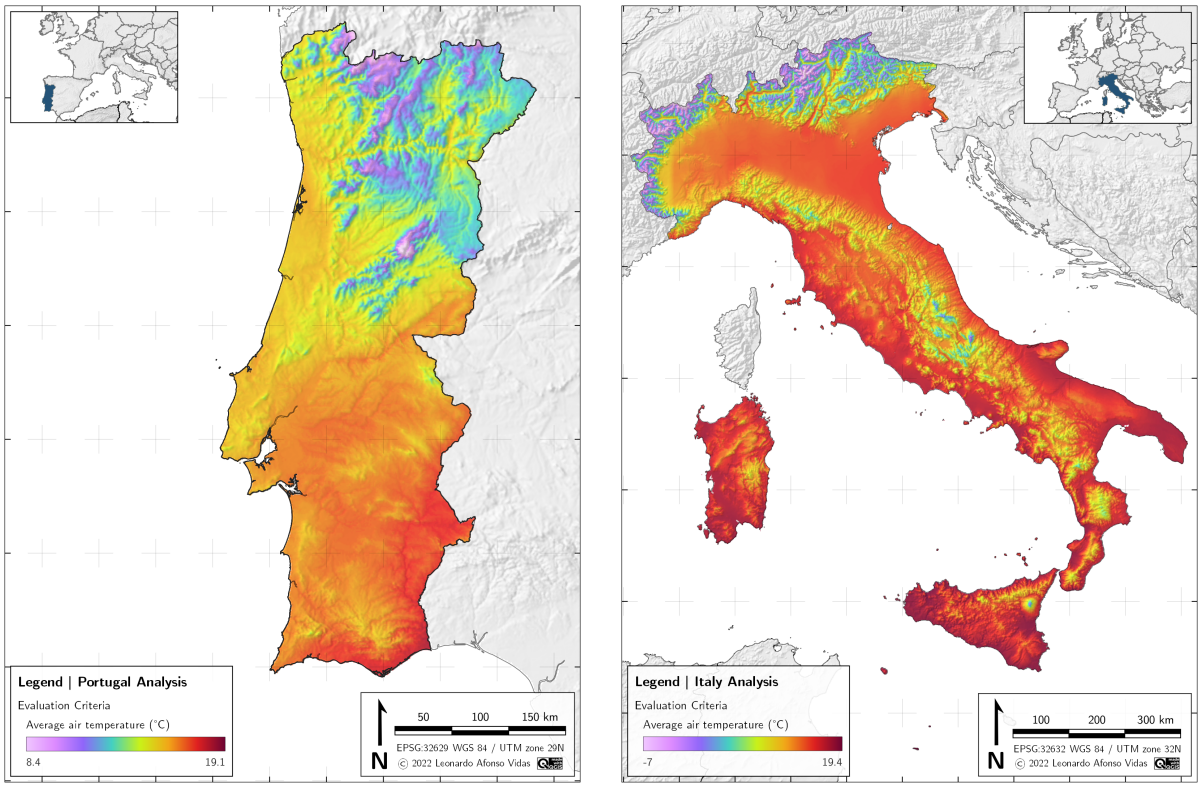

(a) Portugal (b) Italy

Figure 4.8: Evaluation analysis: air temperature criteria.

4.4.4 Seafloor Bathymetry

Bathymetry describes depth variations in the ocean's seabed (analogous to submarine orography). Water depth is a crucial criterion for assessing the siting of offshore wind farms since, typically, these require less than 50 meters of water depth for fixed foundation turbines. On the other hand, floating wind technologies are currently estimated to be economically feasible for water depth down to 1000 meters, mainly due to the mooring, anchorage and cabling works used. This analysis follows the recommendation of Global Wind Atlas [44], which also corroborates most of the published studies consulted in the literature [9, 12, 80].
Table 4.10 gives an overview of the sources and references of the bathymetry layers used for both countries, concerning both technologies. Figure 4.9 presents the restricted seafloor bathymetry of Portugal and Italy.

Table 4.10: Outline of bathymetry data evaluation.

Source	Data layer	Technology	Exclusion threshold	Ref.
[117]	Italy bathymetry raster	Fixed foundation	Below –50 m	[44]
		Floating structure	Below –1000 m	
[118]	Portugal bathymetry raster	Fixed foundation	Below –50 m	
		Floating structure	Below –1000 m	

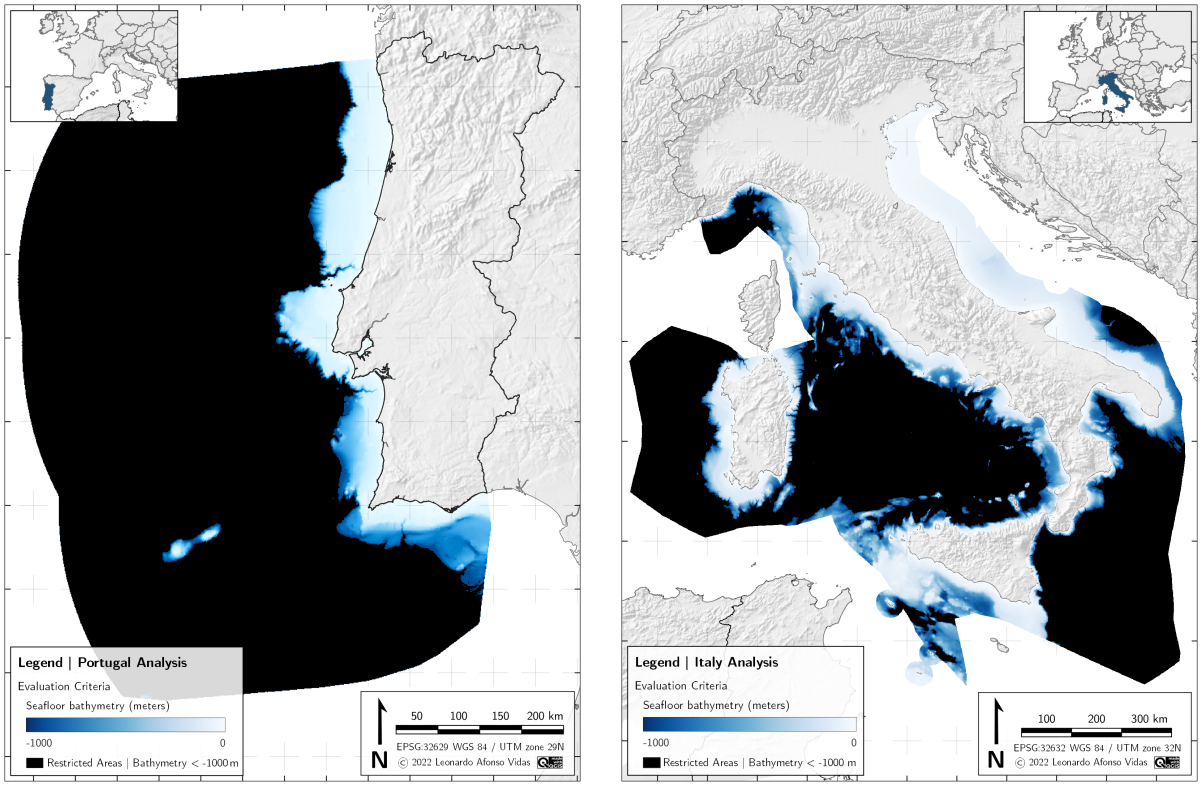

(a) Portugal (b) Italy

Figure 4.9: Evaluation analysis: seafloor bathymetry criteria.

4.4.5 Wind Speed

Mean wind speed is one of the primary ways to measure wind energy resources. In general, the wind velocity profile in the atmosphere increases with height, which is why turbines have steadily become taller and taller over the years. At greater heights is also where the air is less dense, which in turn causes diminishing energy resources since the power of a wind–stream is directly proportional to air density. However, it varies to the cube of wind velocity, so essentially, higher wind speeds correspond to higher energy availability.

Average wind speeds are commonly measured from meteorological observations at 10 metres above ground level and then converted to the desired rotor height. Turbine manufacturers determine cut–in and cut–out speeds at those heights to protect the turbine from damage, usually fixating them between 3 m/s and 25 m/s [119]. These limits are also applied in this analysis, serving as an evaluation criterion.

Table 4.11 gives an outline of wind speed layers fetched of both countries, while Figure 4.10 gives the results after applying the mean wind speed evaluation criterion.

Table 4.11: Outline of wind speed data evaluation.

Source	Data layer	Exclusion threshold	Ref.
[120]	Italy wind speed raster	<3 m/s $\vee$ >25 m/s	[119]
[121]	Portugal wind speed raster		

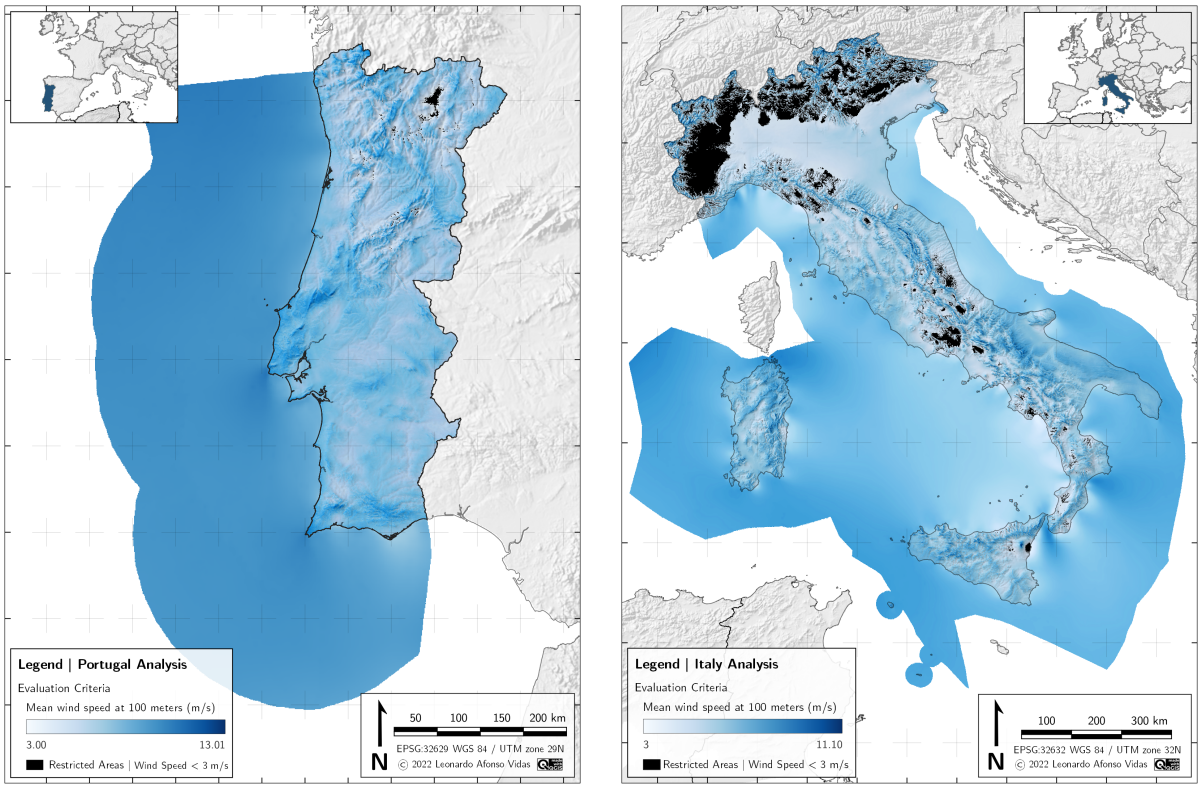

(a) Portugal (b) Italy

Figure 4.10: Evaluation analysis: wind speed criteria.

4.5 Eligible Locations

With the exclusion and evaluation criteria perfectly defined, their respective restricted zones are merged to create a layer of 'incompatible locations'. These locations represent the current regions in each country where it is not possible to install a RES system dedicated to green hydrogen production—either because the land is already occupied by other socioeconomic activities or is buffered (according to the rules applied in the preceding sections).

Afterwards, a geometric subtraction of these polygons is executed from the country's total surface, creating the data layer of the 'eligible locations'. Contrary to the previous ones, these are the available suitable areas for developing green hydrogen projects today—constituting one of the objective deliverables of this thesis. Figure 4.11 illustrates the aforementioned information, depicting both countries in a bicolour way of either *eligible* (in blue) or *incompatible* (in red) locations.

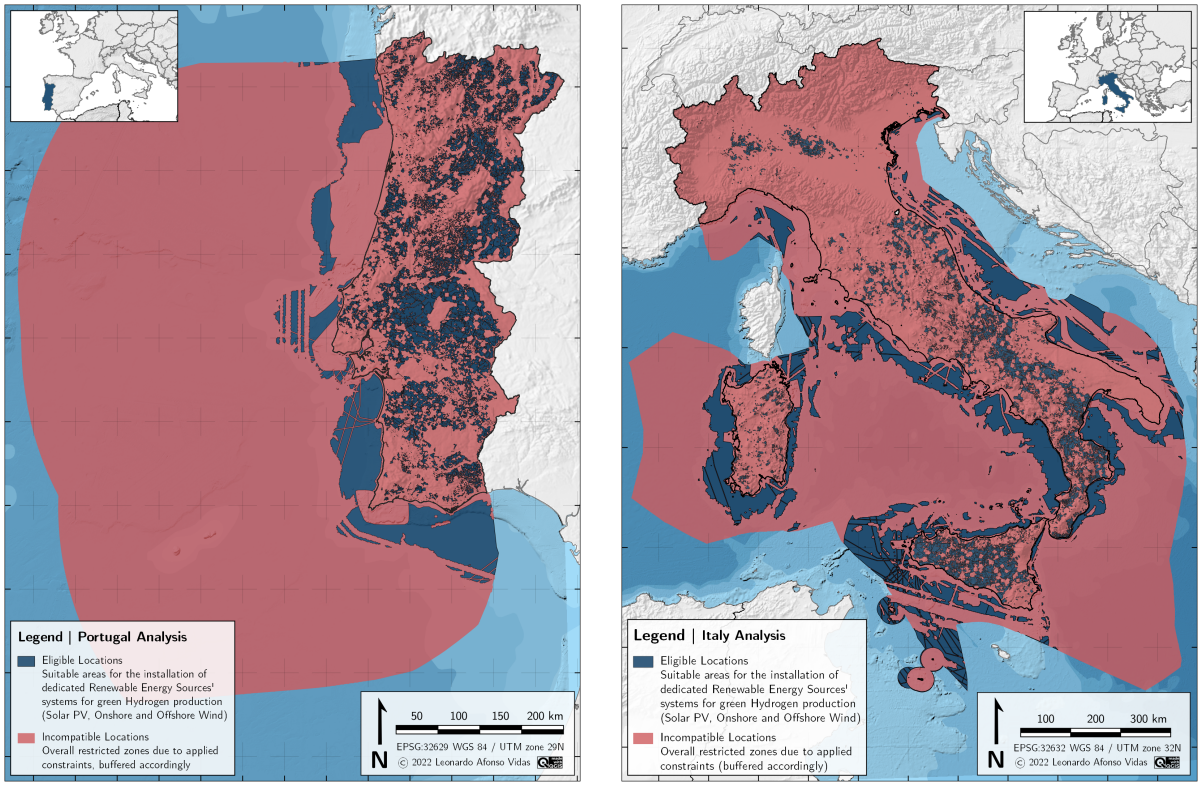

(a) Portugal (b) Italy

Figure 4.11: Country analysis: total eligible locations.

To better assess the visual results of these maps, the available area and the respective percentage fraction of the total area (onshore and offshore) of both countries are computed and displayed in Table 4.12.

Table 4.12: Summary of the results for eligible locations.

	Total Area (km^2)		**Available Area (km^2)**		**Fraction (%)**	
	Onshore	Offshore	Onshore	Offshore	Onshore	Offshore
Italy	300 979	536 654	37 637	104 338	12.50	19.44
Portugal	89 015	315 598	24 734	22 495	27.79	7.13

As expected, most of the total area in Italy and Portugal is already occupied. However, in any case of country–wide analysis, small fractions of available land may correspond to large surface areas in absolute terms—which is the case here. The regions available for installing renewable energy projects have a massive potential to shift the energy mix of both countries.

It is also relevant to look at the distribution of technologies across the available area. From the outset, regions onshore have no restriction that prevents the placement of photovoltaic solar parks or wind turbine farms in a given location. On the other hand, regions offshore have strict rules that differentiate between areas suitable for fixed foundation turbines or floating turbines, as explained in Section 4.4.4. Figure 4.12 presents the maritime zones of each country where bathymetry limits the installation of offshore wind farms.

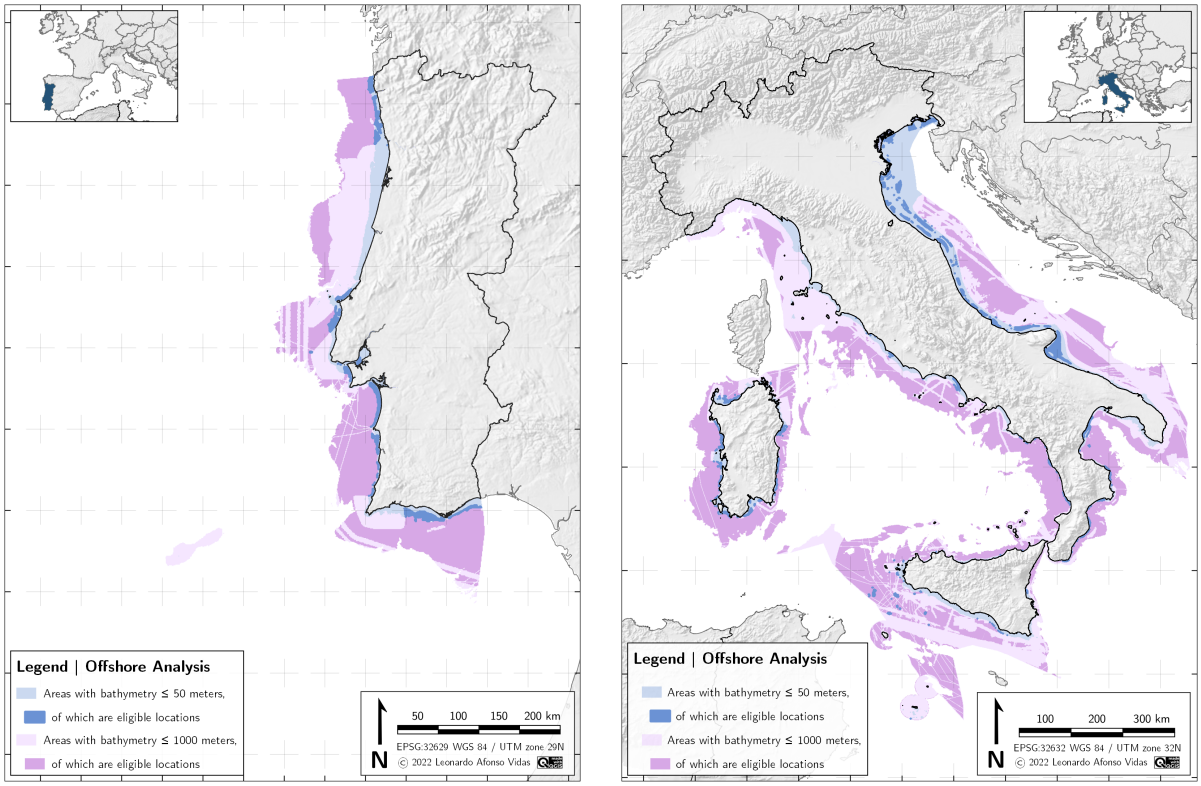

(a) Portugal (b) Italy

Figure 4.12: Country analysis: offshore eligible locations.

Besides being a much larger country, Italy has more of its land bordered by the sea, whereas Spain completely borders continental Portugal to the North and East. This explains why the fraction of available offshore land is more than double from one country to the other.

This process ends the design of the geographical model. Each of the points yielded by the model is a potential eligible location for the installation of a green hydrogen project, whose economic viability is assessed in the following chapter.

5 Numerical Model Layout

Every economic assessment requires the development of a numerical model that computes the outcome predictions from the input data. This chapter minutely describes the development of the two numerical models used in this economic analysis. Section 5.1 first addresses the calculation of both the levelised cost of hydrogen and the levelised cost of electricity (LCOE)—a sub–component of the former—for each one of the four renewable energy sources. Section 5.2 then takes these calculations and employs them into a generalised model to be applied to the whole set of locations of both countries. Finally, Section 5.3 improves on the generalised model and describes the entire development of a specific optimisation model.

5.1 Hydrogen Economic Fairways

In this work, the pathway to define the economic viability of the hydrogen projects is based on the method recently employed by S. Walsh et al. [122]. He and his team performed a study using the Bluecap software and the Hydrogen Economic Fairways Tool, hosted on Geoscience Australia's portal [123]. Likewise, this analysis applies a sub–model developed in Microsoft Excel, which considers all the distinct parameters essential to compute the cost of hydrogen production in the eligible locations obtained in the previous chapter.
The following subsection delves into the specifics of calculating the LCOH, depending on the RES associated with the project; however, there are two general and independent parameters, which are the same for the four calculations: the project lifetime and the inflation rate.

The lifetime of these projects is assumed to be 30 years. This choice reflects the IEA PVPS Task 12 recommendation for life cycle assessment studies and matches the quality of current solar photovoltaic systems [29]. Wind turbine projects have traditionally shorter technical lifetimes (around 20 years). However, since more and more studies are presently looking at turbine life span extension strategies [38, 124], the applied system lifetime is the same. In any case, the operational period of RES projects is expected to increase henceforth [29].

Inflation rates have been changing dramatically for the past decades, reaching an all–time high of 8.90% in July 2022 [125]. Nevertheless, in accordance with E. Vartiainen et al. [29], an inflation rate of 2% is considered the recent historical average of the Eurozone—and thus is used in this analysis. This decision is crucial because it impacts the difference between the nominal and real weighted average cost of capital (WACC). Most projects use this metric as a proxy for the discount rate since it refers to the required return rate to make an investment worthwhile. Inspecting the actual WACC formula means going too much in–depth into financing theory (and out of the scope of this thesis).

In such manner, this work makes only a distinction between nominal and real WACC: the former accounts for inflation, and the latter does not. This contrast is decisive because expenditures happen throughout a project's lifetime (being subjected to each year's inflation rate), while the utility–scale generated electricity locks energy 'costs' at a constant initial rate, hence avoiding the regular fluctuation of inflation rates. Equation 5.1 shows the Fisher equation, with which these values can be computed (following Bjarne Steffen's [126] method).

$$1 + \mathtt{w}_{\mathtt{nom}} = (1 + \mathtt{w})(1 + \mathtt{i}) \tag{5.1}$$

where:

$\mathtt{w}_{\mathtt{nom}}$ is the nominal WACC.

$\mathtt{w}$ is the real WACC.

$\mathtt{i}$ is the inflation rate.

5.1.1 Levelised Cost of Hydrogen

The levelised cost of hydrogen is a benchmark commonly used to determine the feasibility of a hydrogen project. Above all, it measures the cost of producing one unit of hydrogen during the lifetime of the project. Equation 5.2 presents the generalised formulation used in this thesis.

$$\mathtt{LCOH}^{(*)} = \frac{\mathtt{K}_{\mathtt{RES}} + \mathtt{K}_{\mathtt{H_2}}}{\mathtt{Y}_{\mathtt{H_2}}} \tag{5.2}$$

Note: $^{(*)}$ is replaced according to the RES associated with the calculation: **(pv)** for solar photovoltaic parks, **(wd)** for onshore wind farms, **(fx)** for offshore fixed wind farms or **(ft)** for offshore floating wind farms.

where:

$\mathtt{K}_{\mathtt{RES}}$ is the overall cost structure of the RES power plant, in EUR.

$\mathtt{K}_{\mathtt{H_2}}$ is the overall cost structure of the electrolyser, in EUR.

$\mathtt{Y}_{\mathtt{H_2}}$ is the global hydrogen yield, in kg.

The generalised formulation has many sub–components aggregated into progressively broader concepts. These concepts are explored in the following equations, based on the works of M. Minutillo et al. [72], L. Viktorsson et al. [127] and T. A. Gunawan et al. [128]. Equation 5.3 develops the formulation of $\mathtt{K}_{\mathtt{RES}}$.

$$\mathtt{K}_{\mathtt{RES}} = \left[\mathtt{I}_0 + \sum_{\mathtt{n}=1}^{\mathtt{N}} \left(\frac{\mathtt{O}_{\mathtt{K}}}{(1 + \mathtt{w}_{\mathtt{nom}})^{\mathtt{n}}} \right) - \frac{\Delta_{\mathtt{N}}}{(1 + \mathtt{w}_{\mathtt{nom}})^{\mathtt{N}}} \right] \times \mathtt{P}_{\mathtt{RES}} \tag{5.3}$$

where:

$\mathtt{N}$ is the economic lifetime of the system, in years (assumed to be 30).

$\mathtt{n}$ is the year number, ranging from 1 to $\mathtt{N}$.

$\mathtt{I}_0$ is the total capital expenditure of the system, made at $\mathtt{n} = 0$, in EUR/kW.

$\mathtt{O}_{\mathtt{K}}$ is the total all–in expected operational cost of the system, at any given year, in EUR/kW/yr.

$\Delta_{\mathtt{N}}$ is the decommission value of the system, at year N, in EUR/kW (assumed to be zero).

$\mathtt{w}_{\mathtt{nom}}$ is the nominal WACC, in percentage.

$\mathtt{P}_{\mathtt{RES}}$ is the installed capacity of the RES power plant, in kW.

The decommission value of the system at the end of the project's life includes the decommission expenditures (DecEx) of dismantling the hardware, removing the infrastructure and cleaning the area, as well as the end–of–life salvage value of the components (second–hand sales of modules or turbines, and recycling parts). Since there is still no agreed price for such elements [29], the decommission value is here defined to be zero: $\Delta_N = 0$. Nevertheless, this parcel is still relevant to add to the equation because typically, the residual value of a dismantled PV/wind system is positive [129, 130]—and so, if there is any inaccuracy in this formulation, is of an overestimation error, not underestimation (i.e. the final LCOH may be even lower than what is presented).

The total capital expenditure of the RES system includes both hardware and non–hardware components costs, installation or balance of system costs, and soft costs, according to the respective CapEx breakdown structure mentioned in Section 3.1. This expense is assumed to be paid in full before the project begins operation, thus not needing to be discounted to the present.

The total all–in operational expenditure of the system consists of both operations and management and services costs (scheduled and unscheduled) and other expenses. It is a fixed annuity, with a different value for each technology, corresponding to the respective OpEx breakdown structure considered in Section 3.1.
As a series of equal annual payments needed to be discounted to the present value, the constant value of O_K leaves the summation, and the remaining term takes the form of an elementary finite geometric series (which has a perfectly defined formula for its sum to the n–th term). Through Equation 5.4, the capital spread factor is so defined as the inverse of the known capital recovery factor.

$$\sum_{n=1}^{N} \frac{1}{(1+w_{nom})^n} = \frac{(1+w_{nom})^N - 1}{w_{nom} \times (1+w_{nom})^N} \;:=\; S_K \tag{5.4}$$

This factor is used in the following subsections as a multiplication element to systematically discount sets of equal annual amounts. Equation 5.5 now further expands the components of K_{H_2} formulation.

$$K_{H_2} = \left[I_0 + \sum_{n=1}^{N} \left(\frac{O_K}{(1+w_{nom})^n} \right) + \sum_{j=1}^{2} \left(\frac{R_{jN/3}}{(1+w_{nom})^{jN/3}} \right) - \frac{\Delta_N}{(1+w_{nom})^N} \right] \times P_{H_2} \tag{5.5}$$

where:

N is the economic lifetime of the system, in years (assumed to be 30).

n is the year number, ranging from 1 to N.

I_0 is the total capital expenditure of the system, made at $n = 0$, in EUR/kW.

O_K is the total all–in operational expenditure of the system, in EUR/kW/yr.

j is the replacement number, with $j = 1, 2$.

$R_{jN/3}$ is the electrolyser replacement cost, happening at years 10 and 20, in EUR/kW.

Δ_N is the decommission value of the system, at year N, in EUR/kW (assumed to be zero).

w_{nom} is the nominal WACC, in percentage.

P_{H_2} is the electrolyser rated power, in kW.

The total capital expenditure of this system covers the electrolyser (the stack, including costs for the distributed control system, energy management unit, engineering, interconnection), all necessary BOS costs (power supply, drier, cooling, de–oxo, water de–ionisation equipment, and civil works—building and foundations), and soft costs, like certifications, commissioning, and start–up costs; all according to the CapEx breakdown structure presented in Subsection 3.2.2. Similarly to its RES equivalent, it is assumed to be paid in full before the project begins operation, thus not needing to be discounted.

The total all–in operational expenditure of the system consists of fixed and variable operations and management costs. Fixed O&M generally includes the electrolyser's maintenance and respective BOS components, service contract costs, a fixed annual cost for water consumption, direct labour, administration/general overheads, and insurance/local taxes. Variable O&M commonly consists of electricity and water consumption costs; since, in this case, the electricity comes directly from the RES coupled to the electrolyser, that term is dropped. So, O_n is also a fixed annuity discounted to the present value, using the S_K factor computed before.

According to the latest report from the UK's Department for Business, Energy and Industrial Strategy [131], replacement expenditures (ReplEx) for PEM electrolysers are around 60% of the initial CapEx and assumed to be needed every 11 years over a 30–year technical lifetime. For this analysis, two 10–year periods of replacement are presumed instead, happening precisely at years 10 and 20: $R_{jN/3} = 0.6 \times I_0$ with $N = 30 \wedge j = 1, 2$.

Similarly to the previous case, and for the sake of consistency, the decommission value of this system is assumed to be zero.

With both parts from the numerator explained, it remains only to describe the denominator component. Equation 5.6 then presents the formulation for the global hydrogen yield.

$$Y_{H_2} = \sum_{n=1}^{N} \left(\frac{\upsilon \times P_{RES} \times (1 - \delta_{RES})^n}{(1 + w)^n} \times \frac{\eta \times \rho \times (1 - \delta_{H_2})^n}{P_{H_2}} \right) \tag{5.6}$$

where:

N is the economic lifetime of the system, in years (assumed to be 30).

n is the year number, ranging from 1 to N.

υ is the annual utilisation factor of the power plant (full load hours), in kWh/kW.

P_{RES} is the installed capacity of the RES power plant, in kW.

δ_{RES} is the annual power degradation of the RES system, in percentage.

η is the all–round efficiency of the system, from the RES output to the stack input, in percentage.

ρ is the net production rate of the electrolyser, in kg/h.

δ_{H_2} is the annual power degradation of the electrolyser, in percentage.

P_{H_2} is the electrolyser rated power, in kW.

w is the real WACC, in percentage.

The annual utilisation factor of a power plant is usually expressed as its full load hours—the time for which the system has to operate at nominal power to generate the same amount of electrical energy as the system actually generates within a year [132]. This concept is extended to electrolysers as their number of FLHs is related to the type of electricity that powers them. For dedicated RES–to–Hydrogen projects such as the ones in this thesis, FLHs are highly dependent on resources' availability and location.

Degradation rates are considered in this calculation in order to present the most accurate results possible. These values differ depending on the RES technology and are further explained below.
Regarding the annual power degradation of the electrolyser, a value of 0.08% per 1000 hours is chosen, based on Gigastack's latest public report [71]. In consistency with the other degradation rates in the model, this term is converted to a yearly value, as follows: $0.08 \times 8760/1000 = 0.7008\%$.

The system's efficiency and the electrolyser's net production rate are obtained from a collection of several examples currently available on the market. Such devices include the M Series from NEL [133], the HyLYZER system from Cummins [134], GenFuel's ecosystem from PlugPower [135] and Siemens Energy's Silyzer [136]. Since none of those mentioned above provides a complete technical datasheet, feature selections reflect on the ones with the most information available. From this group, production rates typically approach 425 kg/day per MW–installed, which leads to $\rho = 0.01771$ kg/h per kilowatt–installed. The all–round efficiency (from the RES output to the stack input) is set to 60%, supported by the preeminent report of the IEA [4].

Similarly to the case of discounted expenses above, hydrogen production is also discounted to the present value. Note that every aforestated variable is independent of the year number, except for the degradation rates. So, applying a similar reasoning to the calculation of the capital spread factor, all constants leave the summation with the remaining term taking the shape of a finite geometric series. Equation 5.4 thus gives the formula for the yield spread factor.

$$\sum_{n=1}^{N} \frac{(1-\delta_{RES})^n \times (1-\delta_{H_2})^n}{(1+w)^n} = \frac{(\delta_{RES}-1)(\delta_{H_2}-1)(1+w)^N\left[(1-\delta_{RES})^N(1-\delta_{H_2})^N-(1+w)^N\right]}{\delta_{RES}\times\delta_{H_2}-\delta_{RES}-\delta_{H_2}-w} := S_Y \quad (5.7)$$

With the general formulation of the levelised cost of hydrogen perfectly defined, a specific equation can be found for every RES technology. Each of the four is detailed below.

LCOH from Solar Photovoltaic Parks

Equation 5.8 provides the LCOH formula for hydrogen projects connected to solar PV parks.

$$LCOH^{(pv)} = \frac{\left[I_0 + O_K \times S_K\right]_{RES} \times P_{RES} + \left[I_0 + O_K \times S_K - \frac{R_{10}}{(1+w_{nom})^{10}} + \frac{R_{20}}{(1+w_{nom})^{20}}\right]_{H_2} \times P_{H_2}}{\upsilon \times P_{RES} \times \eta \times \rho \times S_Y} \quad (5.8)$$

with:

$$S_Y = \frac{(\delta_{pv}-1)(\delta_{H_2}-1)(1+w)^N\left[(1-\delta_{pv})^N(1-\delta_{H_2})^N-(1+w)^N\right]}{\delta_{pv}\times\delta_{H_2}-\delta_{pv}-\delta_{H_2}-w}$$

Regarding the current value of the nominal WACC in OECD countries, B. Steffen [28] provides a reasonable estimation: $w_{nom} = 5.4\%$. The degradation of PV modules is usually divided into a higher first–year degradation rate and a lower lifetime yearly degradation value. Here, a set of conservative values is rounded and used in accordance with the reports from IEA PVPS Task 13 and ITRPV [29]: $\delta_{pv} = 0.45\%$.

LCOH from Onshore Wind Farms

Following the previous rationale, Equation 5.9 now presents the formulation for the cost of producing hydrogen with electrolysers directly connected to onshore wind farms.

$$\mathrm{LCOH}^{(\mathrm{wd})} = \frac{\left[\mathrm{I}_0 + \mathrm{O}_\mathrm{K} \times \mathrm{S}_\mathrm{K}^{(\mathrm{wd})}\right]_{\mathrm{RES}} \times \mathrm{P}_{\mathrm{RES}} + \left[\mathrm{I}_0 + \mathrm{O}_\mathrm{K} \times \mathrm{S}_\mathrm{K} - \frac{\mathrm{R}_{10}}{(1+\mathrm{w}_{\mathrm{nom}})^{10}} + \frac{\mathrm{R}_{20}}{(1+\mathrm{w}_{\mathrm{nom}})^{20}}\right]_{\mathrm{H_2}} \times \mathrm{P}_{\mathrm{H_2}}}{\upsilon \times \mathrm{P}_{\mathrm{RES}} \times \eta \times \rho \times \mathrm{S}_\mathrm{Y}} \tag{5.9}$$

with:

$$\mathrm{S}_\mathrm{Y} = \frac{(\delta_{\mathrm{wd}} - 1)(\delta_{\mathrm{H_2}} - 1)(1+\mathrm{w})^{\mathrm{N}}\left[(1-\delta_{\mathrm{wd}})^{\mathrm{N}}(1-\delta_{\mathrm{H_2}})^{\mathrm{N}} - (1+\mathrm{w})^{\mathrm{N}}\right]}{\delta_{\mathrm{wd}} \times \delta_{\mathrm{H_2}} - \delta_{\mathrm{wd}} - \delta_{\mathrm{H_2}} - \mathrm{w}}$$

The same paper from B. Steffen [28] recommends a project nominal WACC value for onshore wind of 7.3%, which complies with other sources [21, 35]. R. Byrne [137] et al. wrote a comprehensive study regarding the performance decline of wind turbines, finding that the overall turbine power degradation is around 5% over a 13–year lifetime. In this thesis, an operational period of 30 years is considered instead, making $\delta_{\mathrm{wd}} = 0.39\%$. The caveat of considering this life extension is the additional OpEx costs, reflected in the middle of the traditional lifetime (n = 10 years) and at the end (n = 20 years). T. Rubert et al. [38] suggest that operational expenditures should increase by 10% in the first period and 25% in the second. This way, the conventional structure of the capital spread factor changes to:

$$\mathrm{S}_\mathrm{K}^{(\mathrm{wd})} = \mathrm{S}_{\mathrm{K},10} + \frac{1.1 \times \mathrm{S}_{\mathrm{K},10}}{(1+\mathrm{w}_{\mathrm{nom}})^{10}} + \frac{1.25 \times \mathrm{S}_{\mathrm{K},10}}{(1+\mathrm{w}_{\mathrm{nom}})^{20}}\ , \quad \text{where:} \quad \mathrm{S}_{\mathrm{K},10} := \frac{(1+\mathrm{w}_{\mathrm{nom}})^{10} - 1}{\mathrm{w}_{\mathrm{nom}} \times (1+\mathrm{w}_{\mathrm{nom}})^{10}}$$

LCOH from Offshore Fixed Wind Farms

Moving to offshore RES, Equation 5.10 shows the formula of the LCOH from fixed foundations wind farms.

$$\mathrm{LCOH}^{(\mathrm{fx})} = \frac{\left[\mathrm{I}_0 + \mathrm{O}_\mathrm{K} \times \mathrm{S}_\mathrm{K}^{(\mathrm{wd})}\right]_{\mathrm{RES}} \times \mathrm{P}_{\mathrm{RES}} + \left[\mathrm{I}_0 + \mathrm{O}_\mathrm{K} \times \mathrm{S}_\mathrm{K} - \frac{\mathrm{R}_{10}}{(1+\mathrm{w}_{\mathrm{nom}})^{10}} + \frac{\mathrm{R}_{20}}{(1+\mathrm{w}_{\mathrm{nom}})^{20}}\right]_{\mathrm{H_2}} \times \mathrm{P}_{\mathrm{H_2}}}{\upsilon \times \mathrm{P}_{\mathrm{RES}} \times \eta \times \rho \times \mathrm{S}_\mathrm{Y}} \tag{5.10}$$

with:

$$\mathrm{S}_\mathrm{Y} = \frac{(\delta_{\mathrm{wd}} - 1)(\delta_{\mathrm{H_2}} - 1)(1+\mathrm{w})^{\mathrm{N}}\left[(1-\delta_{\mathrm{wd}})^{\mathrm{N}}(1-\delta_{\mathrm{H_2}})^{\mathrm{N}} - (1+\mathrm{w})^{\mathrm{N}}\right]}{\delta_{\mathrm{wd}} \times \delta_{\mathrm{H_2}} - \delta_{\mathrm{wd}} - \delta_{\mathrm{H_2}} - \mathrm{w}}$$

B. Steffen [28] does not make a distinction between offshore wind technologies, considering just one overall nominal WACC: $\mathrm{w}_{\mathrm{nom}} = 8.3\%$ —which again, is in accordance with other reputable references [21, 35].
Operation and maintenance periodicity is kept the same as onshore wind, and the degradation rate of offshore wind turbines is here assumed to be the same too. Evidence to the contrary has been found in the literature [138], but with insufficient expression.

Lastly, a different value for the electrolyser OpEx is considered here since there is no need to include fixed and variable fees for piped water. In this analysis, the electrolyser is located in an offshore, dedicated and centralised platform, as demonstrated by J. Ezquerra [139] to be the cheapest solution. Hence, the cost of desalinating sea water on–site (using reverse–osmosis desalination) is adopted, using data from the IEA [4].

LCOH from Offshore Floating Wind Farms

Finally, Equation 5.11 shows the formula to compute the LCOH from offshore floating wind farms.

$$\mathrm{LCOH}^{(\mathrm{ft})} = \frac{\left[\mathrm{I}_0 + \mathrm{O}_\mathrm{K} \times \mathrm{S}_\mathrm{K}^{(\mathrm{wd})}\right]_{\mathrm{RES}} \times \mathrm{P}_{\mathrm{RES}} + \left[\mathrm{I}_0 + \mathrm{O}_\mathrm{K} \times \mathrm{S}_\mathrm{K} - \frac{\mathrm{R}_{10}}{(1+\mathrm{w}_{\mathrm{nom}})^{10}} + \frac{\mathrm{R}_{20}}{(1+\mathrm{w}_{\mathrm{nom}})^{20}}\right]_{\mathrm{H_2}} \times \mathrm{P}_{\mathrm{H_2}}}{\upsilon \times \mathrm{P}_{\mathrm{RES}} \times \eta \times \rho \times \mathrm{S}_\mathrm{Y}} \tag{5.11}$$

with:

$$\mathrm{S}_\mathrm{Y} = \frac{(\delta_{\mathrm{wd}} - 1)(\delta_{\mathrm{H_2}} - 1)(1+\mathrm{w})^{\mathrm{N}}\left[(1-\delta_{\mathrm{wd}})^{\mathrm{N}}(1-\delta_{\mathrm{H_2}})^{\mathrm{N}} - (1+\mathrm{w})^{\mathrm{N}}\right]}{\delta_{\mathrm{wd}} \times \delta_{\mathrm{H_2}} - \delta_{\mathrm{wd}} - \delta_{\mathrm{H_2}} - \mathrm{w}}$$

As stated above, following the suggestion of B. Steffen [28], the nominal WACC for floating devices is assumed to be the same as for fixed foundations: $\mathrm{w}_{\mathrm{nom}} = 8.3\%$. Note that all these WACC values are used as a first estimation, reflecting the international investor perception of operational risk: solar PV is a more mature technology than offshore wind, thus has less perceived risk, and thus presents a lower nominal WACC. Still, a sensitivity analysis is always recommended since WACC rates are highly subjective and depend on the country, market segment, investor type, and risk appetite.

With all the technologies revised, Table 5.1 provides a summary of the variables considered in the different formulations of the levelised cost of hydrogen.

Table 5.1: Summary of the LCOH components for every RES formulation.

		Unit	Solar Photovoltaic	Onshore Wind	Offshore Fixed	Offshore Floating	PEM Electrolyser
General parameters							
N	Operational lifetime	years			30		
i	Inflation value	%			2		
Economic factors							
$\mathrm{w}_{\mathrm{nom}}$	Nominal WACC	%	5.40	7.30	8.30	8.30	n/a
w	Real WACC	%	3.33	5.20	6.18	6.18	n/a
I_0	Capital expenditures	EUR/kW	630	1162.48	1703.63	3604.63	1136.20
O_K	Operational costs	EUR/kW/yr	10.89	37.04	61.02	65.45	34.09 / 14.97
R	Replacement cost	EUR/kW		n/a			681.72
Δ_N	Decommission value	EUR/kW			0		
Technical aspects							
δ_n	Degradation value	%/year	0.45	0.39	0.39	0.39	0.70
ρ	Production rate	kg/h/kW		n/a			0,01771
η	System efficiency	%		n/a			60

5.1.2 Levelised Cost of Electricity

While the central purpose of this thesis is to study the levelised cost of hydrogen, the computation of the levelised cost of electricity in energy systems is typically regarded as a valuable asset.
The LCOE is a metric usually associated with the feasibility of an energy project, measuring the cost of production of one energy unit during the lifetime of that project. Equation 5.12 shows the general formula used in this work.

$$\mathtt{LCOE}^{(*)} = \frac{\mathtt{K}_{\mathtt{RES}}}{\mathtt{Y}_{\mathtt{RES}}} \tag{5.12}$$

where:

$\mathtt{K}_{\mathtt{RES}}$ is the overall cost structure of the RES power plant, in EUR.

$\mathtt{Y}_{\mathtt{RES}}$ is the total electricity generation, in kWh.

This formula resembles Equation 5.2—where the levelised cost of hydrogen is presented—, only here there is no cost associated with the electrolyser system, and the yield is electricity instead of hydrogen. $\mathtt{K}_{\mathtt{RES}}$ is defined precisely like in Equation 5.3 and respects all the assumptions made before for each one of the four technologies. $\mathtt{Y}_{\mathtt{RES}}$ comes from the same formulation as in Equation 5.6, neglecting the terms related to the electrolyser system. Equation 5.13 displays the expanded form of the LCOE.

$$\mathtt{LCOE}^{(*)} = \frac{\mathtt{I}_0 + \mathtt{O}_{\mathtt{K}} \times \sum_{\mathtt{n}=1}^{\mathtt{N}} \frac{1}{(1+\mathtt{w}_{\mathtt{nom}})^{\mathtt{n}}}}{\upsilon \times \sum_{\mathtt{n}=1}^{\mathtt{N}} \left(\frac{1-\delta_{\mathtt{RES}}}{1+\mathtt{w}}\right)^{\mathtt{n}}} = \frac{\mathtt{I}_0 + \mathtt{O}_{\mathtt{K}} \times \mathtt{S}_{\mathtt{K}}}{\upsilon \times \mathtt{S}_{\mathtt{Y}}} \tag{5.13}$$

with:

$$\mathtt{S}_{\mathtt{K}} = \frac{(1+\mathtt{w}_{\mathtt{nom}})^{\mathtt{N}} - 1}{\mathtt{w}_{\mathtt{nom}} \times (1+\mathtt{w}_{\mathtt{nom}})^{\mathtt{N}}} \quad \bigwedge \quad \mathtt{S}_{\mathtt{Y}} = \frac{(1-\delta_{\mathtt{RES}}) \times \left[1 - \left(\frac{1-\delta_{\mathtt{RES}}}{1+\mathtt{w}}\right)^{\mathtt{N}}\right]}{\delta_{\mathtt{RES}} \times \mathtt{w}}$$

Note that while the capital spread factor is identical to the one computed in Equation 5.4, the yield spread factor here is simplified (due to the nonexistence of the electrolyser degradation rate).
This formula is to be used as before to calculate the LCOE value of each RES technology for each location.

With the description of these formulations complete, the following section outlines the methodology associated with the simplified model of computing the levelised cost of hydrogen in Portugal and Italy.

5.2 Simplified General Model

Many articles have been published in the literature where a geographic analysis of the LCOH is carried out, from individual countries such as Mexico [10], Morocco [11] and Ireland [13] to whole continents like Europe [8]. In all of these, the global hydrogen yield is assumed to be converted directly from the electricity generated by the renewable energy source, usually using the net production rate of the electrolyser or the lower/higher heating value of hydrogen.

Despite being extremely effective, this method lacks the inherent complexity of a real RES–to–Hydrogen system, a topic further addressed in Section 5.3. Even so, a similar model to those used in the literature is developed here to implement in all eligible locations of both countries. This section describes the creation of the simplified general model (SGM), starting by explaining how to determine the upper–limit of the RES installed capacity for a given available area and then discussing the definition of the localised LCOH computation.

5.2.1 RES Maximum Allowed Capacity

As will be seen in the next subsection, the calculation of the levelised cost of hydrogen starts from the setting of a virtual hydrogen demand, from which the size of the RES capacity is estimated. Still, initially, it is imperative to establish the theoretical maximum limit based on the physical constraint of the available area. For this, a flowchart illustrates the thought process behind the decisions made for both solar panels and wind turbines (onshore and offshore alike).

Figure 5.1 shows the flowchart to compute the maximum allowed solar installed capacity.

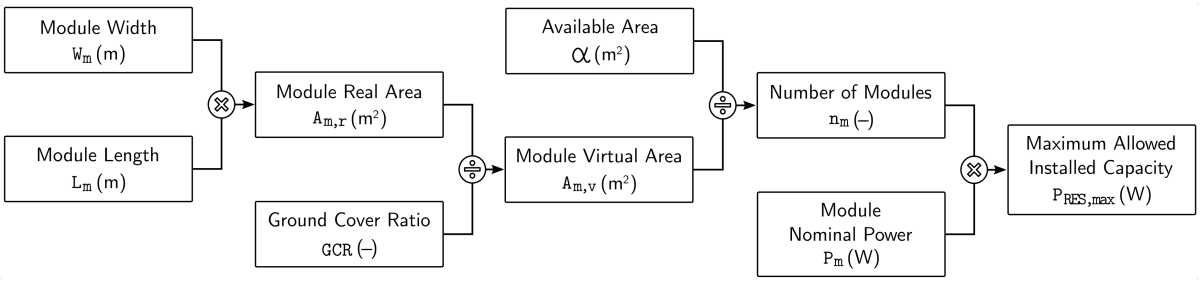

Figure 5.1: Installed capacity upper–limit decision flowchart for photovoltaic solar parks.

The process begins with choosing a generic utility–scale module from Canadian Solar, the company supplying Italy–based EnelX. The CS7L–600MB–AG datasheet [140] states the dimensions of the module as 1303 $\times$ 2172 mm, resulting in an actual area of around 2.83 m^2.

Next, the ground cover ratio (GCR) is obtained to compute the virtual area of the module, taking into account the row space that minimises shading. This inter–row shading is measured by the respective derate factor that accounts for the system's electrical output reduction. According to T. Mahachi and A. Rix [141], it is standard industry practice to optimise land–use on photovoltaic parks by considering a 2.5% shading loss, which translates to a shading derate factor of 0.975. The approximate GCR can now be selected using a series of curves associated with the mounting type of the panels. The mounting types contemplated in this analysis are fixed tilt (four distinct angles), single–axis tracking and dual–axis tracking. Fixed tilt configurations have been found to perform as good as, if not better than, tracking devices for a fraction of the price [142];

this is due to the electric consumption of the actuator, which causes an inherent energy loss at the source. Hence, the mounting configuration chosen is fixed tilt. Following Subsections 4.1.1 and 4.1.2, and in an effort to match the tilt angle of the panels to the average latitude of both countries, a value of 40° is selected. Figure 5.2 illustrates the relation between the shading derate factor and the ground cover ratio for the configurations described above. With the specific data of this analysis, GCR = 0.42.

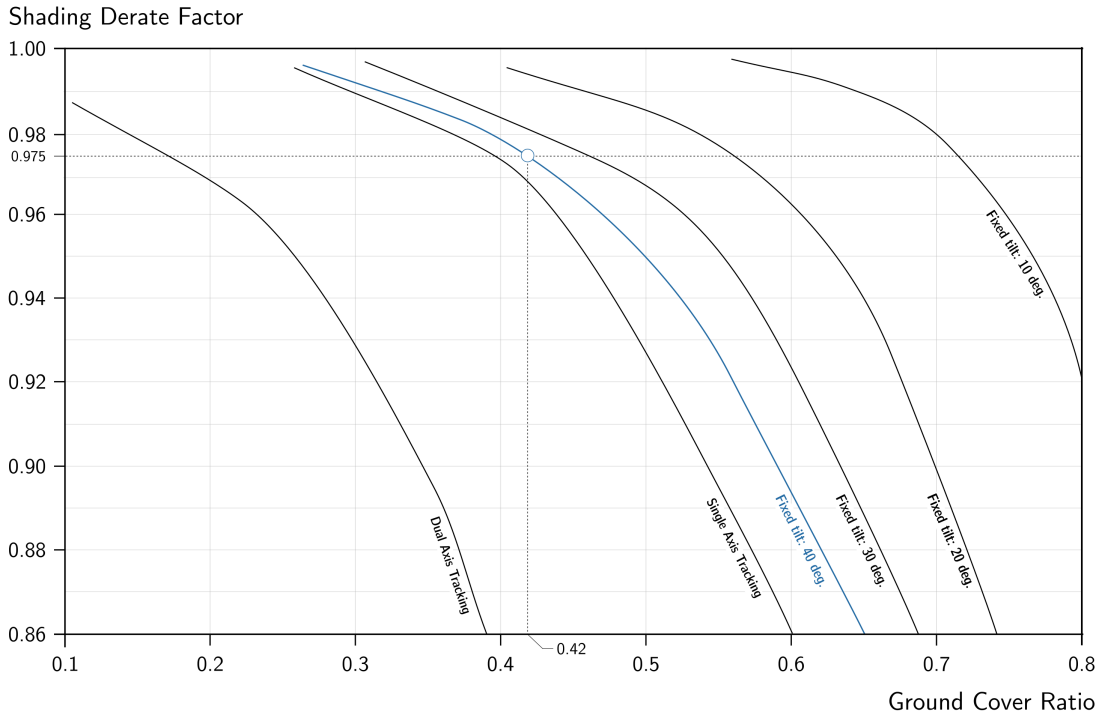

Figure 5.2: Shading derate factor as a function of GCR for multiple module configurations. Adapted from [141].

So, dividing the previous calculated real area of the modules by this ground cover ratio gives the module virtual area: $A_{m,v} = 7.26$ m^2. The choice of the total available area per pixel (α) refers back to Section 4.2, where the spatial resolution of the geographical model is defined. An adjustment is made to accommodate the electrolyser and all balance of system footprint, leaving a space of 780 by 780 meters free for the RES installed capacity. This available area is then divided by the module's virtual area to give the maximum number of panels allowed in each pixel: n_m.

Finally, the same datasheet states a module's nominal power of 600 W under Standard Test Conditions (irradiance of 1000 W/m^2 and cell temperature of 25 °C). Multiplying this value by the number of modules, leads to the solar PV installed capacity upper–limit.

Table 5.2 outlines the value structure of the decision process described so far.

Table 5.2: Summary of components in the computation of the maximum allowed solar installed capacity.

	W_m (m)	L_m (m)	$A_{m,r}$ (m^2)	GCR (–)	$A_{m,v}$ (m^2)	W_{px} (m)	L_{px} (m)	α (m^2)	n_m (–)	P_m (W)	$P_{RES,max}$ (MW)
Solar Photovoltaic	1.30	2.17	2.83	0.39	7.26	780	780	608400	83840	600	**50.30**

Note: colored cells indicate values derived from the formulas described above.

Figure 5.3 now shows the equivalent decision flowchart for wind turbine farms.

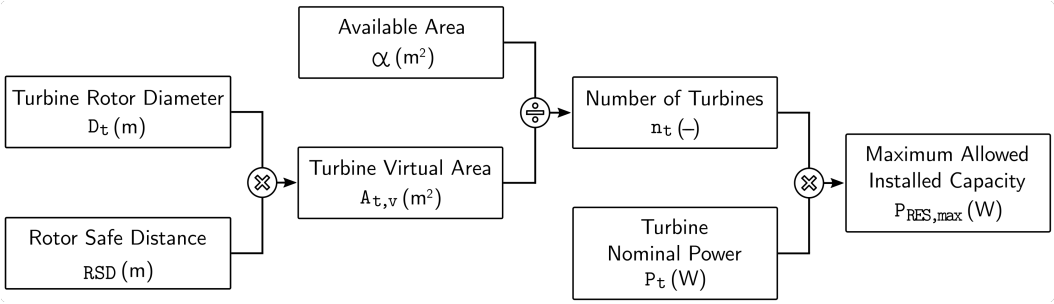

Figure 5.3: Installed capacity upper–limit decision flowchart for wind farms.

Here the process starts with establishing a common diameter size for the turbine rotor. The International Electrotechnical Commission Class II is used as reference [143], where 3.45 MW turbines have a diameter of 126 meters and a hub height of 100 meters. Vestas' 4 MW Platform is chosen, analogously to the decision made in Subsection 4.4.5. Before computing each turbine's virtual area, the safe distance from one another first needs to be defined. This procedure is to avoid any turbine–induced airflow disturbance that may affect the performance of nearby turbines in parallel–string layouts. Nowadays, most sources [144–146] agree on placing onshore turbines seven rotor diameters away from each other downwind and five rotor diameters sidewind. Regarding offshore farms, both these numbers increase to eight since turbines spaced further apart have been found to improve their efficiency and lifetime [144]; besides, covering a larger area is less of a problem on the sea. Multiplying these two quantities gives a virtual rectangle with a turbine on one of its corners and an area $A_{t,v}$. The subsequent procedure is the same as for the solar parks. The total available area is also one pixel with approximately 1 km^2, leading the number of turbines in each pixel to be the quotient between this area and the turbine's virtual area. Finally, the upper–limit wind installed capacity is computed by multiplying the maximum number of turbines in each farm by the nominal power of one said turbine.

Table 5.3 presents the values of each component in the decision process described above for onshore, offshore fixed and offshore floating wind farms.

Table 5.3: Summary of components in the computation of the maximum allowed wind installed capacity.

	D_t	— RSF —			$A_{t,v}$	W_{px}	L_{px}	α	n_t	P_t	$P_{RES,max}$
	(m)	(–)	(–)	(m)	(m^2)	(m)	(m)	(m^2)	(–)	(MW)	(MW)
Onshore Wind	126	7	5	35	4410	780	780	608400	138	3.45	**475.96**
Offshore Fixed	126	8	8	64	8064	780	780	608400	75	7.00	**528.13**
Offshore Floating	126	8	8	64	8064	780	780	608400	75	7.00	**528.13**

Note: colored cells indicate values derived from the formulas described above.

With the installed capacity limit of every RES defined, the following subsection explores the reasoning behind structuring the simplified general model.

5.2.2 Localised LCOH Computation

As explained in the preceding sections, this work employs a generalised LCOH model to cover all the eligible locations resulting from the geographic analysis of Chapter 4. With the fundamental parameters of the electrolyser identified (ρ, η), the SGM starts from the definition of a virtual hydrogen demand, $\mathcal{D}$. This value represents a broad hydrogen need to be fulfilled in the regions where the project's economic feasibility is being evaluated; here is defined as 100 ton/year. Next, from this hydrogen demand, the amount of electricity needed at the stack input is computed using the net production rate of the electrolyser. When the electrolyser system's electric efficiency is considered, one gets the yearly energy needed to be generated by the coupled RES power plant. Finally, to find the size of the RES station, one needs to divide this quantity by the full load hours of the power plant. The annual solar and wind capacity factors are respectively collected from Global Solar Atlas[1] [114, 116] and Global Wind Atlas[2] [120, 121]. After proper data management in QGIS, a list of all capacity factors is converted to FLH and stored in each set $\mathbb{C}^{(*)}$.

The size of the RES power plant is then tested against the upper–limits computed before to comply with the maximum physical allowance of installed capacity. If it is above the upper–limit, then the virtual hydrogen demand is adjusted for that particular location; if instead is below, then it is clear to proceed.

The next step is the sizing of the electrolyser. Most of the consulted literature [8, 10, 11, 13] just considers the electrolyser to have the same size as the RES station—this represents an oversimplified solution. Figure 5.4 illustrates the energy production profile from solar PV (yellow) and onshore wind turbines (blue) during a typical day. The cited articles presume that the rated power of the electrolyser (green) coincides with the nominal installed capacity of the RES power plants, as shown (assuming nominal power is reached during the day).

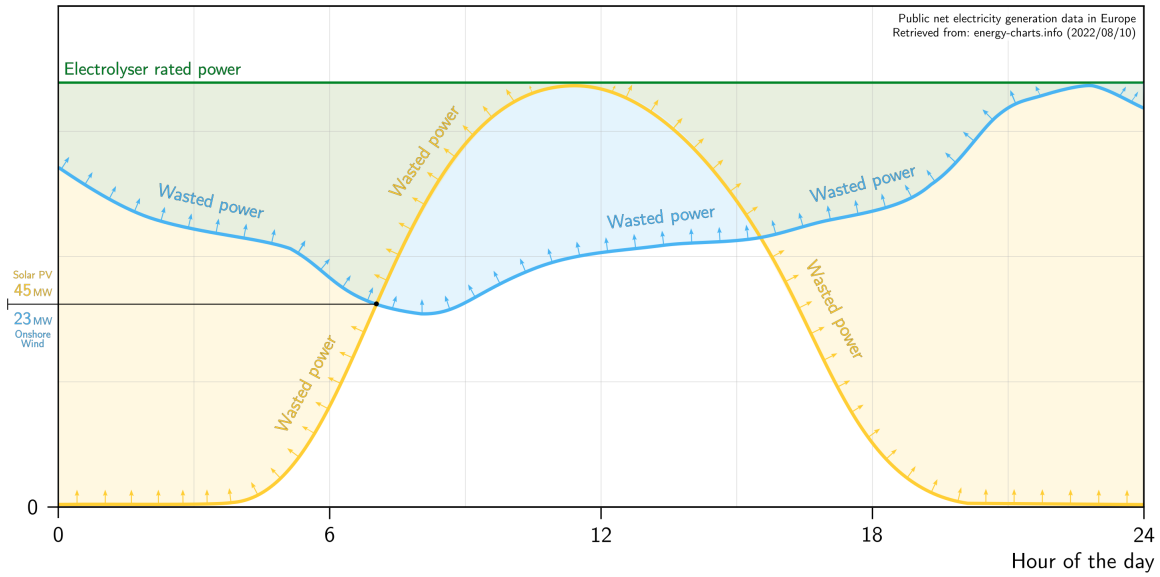

Figure 5.4: RES–to–Hydrogen direct coupling: the oversimplified solution.

[1] Global Solar Atlas delivers a 'PVOUT' dataset encompassing the estimated solar photovoltaic power generation potential (in kWh/kW), computed as the average yearly total electricity production from a 1 kWp solar plant over 25 recent years. The PV system consists of ground–based, free–standing structures with crystalline–silicon modules mounted at a fixed position, with an optimum tilt angle to maximise yearly energy yield (use of high–efficiency inverters is assumed too). The analysis takes into account solar radiation, air temperature and terrain features that simulate losses in the modules; losses due to dirt and soiling are estimated to be 3.5%, while the cumulative effect of other conversion losses (such as preliminary inter–row shading, power mismatches and cables) is assumed to be 7.5%. The power plant availability is considered 100%.

[2] Global Wind Atlas provides a (unitless) capacity factor dataset for three International Electrotechnical Commission classes of 3.45 MW wind turbines, with rotor diameters of 112 m, 126 m, and 136 m, at a hub height of 100 m.

Note that every region bounded by the green line and the yellow/blue line reveals a period when the stack is not entirely in use. This setup inherently drives to waste most of the power from the electrolyser—in this example, around 27% if connected to onshore wind turbines, and up to 58% if connected to solar PV. In other words, this configuration leads to a lower electrolyser capacity factor and, in turn, increased relative costs. For this reason, in this work, an oversize factor ($\mathcal{F}$) is applied instead: a ratio to apply between P_{RES} and P_{H_2} that best optimises the hydrogen output. The method to obtain this factor is described in the next section.

With the size of both the RES power plant and the electrolyser defined, Equations 5.8–5.11 are used to find the respective LCOH. An additional procedure is required in onshore locations to evaluate which technologies yield the lowest cost since only one can be installed. After a direct comparison, the cheapest LCOH is selected for that location.

Algorithm 1 offers a pseudo–code summary of the decision process supporting the simplified general model.

Algorithm 1 Simplified General Model algorithm

Require: $\mathcal{D}$, ρ, η, υ ▷ Parameters of the model

procedure SGM($\hookleftarrow$)
  for all $\upsilon \in \mathbb{C}^{(*)}$ **do**
    $\mathcal{D} \leftarrow$ ▷ Set hydrogen virtual demand
    $\mathcal{D} : \rho : \eta : \upsilon = P_{RES}$ ▷ Compute power plant size
    if $P_{RES} > P_{RES,max}$ **then**
      decrease $\mathcal{D}$
    else
      $\mathcal{F} \leftarrow$ ▷ Set oversize factor
      $P_{RES} : \mathcal{F} = P_{H_2}$ ▷ Compute electrolyser size
    end if
    procedure Onshore LCOH(*)
      if $LCOH^{(pv)}$ **then**
        use Equation 5.8
      else if $LCOH^{(wd)}$ **then**
        use Equation 5.9
      end if
      if $LCOH^{(pv)} < LCOH^{(wd)}$ **then** ▷ Verify lowest local LCOH
        return $LCOH^{(pv)}$
      else
        return $LCOH^{(wd)}$
      end if
    end procedure
    procedure Offshore LCOH(*)
      if $LCOH^{(fx)}$ **then**
        use Equation 5.10
      else if $LCOH^{(ft)}$ **then**
        use Equation 5.11
      end if
    end procedure
  end for
end procedure ▷ Exit SGM

Deliver: $LCOH^{(*)}$

5.3 Optimised General Model

With the disadvantages of the simplified method identified, the need to develop an optimisation algorithm is evident. Looking at Figure 5.4 again, this algorithm would predominantly shift the line of electrolyser rated power up and down during the day until it finds the least–loss level: the one that corresponds to the cheaper LCOH.

Some articles have been published on this subject, from linear approximations of solar–hydrogen systems [14] to particle swarm optimisation of far offshore wind–hydrogen structures [16]. M. Scolaro and N. Kittner [17] explored the possibility of enhancing these systems also to provide ancillary services in the German market, while NREL recently published a technical report [15] on optimising an integrated renewable–electrolysis system.

The model developed in this thesis assimilates learnings from these (and other) works and builds on a traditional optimisation method. The objective of the optimised general model (OGM) is to find the cheapest LCOH in a given set of suitable locations, considering hourly changing values for P_{RES} and P_{H_2}. The algorithm presupposes the existence of a RES power plant and an electrolyser system in each location, with the possibility of having both solar PV and wind in a hybrid onshore configuration. The power plant's installed capacity and the electrolyser's nominal input power are the decision variables, where the latter is upper bound by the former. All the parameters described next are the same scalar value for each location, except for the capacity factor—which is indexed to each point, as seen before.

Following up, Subsection 5.3.1 uncovers the problem setting and the notation used within the algorithm, while Subsection 5.3.2 analyses the mathematical formulation of the model.

5.3.1 Problem Setting and Notation

The OGM is built with Pyomo [147, 148], a Python–based, open–source optimisation modelling language with multiple optimisation capabilities. The first step consists of initialising the abstract mathematical model built on unconstructed components. Secondly, the three basic elements needed to construct a Pyomo model are declared in standard Python objects: sets, parameters and variables. Finally, when a solution is to be obtained, a concrete instance of the model is created with data values being applied via a 'DataPortal'. The following items lay out the definition of said objects.

Index Sets

Pyomo sets provide indexes for parameters, variables and also other sets. Coding starts with the abstract declaration of sets $\mathbb{L}$ and $\mathbb{H}$, respectively, regarding the list of eligible location points and the number of hours in one year. These are followed by loading the concrete values from a prepared CSV file.

Parameters

Parameters refer to a class of data values used to characterise the model. Parameters may be endogenous or exogenous entities, i.e. depend or not on other constants. Most parameters are exogenous (see Section 5.1), with the exception of the real WACC, the capital and production spread factors, and the overall cost structures. As noted before, all these parameters are the same scalar for each location, apart from the capacity factors. Contrary to the yearly SGM analysis, the optimisation model requires an hourly time frame to operate correctly.

For each year's hour, the model assesses the energy production from the RES power plant, and the electrolyser rated power, evaluating which relation results in the lowest LCOH. Neither Global Solar Atlas nor Global Wind Atlas provides hourly capacity factors—instead, the PVGIS tool [149] is used to get values for onshore locations, and Renewablesr.ninja [150, 151] is employed for offshore.

PVGIS enables the extraction of a CSV file per location containing a series of outputs; the specific ones needed are `PV Power` and `Wind Speed at 10 m`. To compute the hourly solar PV energy yield, the software requires some inputs; these correspond to the same assumptions made for the annual capacity factors: 1 kWp power plant with ground–based crystalline–silicon modules, mounted at a fixed optimal slope and azimuth angles. System losses follow the software recommendation of 14%, and the solar radiation database is the most recent year available on PVGIS–SARAH2. With the `PV Power` values calculated, a simple sequence division by the installed peak PV power returns the solar FLH of that location at every hour.

Regarding `Wind Speed at 10m`, the procedure begins with converting wind speed from 10 meters to 100 meters—the selected hub height. For this, Prandtl's relation is used, given by Equation 5.14:

$$u = u_{ref} \times \frac{\ln(z/r)}{\ln(z_{ref}/r)} \tag{5.14}$$

where:

u is the wind speed at the desired height, in m/s.

u_{ref} is wind speed at the reference height, in m/s.

z is the desired height, in meters (assumed to be 100).

z_{ref} is the reference height, in meters (assumed to be 10).

r is the roughness length, in meters.

The roughness length—and respective roughness class (RC)—is a proxy parameter for a length–scale representation of the surface roughness [152]. Higher RC values mean more protruding landscapes, which significantly impact wind patterns. This study considers RC–0 for offshore projects and RC–1 for onshore ones. Having the wind velocity profiles computed at the hub height, a power curve is applied to obtain the power at the turbine's output (P_{out}). The power curve is a piecewise–defined function, expressed by Equation 5.15:

$$P_{out} = \begin{cases} 0, & u < u_{min} \\ f(u), & u_{min} < u < u_{nom} \\ P_{nom}, & u_{nom} < u < u_{max} \\ 0, & u > u_{max} \end{cases} \tag{5.15}$$

where:

P_{nom} is the nominal power of the turbine, in MW.

$f(u) = au^4 + bu^3 + cu^2 + du + e$ is the 4^{th} order polynomial that best fits the real power curve.

u_{min} is the cut–in wind speed, in m/s (assumed to be 3).

u_{nom} is the nominal wind speed, in m/s (assumed to be 13).

u_{max} is the cut–out wind speed, in m/s (assumed to be 25).

The selected power curve follows the characteristic of Vestas V112–3.45 model, used here as a reference to compute the coefficients of the polynomial interpolation. Figure 5.5 illustrates the process.

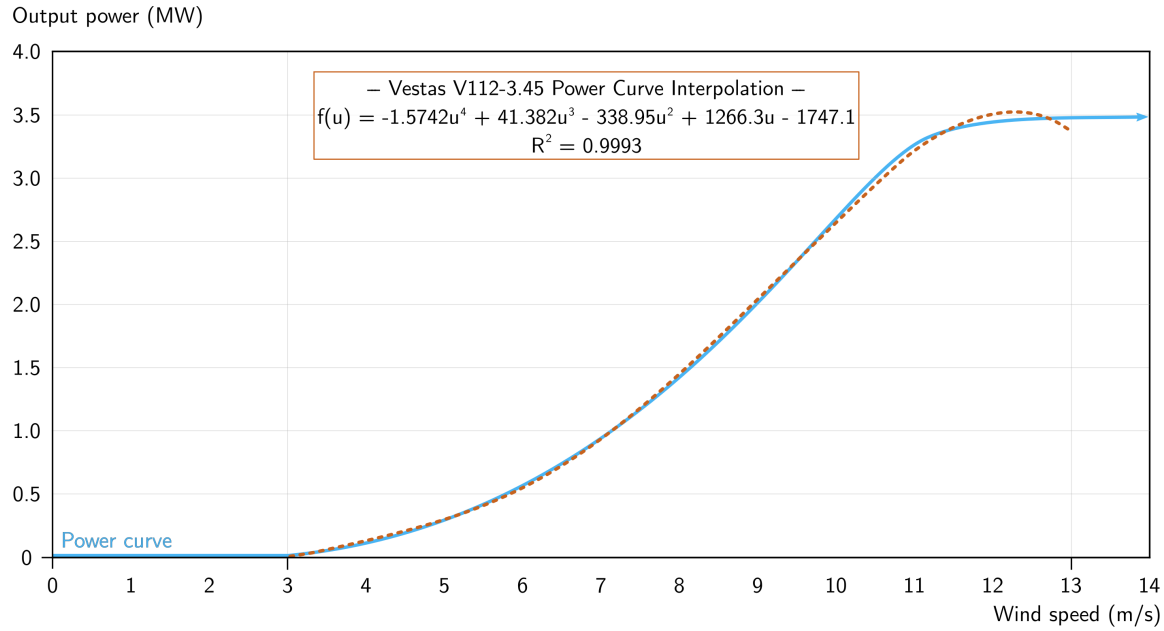

Figure 5.5: Vestas V112–3.45 power curve interpolation.

With the hourly wind power output, a sequence division by the nominal power of the turbine returns the wind FLH of that location at every hour.

Regarding offshore points, Renewables.ninja provides a direct CSV file with the capacity factors. Besides choosing the most recent year in the dataset (MERRA–2), the installed capacity is selected as 1 kW, hub height as 100 meters and turbine model as Vestas V164–9.5.

Variables

Variables represent the unknowns of a model. Ultimately, they are intended to store the values referred to as the 'solution' of the optimisation program. Variables are declared as indexed, bounded elements with a specific domain. This model envisions the existence of three decision variables and four support variables, outlined in Table 5.4. While the former establish the actual solution, the latter exist to execute auxiliary computations.

Table 5.4: Summary of variables in the optimised general model.

	Variable	Index	Domain	Upper–bound	Description
Decision	P_{pv}	$\mathbb{L}$	Non-Negative Reals	$P_{pv,max}$	Solar installed capacity
	P_{wd}	$\mathbb{L}$		$P_{wd,max}$	Wind installed capacity
	P_{H_2}	$\mathbb{L}$		$P_{pv} + P_{wd}$	Electrolyser nominal power
Support	$E_{H_2,h}$	$\mathbb{L}$, $\mathbb{H}$	Non-Negative Reals	$P_{pv} + P_{wd}$	Hourly electrolyser energy
	$Y_{H_2,h}$	$\mathbb{L}$, $\mathbb{H}$		|	Hourly hydrogen production
	Y_{H_2}	$\mathbb{L}$		n/a	Yearly hydrogen production
	Z	$\mathbb{L}$	|	|	Virtual change of variable

5.3.2 Mathematical Formulation

Every optimisation problem requires the mathematical formalism that enables a rigorous description of the reality it is trying to model. The design of an efficient mathematical formulation rests on an understanding to derive innovative approaches to the architecture of the problem. In this thesis, the design aspects of the mathematical formulation undergo several iterations: 1. insight of the question to be assessed; 2. establishment of preliminary relations; 3. model redesign to decrease the number of variables and constraints; 4. refinement of the redesign; and 5. abstraction to a multi–criteria optimisation problem.

The first detail to recognise is the unique structure of the model; it consists of a very–large non–convex optimisation problem with a non–linear objective function. Such a problem may have multiple feasible regions and several locally optimal points within each region. Generally, non–convex optimisation has at least NP–hard[3] complexity, meaning it can take time exponential in the number of variables and constraints to determine: that a non–convex problem is infeasible, that the objective function is unbounded, or that an optimal solution is the 'global optimum' across all feasible regions. Consequently, efforts have been made to turn the objective function from a non–linear configuration into a quadratic one, which speeds up the solving process while maintaining the validity of the results.

The following items address the definitions of the constraints and the objective function.

Constraint Expressions

Constraints establish the functional relationships between variables, using equality or inequality expressions as rules of Python. The equations presented below follow the reasoning to compute the optimised LCOH at each location; the solution then consists of the RES installed capacity values and the nominal input power of the electrolyser. Coloured elements in the expressions indicate decision variables.

— Hourly electricity consumption by the electrolyser

The hourly electricity generation is equal to the solar/wind installed capacity times the respective capacity factor; this electricity can either be directed to the electrolyser or be unused (curtailed). Thus, the electricity consumption by the electrolyser must always be less than or equal to the electricity generated by the RES.

$$\mathrm{E}_{\mathrm{H_2,h}} \leq \mathrm{P}_{\mathrm{pv}} \times \mathrm{CF}_{\mathrm{pv,h}} + \mathrm{P}_{\mathrm{wd}} \times \mathrm{CF}_{\mathrm{wd,h}} \tag{5.16}$$

— Hourly electrolyser electricity use limit

The electrolyser input power always limits the hourly amount of electricity directed to the electrolyser.

$$\mathrm{E}_{\mathrm{H_2,h}} \leq \mathrm{P}_{\mathrm{H_2}} \times 1\ \mathrm{hour} \tag{5.17}$$

— Electrolyser nominal input power upper–bound

The electrolyser input power must be lower than the RES installed capacity.

$$\mathrm{P}_{\mathrm{H_2}} \leq \mathrm{P}_{\mathrm{pv}} + \mathrm{P}_{\mathrm{wd}} \tag{5.18}$$

[3] *def.* The set of decision problems solvable in polynomial time by a nondeterministic Turing machine [153].

— Hourly hydrogen production

The amount of hydrogen produced in each hour is equal to the electricity directed to the electrolyser times the all–round electric efficiency and the net production rate.

$$Y_{H_2,h} = E_{H_2,h} \times \eta \times \rho \tag{5.19}$$

— Lifetime discounted hydrogen production

The amount of hydrogen produced during the entire lifetime of the project is the production spread factor times the yearly sum of the hydrogen yield at each hour.

$$Y_{H_2} = S_Y \times \sum_h Y_{H_2,h} \tag{5.20}$$

— Lifetime hydrogen virtual demand

The total hydrogen demand is equal to the minimum yearly hydrogen demand times the economic lifetime of the system (assumed to be 30 years). The 100 ton value considered is referenced back to the 425 kg–daily mass output of GenFuel's Plug 1 MW electrolyser [135] (adjusted for the utilisation factor).

$$Y_{H_2} \geq 100\,000 \times 30 \tag{5.21}$$

— Area power density limits

The combined installed capacity of both power plants and the electrolyser must not exceed the available area. The power density of each system ($\chi_{pv} = 0.08268\,kW/m^2$, $\chi_{wd} = 0.7823\,kW/m^2$, $\chi_{H_2} = 85.32\,kW/m^2$), is computed by dividing the upper–bound installed capacity of each system by the total available area.

$$\frac{P_{pv}}{\chi_{pv}} + \frac{P_{wd}}{\chi_{wd}} + \frac{P_{H_2}}{\chi_{H_2}} \leq \alpha \tag{5.22}$$

— RES installed capacity limits

The installed solar/wind capacity cannot exceed its respective limit (defined by the area available).

$$\begin{aligned} P_{pv} &\leq P_{pv,max} \\ P_{wd} &\leq P_{wd,max} \end{aligned} \tag{5.23}$$

— Power lower bounds (non–negativity constraint)

Neither one of the variables can assume negative values.

$$\begin{aligned} P_{pv} &\geq 0 \\ P_{wd} &\geq 0 \\ P_{H_2} &\geq 0 \end{aligned} \tag{5.24}$$

— Change of variable in the objective function

For the reasons expressed in Subsection 5.3.2 and corroborated in Subsection 5.3.3, the original non–linear objective function is converted into a quadratic formula.

$$Z \times Y_{H_2} = K_{RES} + K_{H_2} \tag{5.25}$$

Objective Function

The optimisation model concludes with the formulation of the objective function. Primarily, the objective is to minimise the levelised cost of hydrogen. Since this is a deterministic optimisation —in which every point is independent of the adjacent ones—, it is possible to perform a joint minimisation of all eligible locations, where the minimisation of the sum is equal to the sum of the minimisations. Equation 5.26 displays the function for just one point, as it is used in the case under study.

$$\textbf{min } \mathtt{LCOH} = \textbf{min } \frac{\mathtt{K_{RES}} + \mathtt{K_{H_2}}}{\mathtt{Y_{H_2}}} = \textbf{min } \mathtt{Z} \tag{5.26}$$

$$\textbf{s.t. } \text{Equations 5.16 – 5.25}$$

Algorithm 2 outlines a pseudo–code of the decision process in the base of the optimised general model.

Algorithm 2 Optimised General Model algorithm

Require: $\mathtt{P_{pv,max}}$, $\chi_{\mathtt{pv}}$, $\mathtt{CF_{pv}}$, $\mathtt{P_{wd,max}}$, $\chi_{\mathtt{wd}}$, $\mathtt{CF_{wd}}$, $\chi_{\mathtt{H_2}}$, α, $\mathcal{D}$, $\mathtt{N}$, $\mathtt{S_Y}$ ▷ Parameters of the model

1: **procedure** OGM($\hookleftarrow$)
2: **for all** $\mathtt{h} \in \mathbb{H}$ **do**
3: $\mathtt{P_{pv}}$, $\mathtt{P_{wd}}$, $\mathtt{P_{H_2}} \leftarrow$ ▷ Set initial guesses for decision variables
4: **Ensure:** $0 \leq \mathtt{P_{pv}} \leq \mathtt{P_{pv,max}}$
5: $0 \leq \mathtt{P_{wd}} \leq \mathtt{P_{wd,max}}$
6: $0 \leq \mathtt{P_{H_2}} \leq \mathtt{P_{pv}} + \mathtt{P_{wd}}$
7: $\mathtt{P_{pv}} : \chi_{\mathtt{pv}} + \mathtt{P_{wd}} : \chi_{\mathtt{wd}} + \mathtt{P_{H_2}} : \chi_{\mathtt{H_2}} \leq \alpha$
8: $\mathtt{P_{pv}} \times \mathtt{CF_{pv,h}} + \mathtt{P_{wd}} \times \mathtt{CF_{wd,h}} = \mathtt{E_{H_2,h}}$ ▷ Compute electricity use by the electrolyser
9: **if** $\mathtt{E_{H_2,h}} \geq \mathtt{P_{H_2}}$ **then**
10: **return** *to line 3:*
11: *decrease* $\mathtt{P_{pv}}$ *or* $\mathtt{P_{wd}}$
12: **else**
13: $\mathtt{E_{H_2,h}} \times \rho \times \eta = \mathtt{Y_{H_2,h}}$ ▷ Compute hydrogen production
14: **end if**
15: $\mathtt{Y_{H_2}} = \mathtt{S_Y} \times \sum_{\mathtt{h}} \mathtt{Y_{H_2,h}}$
16: **end for**
17: $\mathcal{D} \leftarrow$ ▷ Set hydrogen virtual demand
18: **Ensure:** $\mathtt{Y_{H_2}} \geq \mathcal{D} \times \mathtt{N}$
19: **procedure** LCOH($\odot$)
20: *use* Equation 5.2
21: **end procedure**
22: **end procedure** ▷ Exit OGM

Deliver: $\mathtt{P}^{\odot}_{\mathtt{pv}}$, $\mathtt{P}^{\odot}_{\mathtt{wd}}$, $\mathtt{P}^{\odot}_{\mathtt{H_2}}$, $\mathtt{LCOH}^{\odot}$

Note: the symbol $\odot$ identifies a relation to the optimal solution.

5.3.3 Validation Check

Having the optimisation algorithm entirely written into code, the model runs for one single location to check the validity of the results. The solver assigned for this operation is Octeract Engine [154], a deterministic branch–and–bound global optimisation software, notable for supporting supercomputing.

Table 5.5 shows the summaries and results of different problem structures, further discussed below.

Table 5.5: Algorithm outcomes using Octeract Engine.

1

```
[ 0.7s ] Problem Summary:
         ========================================
         Problem structure      : NLP
         Objective convexity    : non-convex
         Total # variables      : 17525
         -- continuous          : 17525
         -- binary              : 0
         -- integer             : 0
         Total # constraints    : 26285
         -- linear              : 26285
         -- convex              : 0
         -- non-convex          : 1
         ========================================
```

```
[ 0.4s ] Problem Summary:
         ========================================
         Problem structure      : QCQP
         Objective convexity    : linear
         Total # variables      : 17525
         -- continuous          : 17525
         -- binary              : 0
         -- integer             : 0
         Total # constraints    : 26285
         -- linear              : 26285
         -- convex              : 0
         -- non-convex          : 1
         ========================================
```

2

```
-------------------------------------------------------------------------------------------------------
  Iteration          GAP                LLB          BUB              Pool     Time        Mem
-------------------------------------------------------------------------------------------------------
EXIT: Optimal Solution Found.
          1    4.929e+00 (233.95%)    2.107e+00    7.036e+00           1     112.2s     199.0MB
```

3

```
-------------------------------------------------------------------------------------------------------
  Iteration          GAP                LLB          BUB              Pool     Time        Mem
-------------------------------------------------------------------------------------------------------
EXIT: Maximum CPU time exceeded.
        447    3.973e-02 (  1.14%)    3.482e+00    3.522e+00          208   22176.7s     751.0MB
```

- **Row 1** | displays a comparison between the problem summary of a Non–Linear Program structure (left) and a Quadratically Constrained Quadratic Program (right)—note how the objective convexity goes from Non–Convex to Linear. The number of variables and constraints stays the same as it relates to the interactions between each and the 8760 hourly time steps. Since there is a set of possible solutions to this problem, an option is included to stop the algorithm as soon as it finds the first feasible solution.
- **Row 2** | is the output of that QCQP simulation. The columns GAP, LLB and BUB refer respectively to the absolute (and relative) optimality ratio, the Least Lower Bound and the Best Upper Bound. Of the latter, the first indicates the smallest possible value of the objective function (2.107 EUR/kg), while the second indicates the best local optimum found (7.036 EUR/kg). These values hint that although 7.04 is a feasible solution, it may be far from the global optima, which lies closer to 2.11.
- **Row 3** | shows how the optimal global solution can be found if enough time is given to the solver. Here, the program is left running for a different location until it reaches a GAP close to 1%, at which point it is compulsorily shut down. It took more than six hours.

The real–time spent in computing is also an output of the solver (112.2 sec in the first case and 22176.7 sec in the second), as well as the amount of RAM that the solver takes up (119.0 MB and 751.0 MB). These simulations run on a Dell Precision 5520 machine equipped with an Intel Core i7–7820HQ CPU @ 2.90 GHz processor and 32.0 GB of installed RAM memory.

The algorithm is validated and ready to run the simulations, whose results are shown in the next chapter.

6 Results and Discussion

Following the methodologies examined in the previous chapters, a set of results is presented and discussed. This chapter is divided into three sections, each evaluating a different outcome of the material methods considered. Section 6.1 offers a general overview of the current LCOE in both countries, with onshore and offshore technologies. Section 6.2 analyses the bulk of data from the combined use of the geographical and numerical models. Finally, Section 6.3 provides a sensitivity test to the principal parameters of the economic model.

6.1 Electricity Generation Potential

Locations with a lower levelised cost of electricity are generally correlated with higher suitability for green hydrogen projects—thus the relevance of identifying such regions. The LCOE is computed using Equation 5.13, and the values are summarised in Table 6.1.

Table 6.1: Summary of project expenses for every renewable energy source.

	CapEx (EUR_{2020}/kW)				**OpEx (EUR_{2020}/kW/yr)**		
	Hardware	Balance of System	Soft Costs	TOTAL	General Operations	Maintenance and Services	TOTAL
Solar Photovoltaic	190.26	260.19	179.55	**630**	7.63	3.27	**10.89**
Onshore Wind	819.21	255.64	87.15	**1162**	18.52	18.52	**37.04**
Offshore Fixed	797.47	659.45	247.08	**1704**	57.97	3.05	**61.02**
Offshore Floating	800.31	2303.60	501.10	**3605**	62.18	3.27	**65.45**

Figures 6.1 and 6.2 respectively show the current levelised cost of electricity from solar photovoltaic parks and wind farms. Then, Figure 6.3 shows the onshore distribution of the cheapest technology according to the respective LCOE. As expected, most of the territory is filled with solar PV since its CapEx and OpEx are close to half and one–third that of wind, respectively. Moreover, both countries have exceptional solar irradiance during the year, which leads to higher capacity factors, and further favours solar LCOE.

Finally, Figure 6.4 displays the present levelised cost of electricity in the suitable locations of both countries. The dominance of cheap onshore production is evident, with LCOEs oscillating between 17.43 EUR_{2020}/MWh to 37.45 EUR_{2020}/MWh in Portugal and 22.28–40.43 EUR_{2020}/MWh in Italy. On the contrary, offshore wind with floating devices is still the most expensive way to produce electricity nowadays, with LCOEs as high as 110 EUR_{2020}/MWh in Portugal and 435 EUR_{2020}/MWh in Italy. This fact is due to the technology's very high capital and operational expenditures, as well as the low capacity factors of some regions.

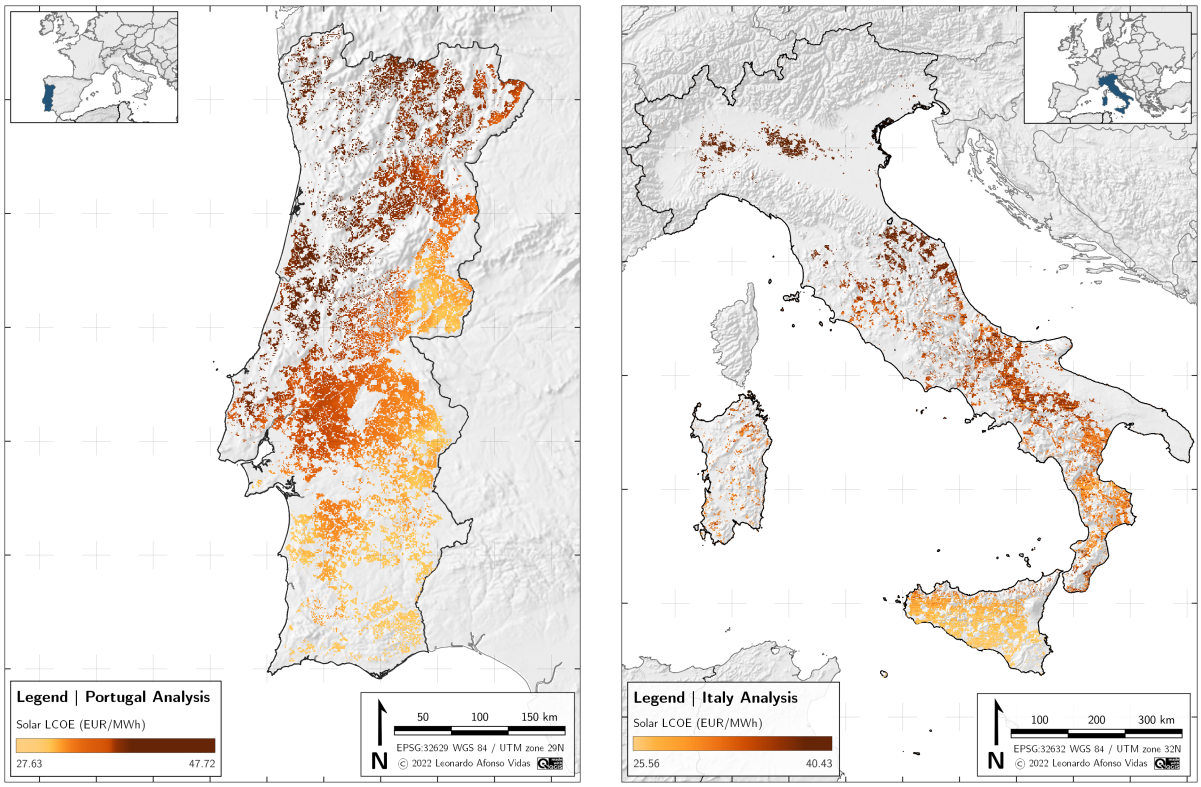

(a) Portugal (b) Italy

Figure 6.1: Current solar levelised cost of electricity in eligible locations of selected countries.

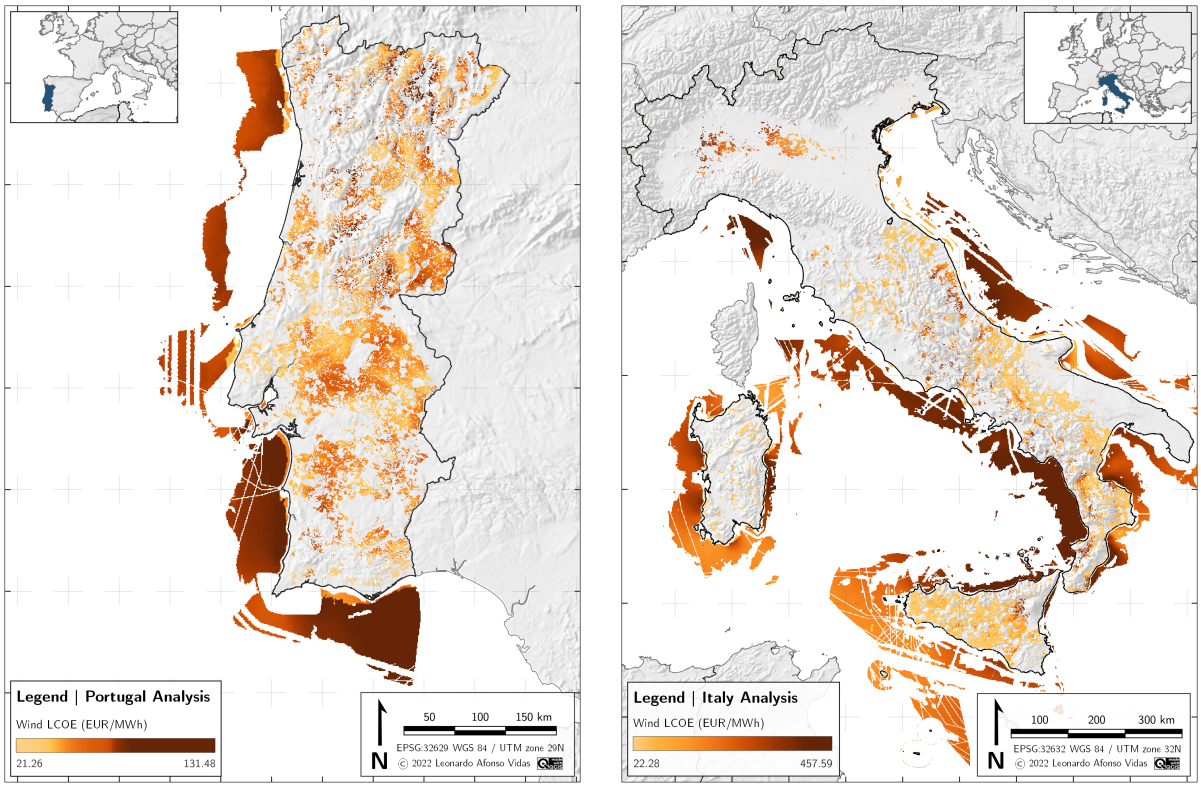

(a) Portugal (b) Italy

Figure 6.2: Current wind levelised cost of electricity in eligible locations of selected countries.

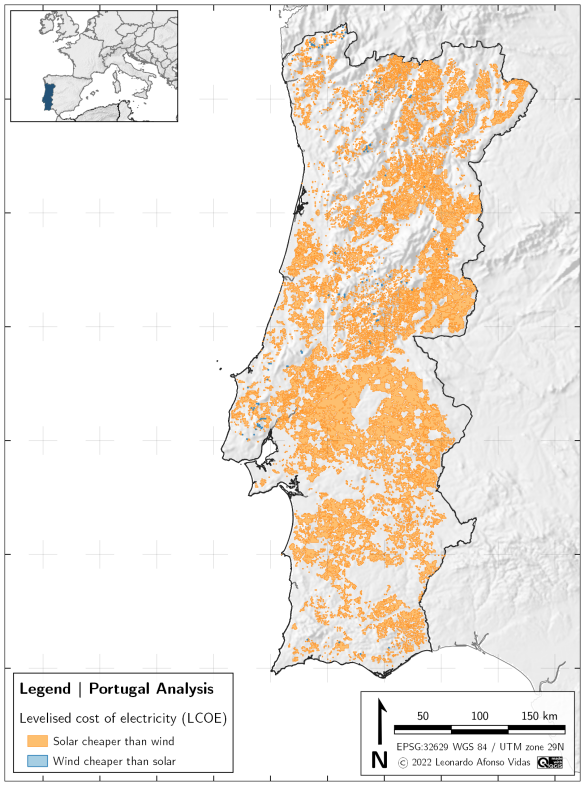

(a) Portugal

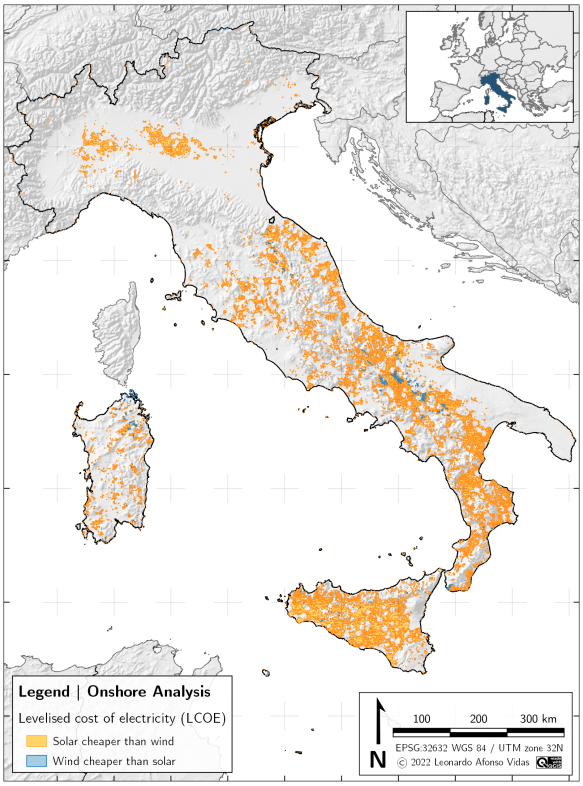

(b) Italy

Figure 6.3: Distribution of onshore RES technologies based on the cheapest levelised cost of electricity.

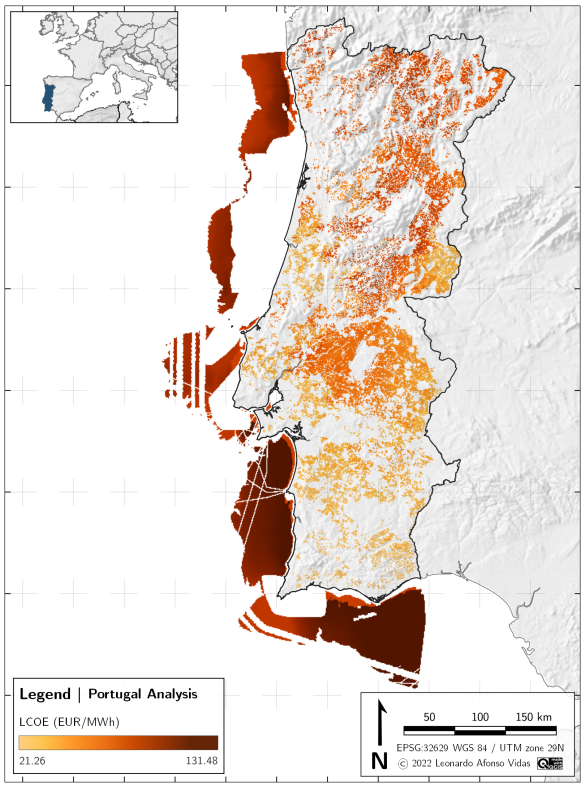

(a) Portugal

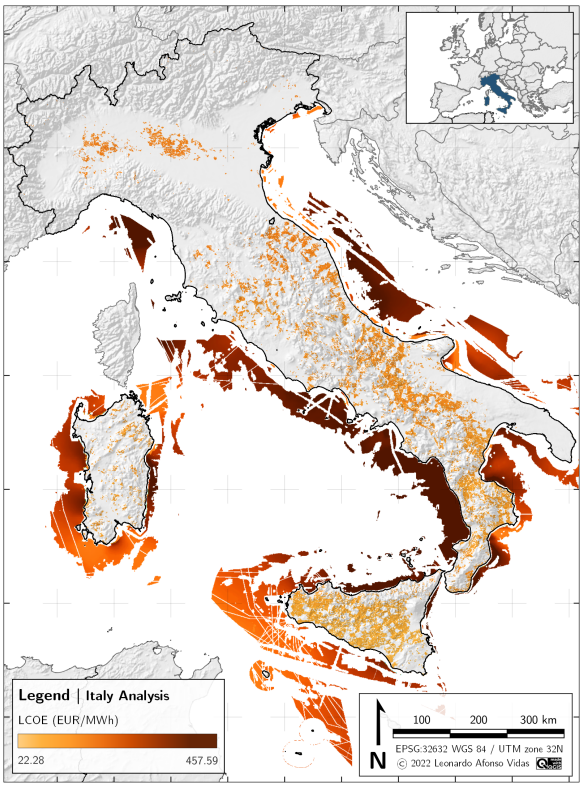

(b) Italy

Figure 6.4: Current levelised cost of electricity in eligible locations of selected countries.

6.2 Hydrogen Production Potential

The oversize factor must first be determined to access the potential for extensive hydrogen production in a meaningful way. This ratio between the RES installed capacity and the electrolyser is computed to yield the lowest LCOH in each suitable location. Hence, the optimisation algorithm is run in three points per technology for each country, with the chosen locations reflecting every set's minimum, average and maximum capacity factors. Table 6.2 outlines the results of said simulations.

Table 6.2: Summary of results: optimisation algorithm.

		Technology		— Point Location — LAT	LON	LCOH (EUR/kg)	LCOH$^{\odot}$ (EUR/kg)	GAP (%)	$P^{\odot}_{RES}$ (MW)	$P^{\odot}_{H_2}$ (MW)	Oversize Factor
ITALY	Onshore	Solar	I	36°45'21.87"	11°59'32.45"	10.89	8.05	26.08	50.27	25.81	1.95
		Solar	II	41°11'35.24"	15°21'54.14"	12.41	9.08	28.83	37.30	18.17	2.05
		Solar	III	46°10'7.52"	12°0'20.73"	13.28	9.64	27.41	27.89	13.35	2.09
		Wind	I	36°45'21.87"	11°59'32.45"	4.57	4.54	0.66	2.51	2.51	1.00
		Wind	II	41°11'35.24"	15°21'54.14"	13.18	12.29	6.75	206.44	129.37	1.59
		Wind	III	46°10'7.52"	12°0'20.73"	19.13	18.81	1.67	309.17	143.37	2.16
	Offshore	Fixed	I	41°11'58.16"	9°33'11.76"	16.41	16.12	1.77	12.07	10.02	1.20
		Fixed	II	42°0'14.88"	15°32'56.79"	22.48	21.05	6.36	56.09	35.34	1.58
		Fixed	III	45°41'49.34"	13°32'0.06"	25.19	24.36	3.30	7.73	6.03	1.28
		Float	I	41°34'3.17"	11°7'40.84"	23.56	23.53	0.12	85.97	84.25	1.02
		Float	II	41°18'44.71"	8°33'59.20"	31.02	30.90	0.39	29.49	27.43	1.08
		Float	III	43°19'39.62"	9°37'13.07"	37.93	37.72	0.55	11.66	10.49	1.11
PORTUGAL	Onshore	Solar	I	37°6'56.93"	-8°26'2.17"	10.26	7.79	24.07	25.43	13.09	1.94
		Solar	II	40°12'20.77"	–8°0'20.88"	12.27	9.02	26.49	50.28	25.10	2.00
		Solar	III	41°52'29.78"	–7°41'54.12"	12.31	9.03	26.65	16.89	7.99	2.11
		Wind	I	37°6'56.93"	–8°26'2.17"	5.02	4.98	0.79	93.17	87.23	1.07
		Wind	II	40°12'20.77"	–8°0'20.88"	23.12	19.96	13.67	72.43	33.74	2.15
		Wind	III	41°52'29.78"	–7°41'54.12"	28.18	23.97	14.93	65.57	31.56	2.07
	Offshore	Fixed	I	39°14'47.66"	–9°23'3.84"	15.06	14.44	4.12	103.61	73.56	1.41
		Fixed	II	41°28'3.53"	–8°48'31.51"	21.68	20.32	6.27	139.88	89.84	1.56
		Fixed	III	36°58'39.17"	–7°48'14.35"	24.62	21.93	10.93	391.63	211.13	1.85
		Float	I	38°33'22.72"	–9°41'38.46"	16.53	16.46	0.42	51.43	47.83	1.08
		Float	II	37°46'40.66"	–9°8'46.95"	15.35	15.27	0.52	11.92	10.93	1.09
		Float	III	36°58'13.86"	–7°48'14.75"	36.05	34.24	5.02	11.39	7.52	1.51

LCOH is the levelised cost of hydrogen computed by the oversimplified model (with $P_{RES} = P_{H_2}$), while **LCOH$^{\odot}$** is the outcome of the optimisation model. **GAP** shows the percentage improvement of the previous results. **P_{RES}** and **P_{H_2}** are respectively the resulting RES installed capacity and the electrolyser's nominal input power. Finally, the **Oversize Factor** is obtained after dividing these last two entities.

The next logical step is to plot this factor against the technologies considered to find a relation that can be used in the remaining points. Figure 6.5 shows just that, identifying the average oversize factor as the centroid of the results belonging to the same technology. Note how this value decreases almost linearly with the renewable energy sources presented.

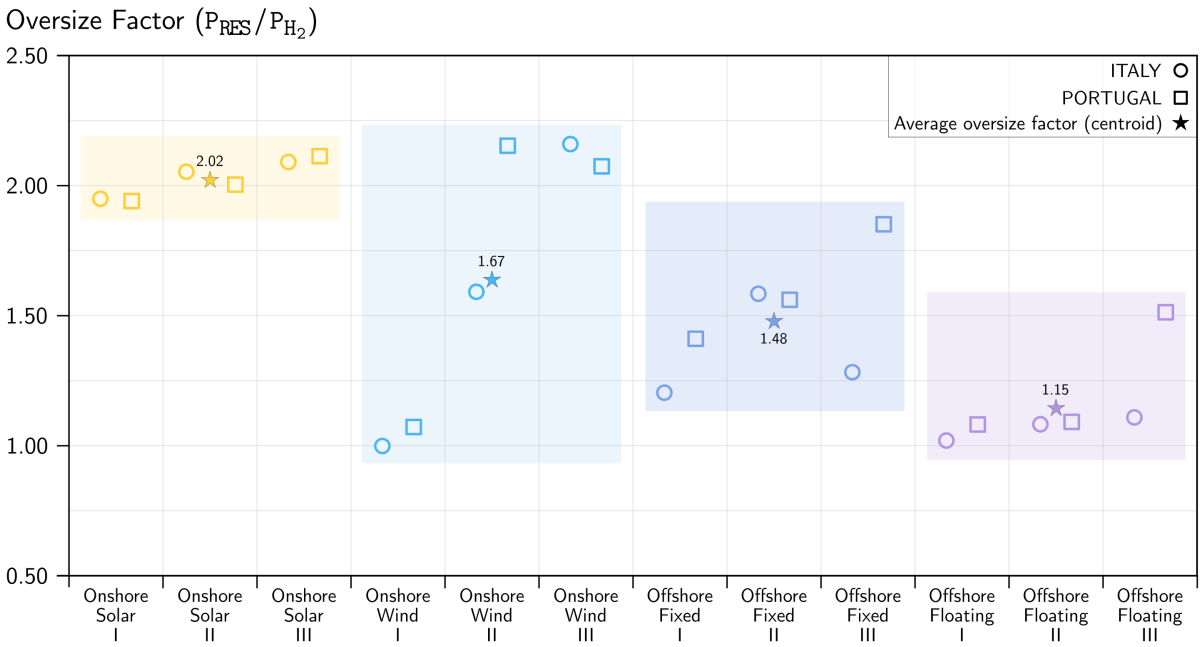

Figure 6.5: Oversize factor as function of RES technology.

Apparently, there is an inverse correlation between the oversize factor and one such entity that increases going from onshore to close–offshore, to far–offshore: most likely, the capacity factor. Figure 6.6 now shows the oversize factor plotted against the full load hours of each of the previous locations' systems. Thereby, the correlation is evident, although not entirely accurate—the green trendline is a power curve with $R^2 = 0.6467$.

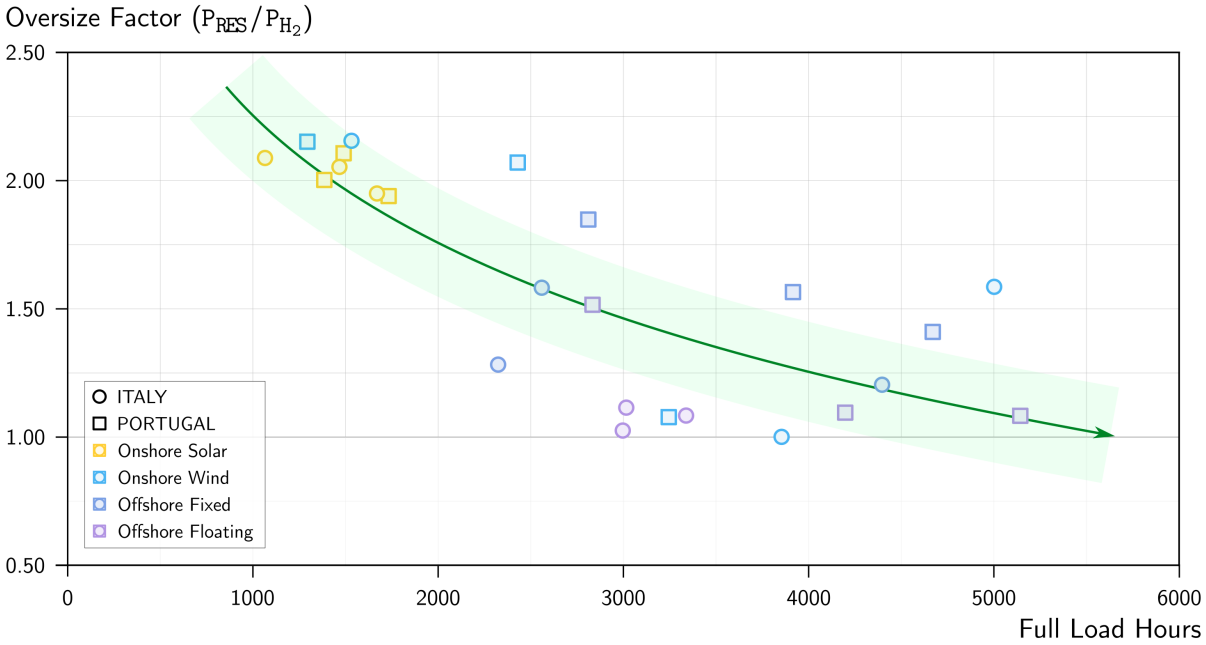

Figure 6.6: Oversize factor as function of RES full load hours.

A careful look at these charts adjudges the independence of results from the selected countries; i.e., Italy and Portugal have optimisation outcomes confirming this correlation. Whether this conclusion is a coincidence from possible similarities between the two countries remains to be determined. Further research should be devoted to this topic by applying the same method to more points in these and other countries, spread geographically around the globe, to achieve a coherent and precise relation.

Nonetheless, this approach gives a first good estimation of a model that better resembles reality—at least, better than the oversimplified solution. Therefore, the centroid values of Figure 6.5 are used to compute the LCOH for the remaining points associated with the respective technology.

Figure 6.7 starts by displaying the levelised cost of hydrogen of systems coupled with solar PV parks.

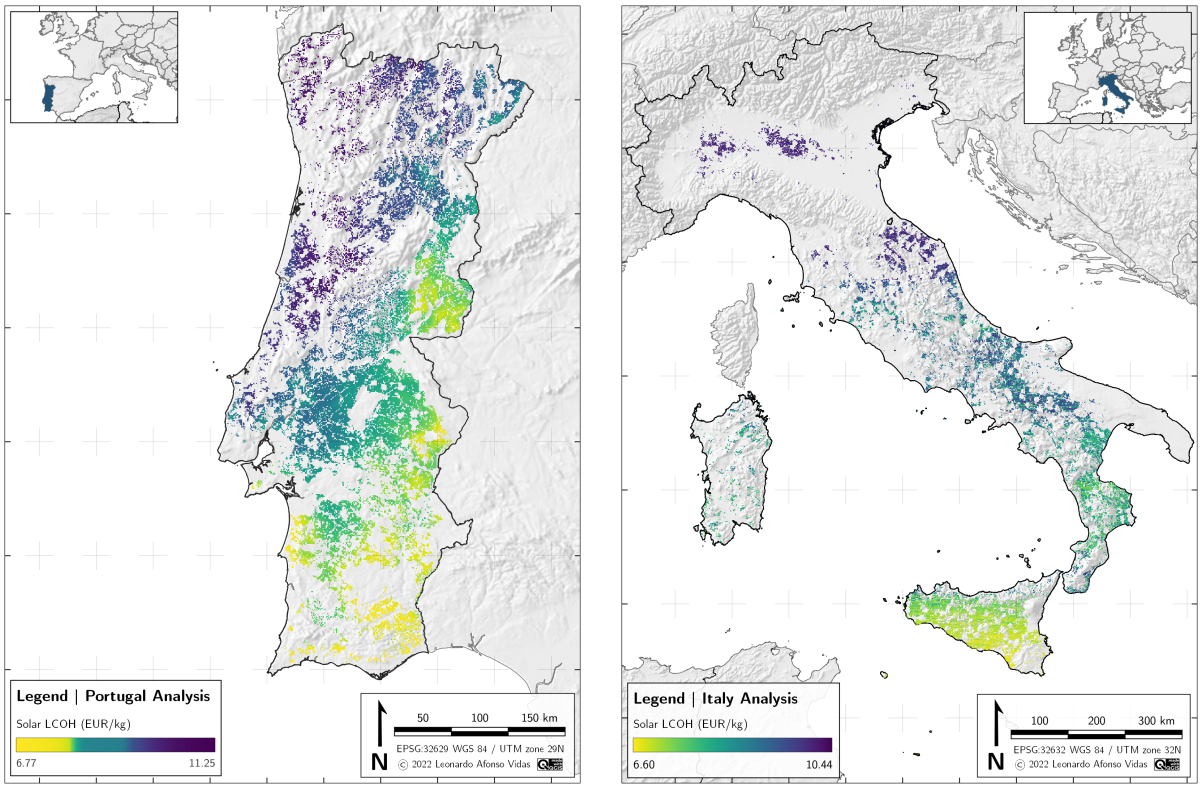

(a) Portugal (b) Italy

Figure 6.7: Current solar levelised cost of hydrogen in eligible locations of selected countries.

Looking at these maps, one main conclusion to take is the clear latitude–stratification of the LCOH in both countries; i.e. the cost of producing solar hydrogen is lower in the South than in the North of Italy and Portugal. As will be seen later, these results are directly linked to the solar capacity factor values in these regions, which are also higher in the South.

The same cannot be said of wind hydrogen production, presented in Figure 6.8. In this case, along with no specific stratification of the LCOH, the relationship with the full load hours of the systems is also not evident. Note that while the highest capacity factors are far–offshore, to be used by floating turbines, these regions do not yield the lowest levelised cost of hydrogen—primarily due to the still excessive capital and operational expenditures, summarised in Table 6.1.

Following a similar procedure to that used with the LCOE, the cheapest onshore RES technology to produce green hydrogen is now determined for each location and mapped out in Figure 6.9.

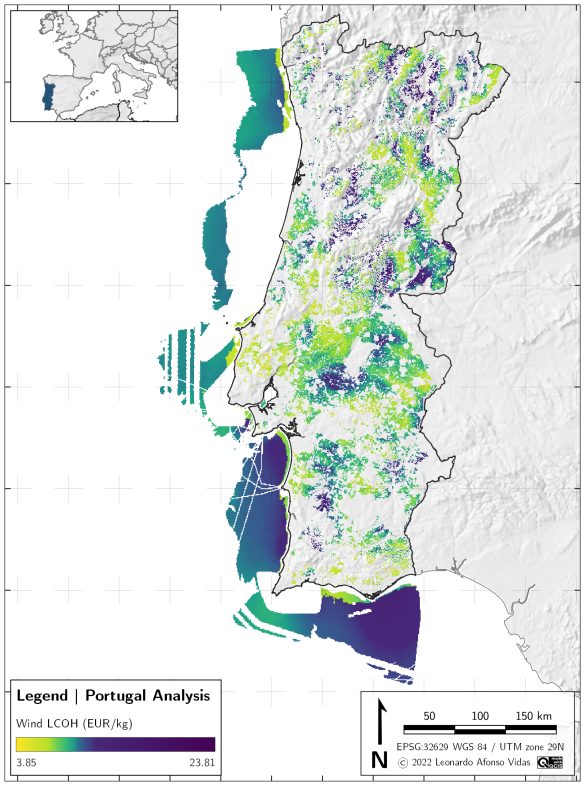

(a) Portugal

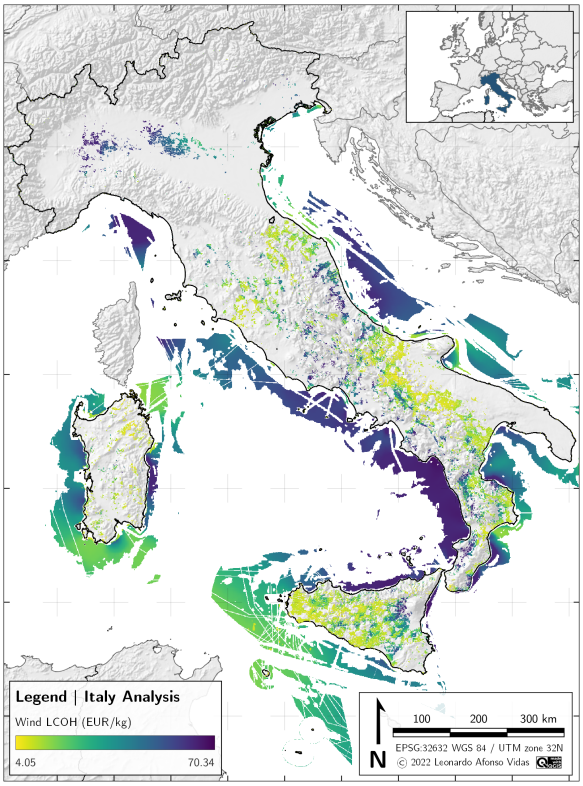

(b) Italy

Figure 6.8: Current wind levelised cost of hydrogen in eligible locations of selected countries.

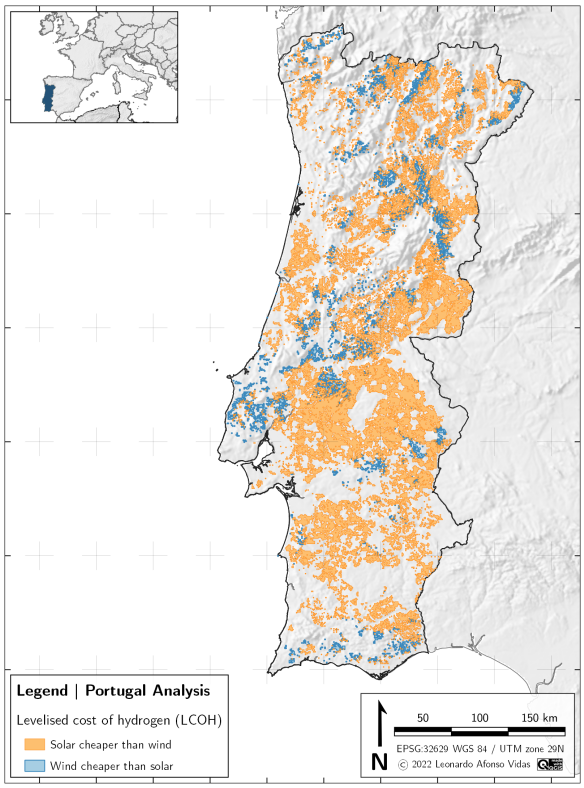

(a) Portugal

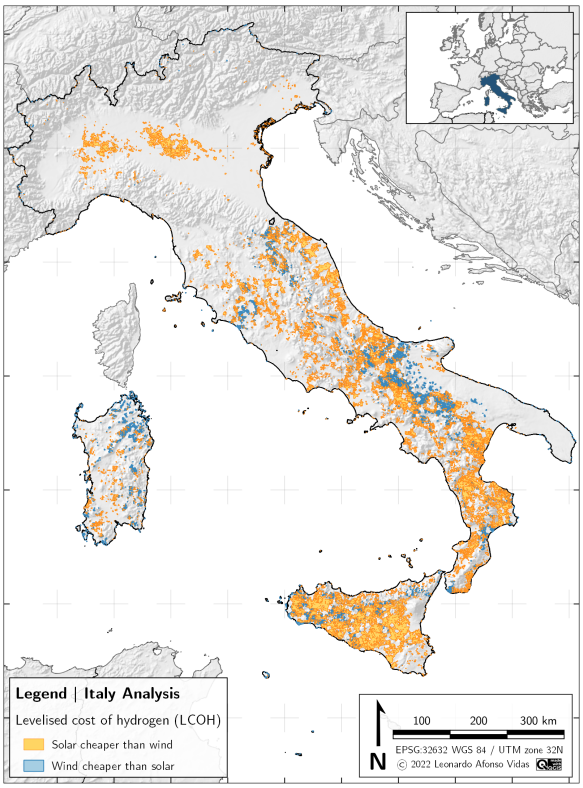

(b) Italy

Figure 6.9: Distribution of onshore RES technologies based on the cheapest levelised cost of hydrogen.

A careful look at these maps discerns some distinction to the ones of Figure 6.3. Contrary to what could be initially assumed, in the onshore regions considered, the technology with the lowest LCOE is not necessarily the technology with the lowest LCOH. This detail is essentially explained by the different WACCs considered, which impact solar and wind costs. The calculation of the LCOH naturally takes into account the costs of the electrolyser and the production of hydrogen, which in turn are affected by the nominal and real WACCs. Since these values are different for solar and wind technologies, it may happen that some regions, despite having a lower solar LCOE, end up having a lower wind LCOH.

With these regions identified, Figure 5.2 maps out the current overall levelised cost of hydrogen in both Portugal and Italy. This illustrates one of the main findings and the second expected deliverable of this thesis, as objectively established in Section 1.3.

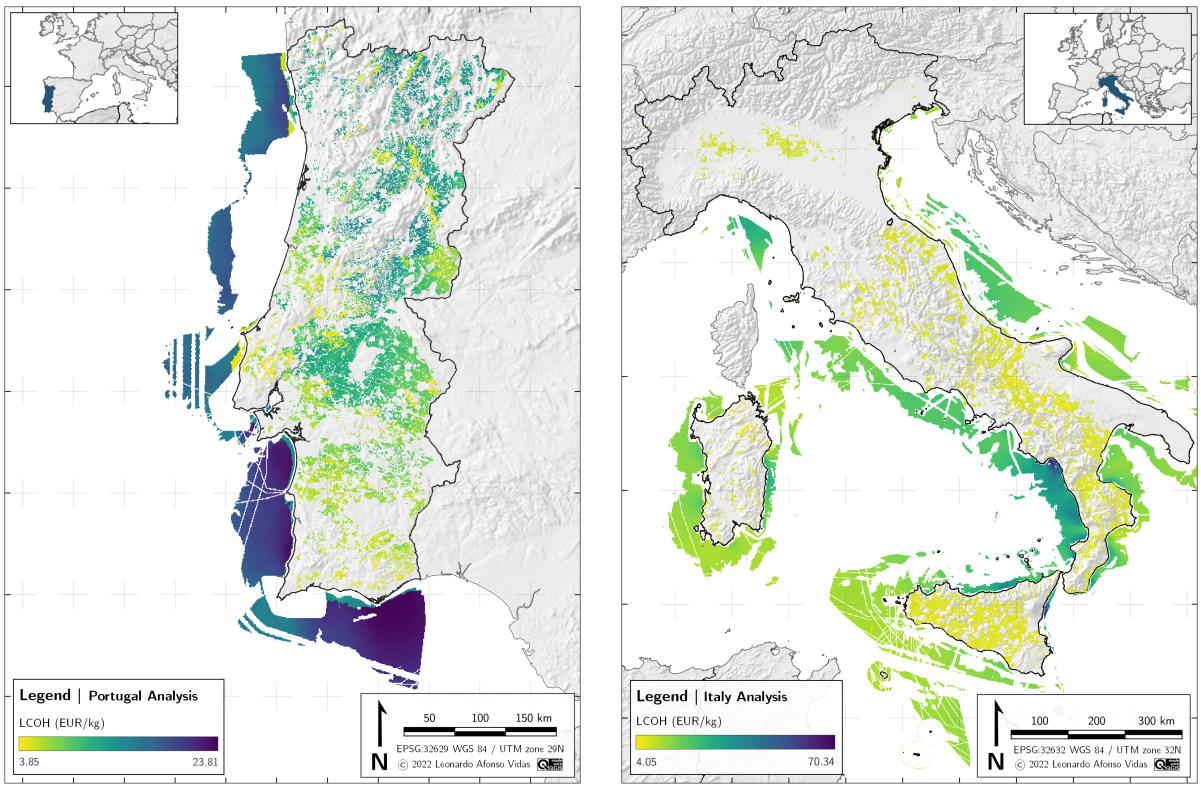

(a) Portugal (b) Italy

Figure 6.10: Current levelised cost of hydrogen in eligible locations of selected countries.

A direct comparison can be made between the two countries, with the initial caveat that the colour–spectrum scale of the legend is not the same. Without this notice, most places along the coast of Portugal might look much more expensive than along the Italian coast—which is indeed not the case.

Either way, the LCOH is generally lower onshore than offshore; in Portugal, onshore costs averages at 6.85 EUR/kg, while in Italy, the average is 7.25 EUR/kg (as opposed to 10.48 EUR/kg and 15.81 EUR/kg, respectively, offshore). While the main reason for the disparity between on/offshore costs is the cost structure of each technology (summarised in Table 6.1), the primary cause for the discrepancy in values between the two countries is related to solar and wind exposure. This quantity is commonly measured by the capacity factors, whose obtainment is clarified in footnotes 1 and 2 of Subsection 5.2.2. The maps of Figures 6.11 and 6.12 respectively depict both countries' annual average solar and wind capacity factors.

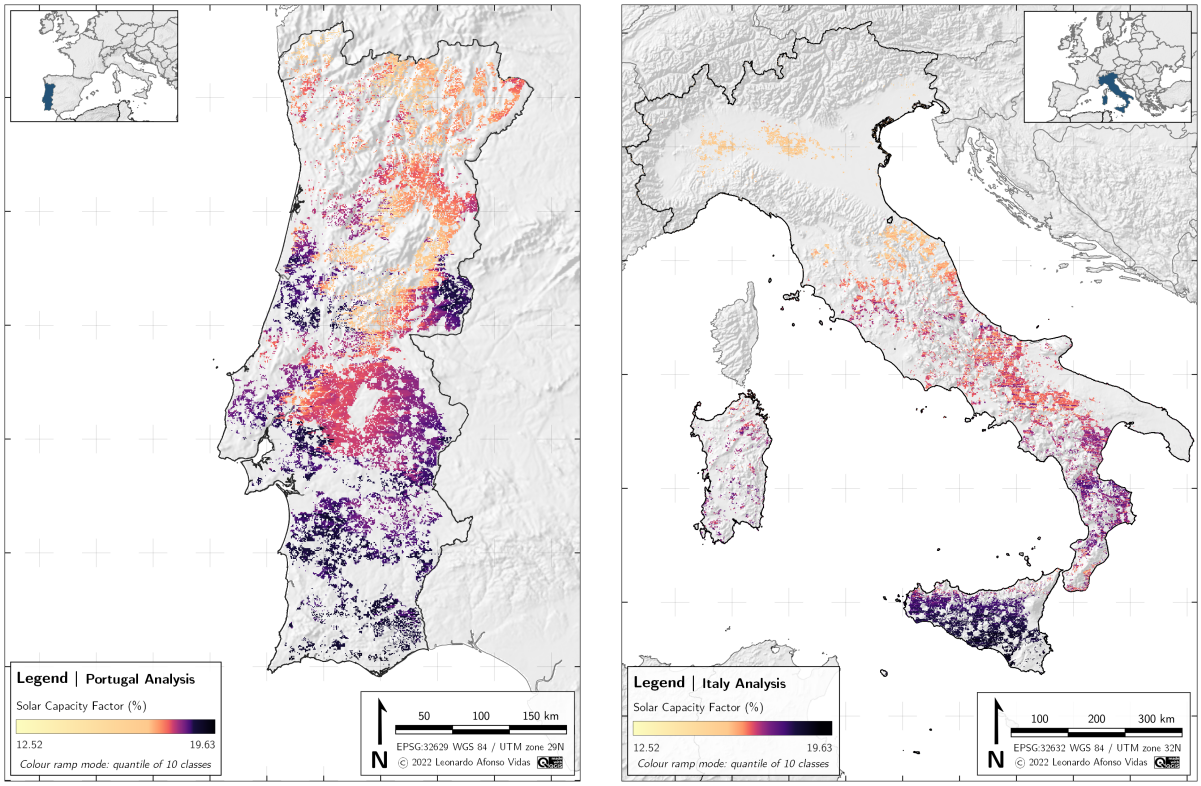

(a) Portugal (b) Italy

Figure 6.11: Yearly average solar capacity factor in onshore eligible locations of selected countries.

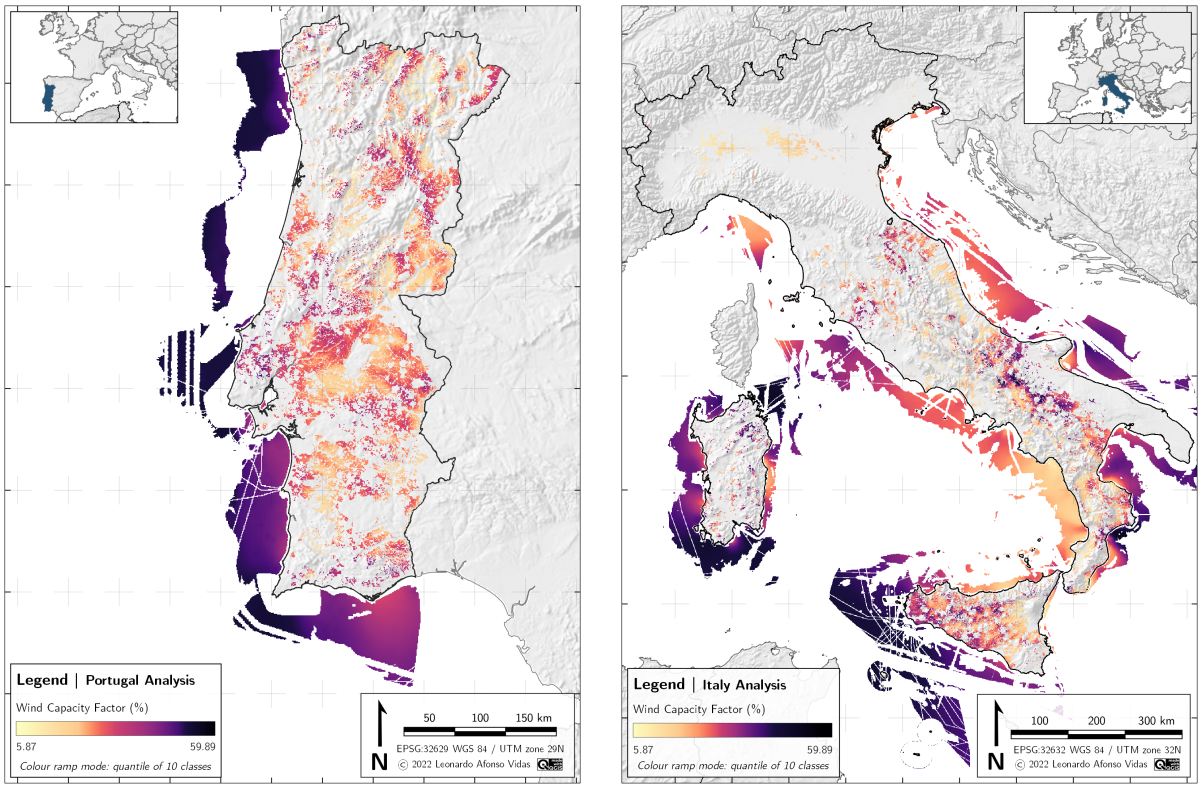

(a) Portugal (b) Italy

Figure 6.12: Yearly average wind capacity factor in eligible locations of selected countries.

Regarding solar exposure, both countries have a clear North–South separation. The South is predominantly more exposed to the sun, especially Sicily in Italy and the Algarve and Alentejo regions in Portugal; these territories consistently have FLH values approaching 1700 hours. The Center and North zones, not so much, reaching just above 1000 full load hours. However, Portugal does have some northern regions with high solar exposure, namely close to the shore and the eastern border, in the district of Castelo Branco. This characteristic is the preeminent explanation for the lower LCOH average presented before.

Concerning wind exposure, there is a crucial acknowledgement of the differences between onshore and offshore locations. Portugal, in particular, has significant disparities between inland full load hours, which average about 2423 hours, and locations in its exclusive economic zone, that approach 4200 FLH on average. This phenomenon is not so pronounced in Italy, perhaps due to its EEZ being enclosed within the Mediterranean Sea instead of out in the open of the Atlantic Ocean—as Portugal's is. As mentioned in Subsection 5.3.1, higher wind speeds (which correlate to higher capacity factors) depend on lower roughness lengths, which ascribe to protruding landscapes that impact wind patterns.
So, although the whole coast of Sardinia and the West coast of Sicily display high capacity factors, the onshore/offshore average is not that much different: 2103 FLH for the former and 2995 FLH for the latter.

Onshore Hybrid Optimisation

In addition to the results obtained from the traditional optimisation process—shown in Table 6.2—, the model is further used to perform a specialised hybrid optimisation in selected onshore locations of both countries. Together with the algorithm procedure mentioned above, this operation constitutes the third and last objective expected to be delivered from this thesis, as stated in Section 1.3.
Table 6.3 summarises the algorithm outcomes of the hybrid optimisation.

Table 6.3: Summary of results: hybrid optimisation.

	Onshore Technology		**— Point Location —** LAT	LON	**LCOH** (EUR/kg)	**LCOH$^{\odot}$** (EUR/kg)	**$P^{\odot}_{pv}$** (MW)	**$P^{\odot}_{wd}$** (MW)	**$P^{\odot}_{H_2}$** (MW)
ITALY	Solar Wind	I	36°45'21.87"	11°59'32.445"	10.89 4.57	**3.73**	0.01	164.90	164.59
	Solar Wind	II	41°11'35.243"	15°21'54.14"	12.41 13.18	**7.74**	10.59	7.06	7.07
	Solar Wind	III	46°10'7.516"	12°0'20.729"	13.28 19.13	**9.15**	41.84	0.03	20.87
PORTUGAL	Solar Wind	I	37°6'56.929"	–8°26'2.165"	10.26 5.02	**4.06**	1.77	7.24	7.06
	Solar Wind	II	40°12'20.773"	–8°0'20.882"	12.27 23.12	**8.57**	27.48	0.00	14.01
	Solar Wind	III	41°52'29.78"	–7°41'54.121"	12.31 28.18	**8.58**	20.95	0.10	10.41

This procedure aims to join both onshore technologies in the same location and compute each installed capacity to minimise the levelised cost of hydrogen; a generalised use of this method was not possible due to insufficient computational resources.

In Table 6.3, the simplified solar/wind LCOH is first provided for every point and then the optimised LCOH, followed by each technology's nominal power. As expected, $\mathbf{LCOH}^{\odot}$ is always (much) lower than any individual **LCOH**, which inherently validates the model. Another relevant aspect to notice in these results is the predominant correlation of the preferred RES technology and the respective **LCOH**; i.e., for each location, the renewable source with the lowest **LCOH** is the one that later has the highest installed capacity in the $\mathbf{LCOH}^{\odot}$ computation. Moreover, $\mathbf{P_{H_2}}$ is always smaller than the sum of $\mathbf{P_{pv}}$ and $\mathbf{P_{wd}}$, as initially constrained.

To better understand the scale of improvement provided by the optimisation algorithm, Figure 6.13 illustrates the central columns of Table 6.3 as a bar chart.

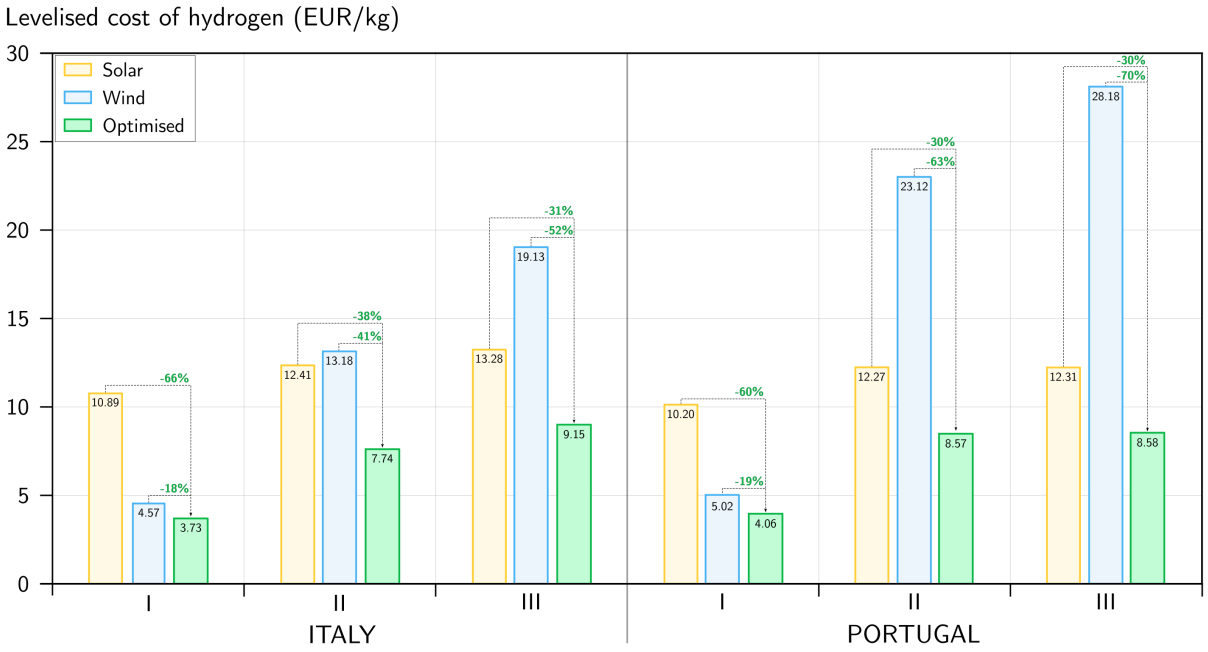

Figure 6.13: Onshore hybrid optimisation.

The yellow and blue bars respectively depict the LCOH from solar and wind systems alone, while the green bars represent the optimised hybridisation of both technologies.

The true power of the algorithm is evident in the relative reductions displayed; in the specific case of these locations, it can be as high as 70%. It could be even higher for other locations, not addressed in this analysis. These reductions may lead to savings to the project owner in the order of €2 million for a 100–ton annual demand. With an annual demand of just 500 tons, the savings can reach close to €10 million.

With the paramount results presented, all that remains is a sensitivity analysis for the most relevant parameters of the economic model.

6.3 Sensitivity Analysis

Any benchmark economic analysis benefits from an in–depth sensitivity analysis. Such assessment intends to determine how the objective variable is influenced by changes in the input parameters in a way that aims to predict the outcome of a decision given a specific range of variability.

In the particular case of this thesis, the objective variable is the levelised cost of hydrogen; its sensitivity is tested against several input parameters, comprised of the most significant variables of the economic model: the system full load hours, the lifetime of the project, the selected nominal WACC, inflation, the RES CapEx, OpEx and degradation rate, and the electrolyser CapEx, OpEx, ReplEx and degradation rate.

Each of these parameters is alternately subjected to a relative variation of -50% to $+50\%$, in intervals of 10%. The LCOH variance is computed through a traditional relative percent error formula for each evaluation. The process is repeated for the four RES technologies and illustrated in appropriate charts.

Figure 6.14 shows the results of the sensitivity analysis applied to solar LCOH.

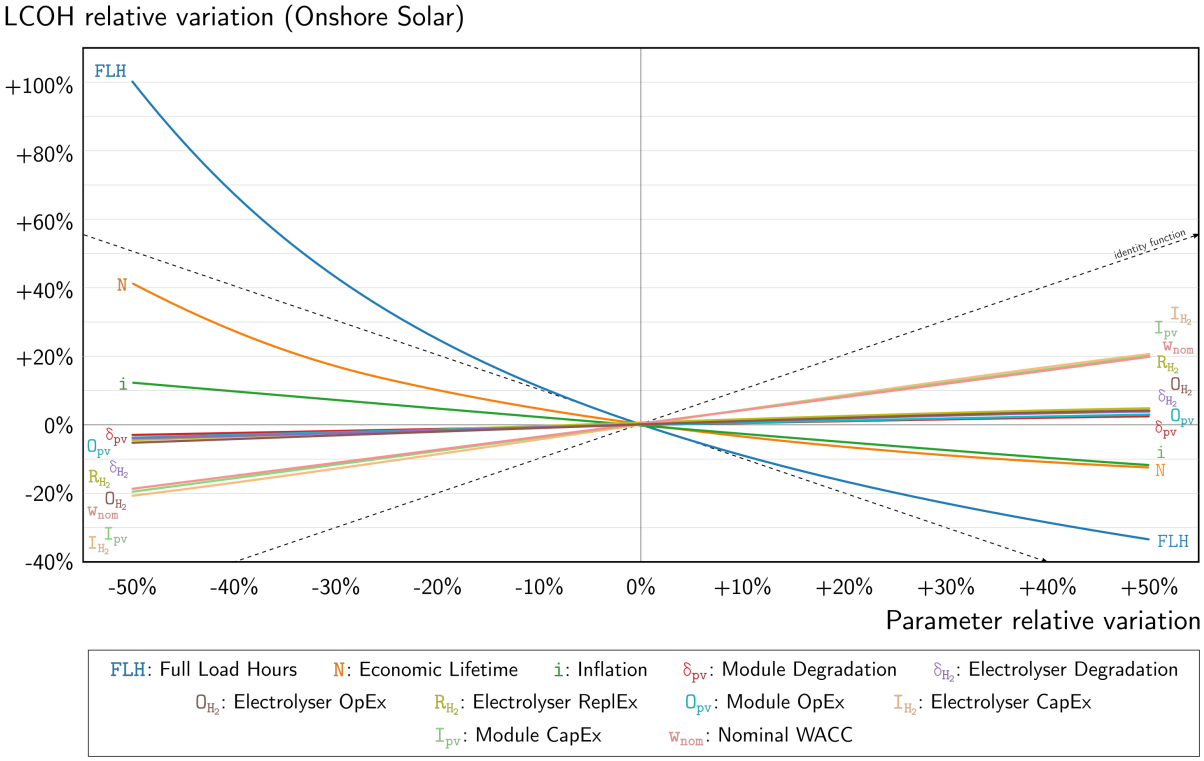

Figure 6.14: Sensitivity analysis: onshore solar.

At first glance, three distinct groups can be discerned: one comprising the full load hours, the economic life of the project and inflation, which are inversely proportional to the levelised cost of hydrogen; a second group that consists of both degradations, both operational expenses and the electrolyser replacement cost, which directly affect the LCOH but not more than 10%; and a third group, including both capital expenditures and the nominal WACC, that directly impact the LCOH by more than 10%.

This pattern repeats for the sensitivity analysis of onshore wind LCOH, represented in Figure 6.15.

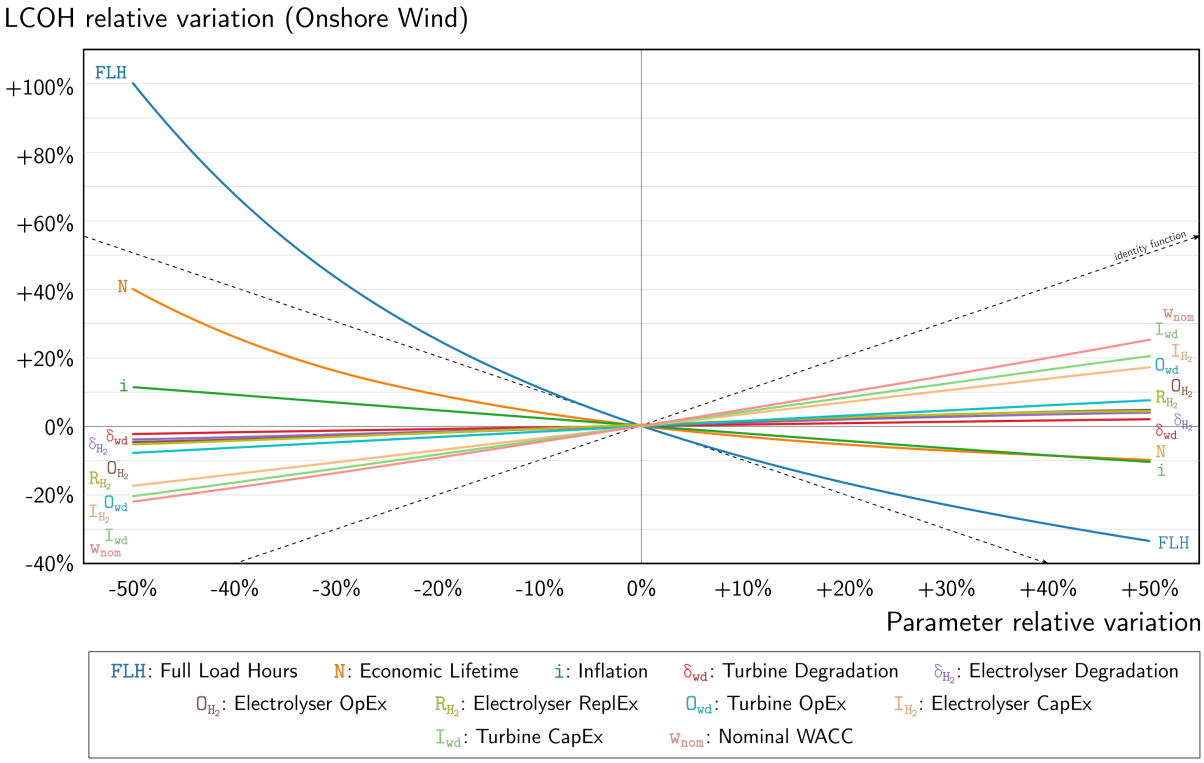

Figure 6.15: Sensitivity analysis: onshore wind.

Concerning these two charts, it is evident how the full load hours are the predominant variable that most influences the levelised cost of hydrogen—locations whose FLHs are half as many as others have double the LCOH. The project lifetime and inflation are the subsequent most relevant variables, respectively varying the levelised cost of hydrogen by up to 40% and 10% when reduced to half. It makes sense that the LCOH would vary inversely with these three parameters since 1) a lower capacity factor leads to less energy being generated and less hydrogen being produced for the same plant capacity—thus increasing the share of the overall cost structures; 2) a shorter economic life gives projects limited time for the production to compensate the investment costs, then increasing each unit–cost of hydrogen; and 3) a lower inflation rate means diminished differences between total expenditures and global hydrogen yield, which removes the advantage of locking energy 'costs' at a constant initial rate—as explained in Subsection 5.1.2.

The next group essentially consists of the same variables, although in distinct orders for both onshore technologies. Either way, degradation rates and operational expenses represent the most negligible influences of all the variables analysed; future reductions of up to 50% in these variables would only decrease the LCOH by about 5%. Therefore, although necessary, this should not be the focus of forthcoming developments.

Finally, the third group, comprising capital expenditures and nominal WACC, makes up the set of input parameters that directly impact hydrogen's levelised cost the most. Expected reductions in turbine/module and electrolyser CapEx can lead to hydrogen being 20% cheaper; so, for an initial LCOH of 5 EUR/kg and a scenario of 1000–ton yearly hydrogen demand, this implies savings in the order of one million euros.

Figures 6.16 and 6.17 respectively display the corresponding charts for offshore wind with fixed foundations and floating devices. The general look is similar to the previous ones, with a few notable distinctions identified and described below.

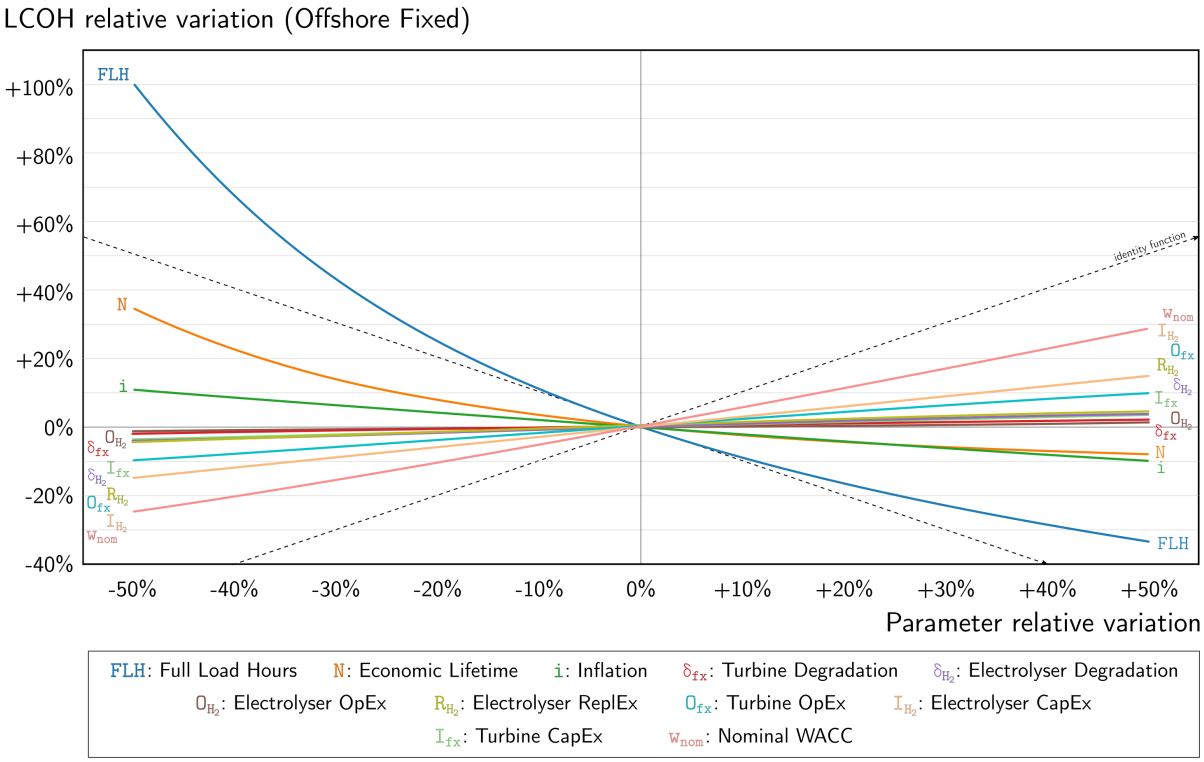

Figure 6.16: Sensitivity analysis: offshore fixed.

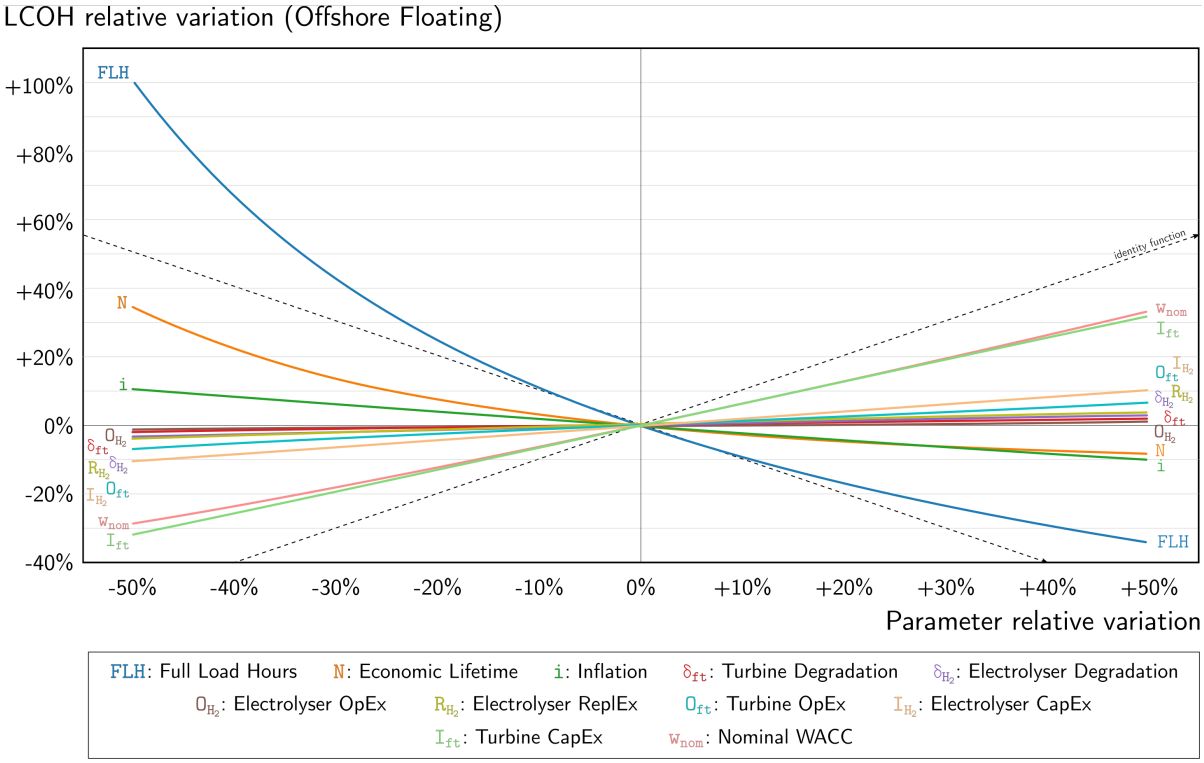

Figure 6.17: Sensitivity analysis: offshore floating.

The fundamental disparities concern the aforementioned two last groups. Here they are not as well defined as before but instead seem to merge into a single extended group with relative variations ranging from less than 1% to more than 30%.

Both turbine and electrolyser degradations and operational expenses continue to be the least impactful parameters (less than 10%) to the offshore LCOH. On the other hand, the variables with the most significant influence are the electrolyser CapEx, the nominal WACC and the RES CapEx. The latter is especially relevant to offshore floating devices, which have the highest capital expenditures of all renewable energy sources. Hence, future research aimed at decreasing this LCOH component should be incentivised.

Two more important elements remain to be analysed: the electrolyser electric efficiency (η) and net production rate (ρ). These two were purposefully left out of the previous charts since, in addition to having the same line profile between them, they have the same profile as the capacity factor; this coincidence would make the chart harder to read. So, Figure 6.18 illustrates both variables as a set of four superimposed curves, one for each RES technology.

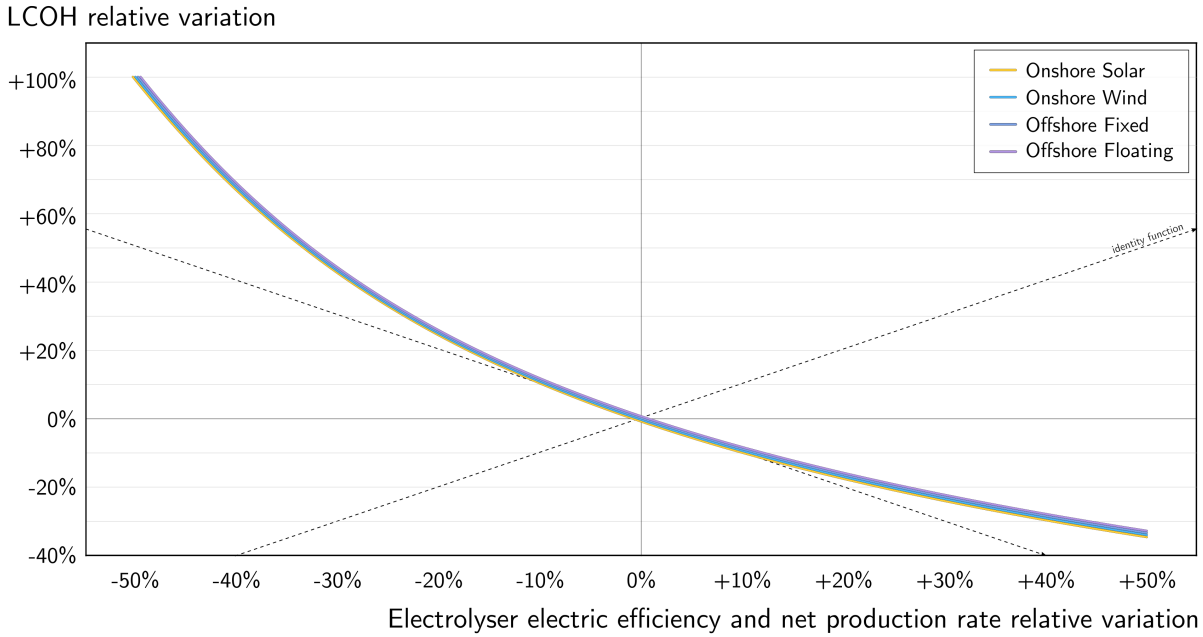

Figure 6.18: Sensitivity analysis: electrolyser efficiency and production rate.

These two parameters undoubtedly show the most considerable potential for improvement on the levelised cost of hydrogen; when combined, even small positive developments can lead to steep decreases in the future cost of producing hydrogen—thus, should be placed at the forefront of electrolyser development research.

7 Conclusions

This chapter concludes the investigation described so far. Section 7.1 summarises the key findings related to the research questions, discussing the value and contributions thereof, while Section 7.2 presents a review of the study's limitations, proposing opportunities for future research.

7.1 Achievements

This study aimed to identify eligible regions to install green–hydrogen production facilities. Moreover, this study intended to find the configurations of renewable energy sources and electrolysers that return the lowest lifetime production cost in specific locations while also obtaining a preliminary oversize factor to apply in extensive geographical analysis.

The land availability of both countries is accomplished through a comprehensive 3–part methodology, based on state–of–the–art literature. The three phases comprise the different stages of any standard geographical information system analysis, from data collection and handling to data exclusion and further evaluation. After establishing an on/offshore geospatial framework, the land–eligibility operation gathered multiple datasets that are managed to map out the desired outcome. In this particular case, datasets are collected from multiple sources and assigned to environmental, legislative, safety and technical criteria. Further evaluation includes region–specific physical attributes, such as ground elevation and slope, air temperature, wind speed and seafloor bathymetry.

The geometric subtraction of these incompatible regions from the total surface of the countries yields the final eligible locations. The main findings are the following:

- Italy has 37 637 km^2 and 104 338 km^2 of onshore and offshore area available, respectively, corresponding to 12.50% and 19.44% of the total area.
- Portugal has 24 734 km^2 and 22 495 km^2 of onshore and offshore area available, respectively, corresponding to 27.79% and 7.13% of the total area.
- Despite the eligible locations being only small percentages of the total surface of the countries, their thorough use would be enough to produce millions of tons of hydrogen annually.

These findings represent an unprecedented achievement for both Italy and Portugal in the sense that they close a critical research gap related to these two countries. Such material data may be a valuable asset to any economic analysis conducted by municipalities and even the central government.

The study then examines the hydrogen economic fairways in the locations mentioned earlier, computing the levelised cost of hydrogen through an extensive sequence of formulations. A simplified general model is created per present–day international literature, based on the maximum allowed capacity of the renewable power plants. Still, this model improves on the existing ones by using an oversize factor determined via an optimisation algorithm. Regarding this finding, the main conclusions are:

- There is an apparent inverse correlation between the oversize factor and the full load hours of the renewable energy system contemplated. This means that for RES technologies with higher capacity factors, the coupled electrolyser should approximate the size of the renewable power plant.
- Making use of this factor, the LCOH generally yields lower values onshore than offshore. The averages for Italy and Portugal are respectively 7.25 EUR/kg and 6.85 EUR/kg (onshore), and 15.81 EUR/kg and 10.48 EUR/kg (offshore).
- The fundamental cause of disparity between onshore and offshore values is the cost structure of each technology; the leading explanation for the value discrepancy between both countries is the solar/wind exposure. The capacity factor is one of the most predominant aspects affecting the levelised cost of hydrogen.

The introduction of this oversize factor significantly improved the study's credibility, producing results ever closer to reality. This procedure constructively challenges the standard way of assessing large–scale green–hydrogen projects and thus may be replicated in subsequent analysis as a means to make estimations better resemble the real world.

Lastly, the algorithm developed to obtain the oversize factor, as part of the optimised general model, is in itself one of the major outcomes of this thesis. Its foundation is grounded on a comprehensive problem setting and mathematical formulation, comprising the detailed definition of index sets, parameters, support and decision variables, as well as an objective function constrained by ten equations. When used on a country–specific set of points, the following was concluded:

- Single configurations, where only one renewable energy source is coupled to the electrolyser, obtained LCOH reductions in Italy and Portugal of up to 7% and 11% (offshore), and 29% and 27% (onshore), respectively. Such cutbacks could translate to hundreds of thousands of euros in savings for the project investors, if not more, depending on the established hydrogen demand.
- Hybrid onshore configurations, where both solar and wind power plants are connected to the electrolyser, generated the highest reductions in the cost of producing hydrogen. In the cluster of three selected locations, the LCOH decreased as far as 52% in Italy and 70% in Portugal. Reductions such as these could lead to €10 million in savings to the project owner, for a 500–ton annual demand.

These results validate the initial premise of the algorithm in providing the optimal computation of the levelised cost of hydrogen with notable success. A model with such attributes was yet to be found in the literature, evidencing its important contribution towards addressing this gap.

In the end, an in–depth sensitivity analysis of the economic model is presented, encompassing five symmetric relative variations of 11 parameters assigned to each renewable energy source. The tests originated three unique groups of variables:

- The first group, including the full load hours, the electrolyser electric efficiency and net production rate, the project's economic lifetime and inflation, inversely affect the LCOH the most—ranging from $+100\%$ to -32%.
- The second group comprises the nominal WACC and both systems' capital expenditures, and most directly impact the LCOH—from -32% to $+39\%$.
- The third group, containing both system' degradation rates and operational expenses, and the replacement cost of the electrolyser, has the least impact on the levelised cost of hydrogen—from -7% to $+8\%$.

7.2 Future Work

Despite the conscious effort to make this thesis as complete an investigation as possible, limitations exist that, once settled, could further increase the potential of its results. The following is a non–exhaustive list of such limitations, alongside recommendations to future studies that might address and build upon the findings of this work.

- Concerning the computation of the levelised cost of hydrogen:
  - Consider regional water consumption costs (instead of a general national price) since municipalities regulate these prices according to the size of the water reserves and expected rainfall.
  - Improve the assumptions around technological learning curves, thus updating expenditure costs in long–term analysis.
  - Adjust the inflation rate and specify the financial assumptions over the weighted average cost of capital (corporate tax rate, debt:equity ratio, loan interest rate and return on equity).
  - Instead of releasing it into the atmosphere, consider the sale of the byproduct oxygen gas, which would considerably decrease the cost of producing hydrogen.
  - Include costs associated with compression, storage, transmission, distribution and delivery of hydrogen, as well as end–use adaptation costs (taking into account the potential charges that producers may face for using hydrogen storage, transmission and distribution networks).
  - Employ advanced artificial intelligence techniques to run the optimisation algorithm in both countries' complete set of locations.
- Regarding the modeling of the electrolyser:
  - Consider the non–linearities of the dynamic efficiency of the electrolyser, which decays with increasing operating time.
  - Deepen the electrochemical model description of the electrolyser, considering the reverse voltage's operational behaviour and the resistive and electrodes overpotential, among others.

- Concerning the systems of renewable energy sources:
  - Consider the regime of financial incentives for renewable energy systems of each country, which may decrease investment costs.
  - Consider the additional installation of electric batteries to store excess electricity and later use at times of insufficient generation—thus increasing the utilisation factor of the electrolyser.
  - Consider the electrolyser also connected to the grid, which is expected to be much greener in the future, thus increasing the system's utilisation factor and reducing the LCOH.

As a concluding remark, one has to acknowledge that the evidence base is fast–moving and so there can be expected gaps in the knowledge. Nonetheless, this work improves on the body of research published so far and contributes to the development of this field of study.

References

[1] International Renewable Energy Agency. *Global hydrogen trade to meet the 1.5°C climate goal: Part I – Trade outlook for 2050 and way forward*. Technical Report, ISBN: 978-92-9260-430-1. Abu Dhabi: IRENA, 2022.

[2] International Renewable Energy Agency. *Geopolitics of the Energy Transformation: The Hydrogen Factor*. Technical Report, ISBN: 978-92-9260-370-0. Abu Dhabi: IRENA, 2022.

[3] Leonardo Vidas, Rui Castro, and Armando Pires. "A Review of the Impact of Hydrogen Integration in Natural Gas Distribution Networks and Electric Smart Grids". In: *Energies* (2022). DOI: 10.3390/en15093160.

[4] International Energy Agency. *The Future of Hydrogen*. Technology Report. Available online: www.iea.org/reports/the-future-of-hydrogen (accessed on 21 July 2022). IEA, June 2019.

[5] International Renewable Energy Agency. *Hydrogen: A renewable energy perspective*. Technical Report, ISBN: 978-92-9260-151-5. Abu Dhabi: IRENA, Sept. 2019.

[6] Brais Armiño Franco. "Techno-economic assessment of hydrogen offloading systems for offshore wind farms". Available online: fenix.tecnico.ulisboa.pt/cursos/mege/dissertacao/846778572212432 (accessed on 26 August 2022). MA thesis. Instituto Superior Técnico, Oct. 2020.

[7] Karan Ramesh Narayan. "Hydrogen-Powered Long-Distance Transportation for Portugal". Available online: fenix.tecnico.ulisboa.pt/cursos/mege/dissertacao/846778572212854 (accessed on 26 August 2022). MA thesis. Instituto Superior Técnico, Jan. 2021.

[8] Charlie Groenewegen. "GIS-based site suitability analysis for solar and win to hydrogen potential in Europe and Mediterranean region in 2030 and 2040". Available online: repository.tudelft.nl/islandora/object/uuid:08a61dd0-21c0-496b-8db9-f43642f9054c (accessed on 08 August 2022). MA thesis. Delft University of Technology, Sept. 2021.

[9] Dimitra G. Vagiona and Manos Kamilakis. "Sustainable Site Selection for Offshore Wind Farms in the South Aegean—Greece". In: *Sustainability* (2018). DOI: 10.3390/su10030749.

[10] Valeria Juárez-Casildo, Ilse Cervantes, and R. de G. González-Huerta. "Solar hydrogen production in urban areas of Mexico: towards hydrogen cities". In: *International Journal of Hydrogen Energy* (2022). DOI: doi.org/10.1016/j.ijhydene.2022.06.137.

[11] Benyounes Raillani, Abdelhamid Mezrhab, Samir Amraqui, Mohammed Amine Moussaoui, and Ahmed Mezrhab. "Regression-based spatial GIS analysis for an accurate assessment of renewable energy potential". In: *Energy for Sustainable Development* (2022). DOI: doi.org/10.1016/j.esd.2022.06.003.

[12] Pandora Gkeka-Serpetsidaki and Theocharis Tsoutsos. "A methodological framework for optimal siting of offshore wind farms: A case study on the island of Crete". In: *Energy* (2022). DOI: 10.1016/j.energy.2021.122296.

[13] Tubagus Aryandi Gunawan, Alessandro Singlitico, Paul Blount, James Burchill, James G. Carton, and Rory F. D. Monaghan. "At What Cost Can Renewable Hydrogen Offset Fossil Fuel Use in Ireland's Gas Network?" In: *Energies* (2020). DOI: 10.3390/en13071798.

[14] Ozcan Atlam, Frano Barbir, and Dario Bezmalinovic. "A method for optimal sizing of an electrolyzer directly connected to a PV module". In: *International Journal of Hydrogen Energy* (2011). DOI: doi.org/10.1016/j.ijhydene.2011.03.073.

[15] Josh Eichman, Mariya Koleva, Omar J. Guerra, and Brady McLaughlin. *Optimizing an Integrated Renewable Electrolysis System*. Technical Report NREL/TP-5400-75635. TN 37831-0062, USA: National Renewable Energy Laboratory, Mar. 2020.

[16] Yuewen Jiang, Weijie Huang, and Guoming Yang. "Electrolysis plant size optimization and benefit analysis of a far offshore wind-hydrogen system based on information gap decision theory and chance constraints programming". In: *International Journal of Hydrogen Energy* (2022). DOI: doi.org/10.1016/j.ijhydene.2021.11.211.

[17] Michele Scolaro and Noah Kittner. "Optimizing hybrid offshore wind farms for cost-competitive hydrogen production in Germany". In: *International Journal of Hydrogen Energy* (2022). DOI: doi.org/10.1016/j.ijhydene.2021.12.062.

[18] European Central Bank — EUROSYSTEM. *Euro foreign exchange reference rates*. 2022.

[19] A Photovoltaic Power Systems Programme. *National Survey Report of PV Power Applications in Italy*. Report. Available online: iea-pvps.org/publications/ (accessed on 19 April 2022). International Energy Agency, 2020.

[20] International Renewable Energy Agency. *Data & Statistics*. Available online: www.irena.org/statistics (accessed on 16 July 2022). 2022.

[21] International Renewable Energy Agency. *Renewable Power Generation Costs in 2021*. Technical Report, ISBN: 978-92-9260-452-3. Abu Dhabi: IRENA, July 2022.

[22] International Renewable Energy Agency. *Renewable Power Generation Costs in 2020*. Technical Report, ISBN: 978-92-9260-348-9. Abu Dhabi: IRENA, June 2021.

[23] Tyler Stehly and Patrick Duffy. *2020 Cost of Wind Energy Review*. Technical Report NREL/TP-5000-81209. TN 37831-0062, USA: National Renewable Energy Laboratory, Jan. 2022.

[24] International Energy Agency. *Renewables 2021*. Technical Report. Paris: IEA, 2021.

[25] International Energy Agency. *Solar PV*. Technical Report. Paris: IEA, 2021.

[26] Federico Annese. "Large Scale Photovoltaic Market Analysis In Italy". Available online: kth.diva-portal.org/smash/get/diva2:1528806/FULLTEXT01.pdf (accessed on 21 April 2022). MA thesis. SE-100 44 Stockholm: KTH School of Industrial Engineering and Managemen, Feb. 2021.

[27] R. Wiser, M. Bolinger, and J. Seel. "Benchmarking Utility-Scale PV Operational Expenses and Project Lifetimes: Results from a Survey of U.S. Solar Industry Professionals". In: *Lawrence Berkeley National Laboratory* (2020). URL: escholarship.org/uc/item/2pd8608q.

[28] Bjarne Steffen, Martin Beuse, Paul Tautorat, and Tobias S. Schmidt. "Experience Curves for Operations and Maintenance Costs of Renewable Energy Technologies". In: *Joule* (2020). DOI: 10.1016/j.joule.2019.11.012.

[29] Eero Vartiainen, Gaëtan Masson, Christian Breyer, David Moser, and Eduardo Román Medina. "Impact of weighted average cost of capital, capital expenditure, and other parameters on future utility-scale PV levelised cost of electricity". In: *Progress in Photovoltaics: Research and Applications* (2020). DOI: doi.org/10.1002/pip.3189.

[30] Naeimeh Mozaffari et al. "Above 23% Efficiency by Binary Surface Passivation of Perovskite Solar Cells Using Guanidinium and Octylammonium Spacer Cations". In: *Solar RRL* (2022). DOI: 10.1002/solr.202200355.

[31] Bryan A. Rosales, Laura E. Mundt, Taylor G. Allen, David T. Moore, Kevin J. Prince, Colin A. Wolden, Garry Rumbles, Laura T. Schelhas, and Lance M. Wheeler. "Reversible multicolor chromism in layered formamidinium metal halide perovskites". In: *Nature Communications* (2020). DOI: 10.1038/s41467-020-19009-z.

[32] Stuart Macpherson et al. "Local nanoscale phase impurities are degradation sites in halide perovskites". In: *Nature* (2022). DOI: 10.1038/s41586-022-04872-1.

[33] Takuro Kusashio and Yuki Misumi. *Solar power anywhere: Lightweight organic cells aim beyond rooftops*. Available online: asia.nikkei.com/Business/Energy/Solar-power-anywhere-Lightweight-organic-cells-aim-beyond-rooftops (accessed on 17 July 2022). 2022.

[34] Elnaz H. Adeh, Stephen P. Good, M. Calaf, and Chad W. Higgins. "Solar PV Power Potential is Greatest Over Croplands". In: *Scientific Reports* (2019). DOI: 10.1038/s41598-019-47803-3.

[35] International Renewable Energy Agency. *Renewable Technology Innovation Indicators: Mapping progress in costs, patents and standards*. Technical Report, ISBN: 978-92-9260-424-0. Abu Dhabi: IRENA, Mar. 2022.

[36] International Energy Agency. *Wind Power*. Technical Report. Paris: IEA, 2021.

[37] Wind Europe. *Financing and investment trends: The European wind industry in 2021*. Technical Report. Belgium: Wind Europe, Apr. 2022.

[38] T. Rubert, D. McMillan, and P. Niewczas. "A decision support tool to assist with lifetime extension of wind turbines". In: *Renewable Energy* (2018). DOI: 10.1016/j.renene.2017.12.064.

[39] WindEurope. *Wind energy in Europe: 2021 Statistics and the outlook for 2022-2026*. Technical Report. Belgium: WindEurope, Feb. 2022.

[40] International Renewable Energy Agency. *Future of wind: Deployment, investment, technology, grid integration and socio-economic aspects (A Global Energy Transformation paper)*. Technical Report, ISBN: 978-92-9260-155-3. Abu Dhabi: IRENA, Oct. 2019.

[41] Wind Trust. *Designing the wind turbine of the future*. Technical Report, Wind Trust, 2016.

[42] Daniel Liu. *Unplanned wind turbine repairs to cost industry $8 billion+ in 2019*. Available online: www.woodmac.com/press-releases/unplanned-wind-turbine-repairs-to-cost-industry-$8-billion-in-2019 (accessed on 18 July 2022). 2019.

[43] WindEurope. *Discussion paper on managing composite blade waste*. Technical Report. Belgium: WindEurope, Mar. 2017.

[44] Global Wind Atlas. *Bathymetry Terrain Layer*. GIS data. Available online: globalwindatlas.info/ (accessed on 26 April 2022). OpenStreetMap, 2021.

[45] International Renewable Energy Agency. *Offshore Renewables: An Action Agenda for Deployment*. Technical Report, ISBN: 978-92-9260-349-6. Abu Dhabi: IRENA, July 2021.

[46] BVG Associates. *Guide to an offshore wind farm - Updated and extended*. Technical Guide. UK: Published on behalf of The Crown Estate and the Offshore Renewable Energy Catapult, Jan. 2019.

[47] Walter Musial, Paul Spitsen, Philipp Beiter, Patrick Duffy, Melinda Marquis, Aubryn Cooperman, Rob Hammond, and Matt Shields. *Offshore Wind Market Report: 2021 Edition*. Market Report DOE/GO-102021-5614. National Renewable Energy Laboratory, Aug. 2021.

[48] International Renewable Energy Agency. *Global energy transformation: A roadmap to 2050 (2019 edition)*. Technical Report, ISBN: 978-92-9260-121-8. Abu Dhabi: IRENA, Apr. 2019.

[49] John Rogers. *New Offshore Wind Turbine Can Power a Home for a Day in Just 7 Seconds*. Available online: blog.ucsusa.org/john-rogers/new-wind-turbine-power-home-for-day-in-7-seconds/ (accessed on 19 July 2022). Dec. 2020.

[50] Verónica Díaz. *Powered by change: Siemens Gamesa launches 14 MW offshore Direct Drive turbine with 222-meter rotor*. Available online: www.siemensgamesa.com/en-int/newsroom/2020/05/200519-siemens-gamesa-turbine-14-222-dd (accessed on 19 July 2022). May 2020.

[51] Adnan Memija. *Dutch Company to Build Prototype Crane for 20 MW Offshore Wind Turbines*. Available online: www.offshorewind.biz/2022/07/08/dutch-company-to-build-prototype-crane-for-20-mw-offshore-wind-turbines/ (accessed on 19 July 2022). July 2022.

[52] Bruno Maques, Alexandre Laíño, Juan Francisco Martínez-Tebar, and Fáktica Analytics. *The next generation monopile foundations for offshore wind turbines*. Technical Report. Boslan, 2022.

[53] Joachim Toftegaard Hansen, Mahak Mahak, and Iakovos Tzanakis. "Numerical modelling and optimization of vertical axis wind turbine pairs: A scale up approach". In: *Renewable Energy* (2021). DOI: 10.1016/j.renene.2021.03.001.

[54] WindEurope. *Offshore wind in Europe - key trends and statistics 2020*. Technical Report. Belgium: WindEurope, Feb. 2021.

[55] Bruce Beaubouef. *WindFloat Atlantic represents major offshore wind milestone*. Available online: www.offshore-mag.com/renewable-energy/article/14188688/windfloat-atlantic-represents-major-offshore-wind-milestone (accessed on 20 July 2022). Dec. 2020.

[56] GlobalData. *Floating Foundations: the Future of Deeper Offshore Wind*. Technical Report. London: GlobalData, June 2019.

[57] International Renewable Energy Agency. *Hydrogen from renewable power: Technology outlook for the energy transition*. Technical Report, ISBN: 978-92-9260-077-8. Abu Dhabi: IRENA, Sept. 2018.

[58] Nick Connell et al. *Green Hydrogen Guidebook*. Guidebook. Available online: www.ghcoalition.org/education (accessed on 22 July 2022). Apr. 2022.

[59] Flaticon. *Flaticon: the largest database of free icons*. Available online: www.flaticon.com/ (accessed on 29 July 2022). 2022.

[60] Leonardo Vidas and Rui Castro. "Recent Developments on Hydrogen Production Technologies: State-of-the-Art Review with a Focus on Green-Electrolysis". In: *Applied Sciences* (2021). DOI: 10.3390/app112311363.

[61] PV Magazine. *The weekend read: Hydrogen is getting cheaper*. Available online: www.pv-magazine.com/2020/03/21/the-weekend-read-hydrogen-is-getting-cheaper/ (accessed on 22 July 2022). Mar. 2020.

[62] International Renewable Energy Agency. *Green Hydrogen Cost Reduction: Scaling up Electrolysers to Meet the 1.5°C Climate Goal*. Technical Report, ISBN: 978-92-9260-295-6. Abu Dhabi: IRENA, 2020.

[63] NEL. *Atmospheric Alkaline Electrolyser Specifications*. Available online: nelhydrogen.com/product/atmospheric-alkaline-electrolyser-a-series (accessed on 21 July 2022).

[64] HyBalance. *HyLYZER-5.000-30*. Available online: hybalance.eu/Large-scale-PEM-electrolysis.pdf (accessed on 22 July 2022).

[65] International Energy Agency. *Global Hydrogen Review 2021*. International Energy Agency, 2021. DOI: 10.1787/39351842-en.

[66] Adam Christensen. *Assessment of Hydrogen Production Costs from Electrolysis: United States and Europe*. Tech. rep. Three Seas Consulting, June 2020.

[67] Gunther Glenk and Stefan Reichelstein. "Economics of converting renewable power to hydrogen". In: *Nature Energy* (2019). DOI: 10.1038/s41560-019-0326-1.

[68] Ramchandra Bhandari and Ronak Rakesh Shah. "Hydrogen as energy carrier: Techno-economic assessment of decentralized hydrogen production in Germany". In: *Renewable Energy* (2021). DOI: 10.1016/j.renene.2021.05.149.

[69] Yuanrong Zhou and Stephanie Searle. *Cost of Renewable Hydrogen Produced Onsite at Hydrogen Refueling Stations in Europe*. White Paper, Washington, DC 20005: International Council on Clean Transportation, Feb. 2022.

[70] Making Mission Possible Series. *Making the Hydrogen Economy Possible: Accelerating Clean Hydrogen in an Electrified Economy*. Tech. rep. Energy Transitions Commission, Apr. 2021.

[71] Gigastack. *Gigastack Phase 2: Pioneering UK Renewable Hydrogen*. Public Report. Sept. 2019.

[72] M. Minutillo, A. Perna, A. Forcina, S. Di Micco, and E. Jannelli. "Analyzing the levelized cost of hydrogen in refueling stations with on-site hydrogen production via water electrolysis in the Italian scenario". In: *International Journal of Hydrogen Energy* (2021). DOI: 10.1016/j.ijhydene.2020.11.110.

[73] Bloom Energy. *Bloom Electrolyzer Data Sheet*. Available online: www.bloomenergy.com/bloomelectrolyzer/#download (accessed on 22 July 2022). 2022.

[74] Enapter. *AEM Electrolyser EL 4.0 Specifications / Key Features*. Available online: www.enapter.com/aem-electrolyser (accessed on 27 July 2022). 2022.

[75] Aaron Hodges, Anh Linh Hoang, George Tsekouras, Klaudia Wagner, Chong-Yong Lee, Gerhard F. Swiegers, and Gordon G. Wallace. "A high-performance capillary-fed electrolysis cell promises more cost-competitive renewable hydrogen". In: *Nature Communications* (2022). DOI: 10.1038/s41467-022-28953-x.

[76] M. Khalfallah et al. *Mediterranean: updated catch reconstructions to 2018*. Report. Fisheries Centre Research, 2020, pp. 251–294.

[77] Current Results Publishing Ltd. *Average Sunshine a Year in Italy*. Available online: currentresults.com/Weather/Italy/annual-days-of-sunshine.php (accessed on 30 May 2022).

[78] OECD. *Disclaimers*. OECD Style Guide: Third Edition. Paris: OECD Publishing, 2015. DOI: 10.1787/9789264243439-10-en.

[79] Fida Ali, Adul Bennui, Shahariar Chowdhury, and Kuaanan Techato. "Suitable Site Selection for Solar-Based Green Hydrogen in Southern Thailand Using GIS-MCDM Approach". In: *Sustainability* (2022). DOI: 10.3390/su14116597.

[80] H Díaz, R. B. Fonseca, and C. Guedes Soares. *Site selection process for floating offshore wind farms in Madeira Islands*. London: Taylor & Francis Group, 2019. ISBN: 978-1-138-58535-5.

[81] QGIS Development Team. *QGIS Geographic Information System*. QGIS Association. 2022. URL: www.qgis.org.

[82] QGIS Development Team. *Documentation for QGIS Desktop 3.22*. User Guide. Apr. 2022.

[83] MapTiler Team. *EPSG:32632 - WGS 84/UTM zone 32N*. Available online: epsg.io/32632 (accessed on 04 June 2022). 2022.

[84] MapTiler Team. *EPSG:32629 - WGS 84/UTM zone 29N*. Available online: epsg.io/32629 (accessed on 04 June 2022). 2022.

[85] David Ryberg, Martin Robinius, and Detlef Stolten. *Methodological Framework for Determining the Land Eligibility of Renewable Energy Sources*. 2017.

[86] Carlos Efraín Porto Tapiquén. *Geografía, SIG y Cartografía Digital*. Available online: www.efrainmaps.es (accessed on 05 June 2022). Valencia, Spain, 2022.

[87] Robert J. Hijmans. *Boundary of Italy*. Available online: earthworks.stanford.edu (accessed on 31 March 2022). University of California, USA, 2015.

[88] European Environment Agency. *Hillshade Europe DEM*. Available online: www.eea.europa.eu/data-and-maps (accessed on 13 April 2022). 2004.

[89] Robert J. Hijmans. *First-level Administrative Divisions of Italy*. Available online: earthworks.stanford.edu (accessed on 01 April 2022). University of California, USA, 2015.

[90] ICPAC Geoportal. *Africa - Admin Level 0*. Available online: geoportal.icpac.net (accessed on 05 June 2022). Nairobi, Kenya, 2017.

[91] European Marine Observation and Data Network. *Exclusive Economic Zone areas in European seas*. Available online: www.emodnet-humanactivities.eu/ (accessed on 3 May 2022). 2021.

[92] ForestGIS. Available online: forest-gis.com/shapefiles-de-portugal/ (accessed on 16 May 2022).

[93] EMODnet Bathymetry Consortium. *EMODnet Digital Bathymetry (DTM 2020)*. 2020. DOI: 10.12770/bb6a87dd-e579-4036-abe1-e649cea9881a.

[94] Directorate-General for Maritime Affairs European Commission and Fisheries. *EMODnet Digital Bathymetry*. Available online: data.europa.eu (accessed on 28 April 2022).

[95] David Ryberg, Martin Robinius, and Detlef Stolten. "Evaluating Land Eligibility Constraints of Renewable Energy Sources in Europe". In: *Energies* (2018). DOI: 10.3390/en11051246.

[96] EPIC WebGIS Portugal. *Ecological Planning, Investigation and Cartograph*. Available online: epic-webgis-portugal.isa.ulisboa.pt/ (accessed on 18 May 2022). 2022.

[97] Geofabrik GmbH and OpenStreetMap Contributors. *OpenStreetMap Data Extracts*. Available online: download.geofabrik.de/europe.html (accessed on 2 April 2022). 2022.

[98] Directorate-General for Maritime Affairs and Fisheries. *Unlocking seabed habitat data in Europe*. Available online: www.emodnet-seabedhabitats.eu (accessed on 28 April 2022).

[99] European Marine Observation and Data Network. *Data Services*. Available online: www.emodnet-humanactivities.eu/search.php (accessed on 3 May 2022). 2022.

[100] C. Maienza, A. M. Avossa, F. Ricciardelli, D. Coiro, and C. T. Georgakis. "Sensitivity analysis of cost parameters for floating offshore wind farms: an application to Italian waters". In: *Journal of Physics: Conference Series* (2020). DOI: 10.1088/1742-6596/1669/1/012019.

[101] UK Maritime and Coastguard Agency. *Offshore Renewable Energy Installations Safety Response*. Technical Report MGN 654 (M+F). National Renewable Energy Laboratory, Apr. 2021.

[102] Info GIS Map. Available online: map.igismap.com/gis-data (accessed on 2 April 2022). 2022.

[103] Global Energy Monitor. *Global Fossil Infrastructure Tracker*. Available online: globalenergymonitor.org/ (accessed on 19 May 2022). 2022.

[104] C. Arderne, C. Zorn, C. Nicolas, and E. E. Koks. "Predictive mapping of the global power system using open data". In: *Scientific Data* (2020). DOI: 10.1038/s41597-019-0347-4.

[105] P. Argyle and S.J. Watson. "Offshore Turbine Wake Power Losses: Is Turbine Separation Significant?" In: *Energy Procedia* (2017). DOI: 10.1016/j.egypro.2017.10.340.

[106] Division for Ocean Affairs and the Law of the Sea. *United Nations Convention on the Law of the Sea*. Technical Report. United Nations, Feb. 2022.

[107] TeleGeography. *Submarine Cable Map*. Available online: www.submarinecablemap.com/ (accessed on 26 April 2022). 2022.

[108] ICPC Marine Environmental Adviser Mike Clare. *Submarine Cable Protection and the Environment - An Update from the ICPC*. Technical Report Issue 4. The International Cable Protection Committee, Mar. 2022.

[109] European Environment Agency. *Copernicus Land Monitoring Service - EU-DEM*. Available online: www.eea.europa.eu/data-and-maps/data/copernicus-land-monitoring-service-eu-dem (accessed on 4 May 2022). 2017.

[110] Ketan Ramaneti, Pranavi Kakani, and Surya Prakash. "Improving Solar Panel Efficiency by Solar Tracking and Tilt Angle Optimization with Deep Learning". In: *2021 5th International Conference on Smart Grid and Smart Cities (ICSGSC)*. 2021. DOI: 10.1109/ICSGSC52434.2021.9490485.

[111] Giuseppe Amatulli, Sami Domisch, Mao-Ning Tuanmu, Benoit Parmentier, Ajay Ranipeta, Jeremy Malczyk, and Walter Jetz. "A suite of global, cross-scale topographic variables for environmental and biodiversity modeling". In: *Scientific Data* (2018). DOI: 10.1038/sdata.2018.40.

[112] EarthEnv. *Global 1,5,10,100-km Topography*. Available online: www.earthenv.org/topography (accessed on 2 April 2022). 2020.

[113] Solargis. *Global Solar Atlas 2.0 : Technical Report*. ESMAP Paper. World Bank Group, Nov. 2019.

[114] Global Solar Atlas. *Map and data downloads: Italy*. GIS data. Available online: globalsolaratlas.info/download/italy (accessed on 10 April 2022). Solargis, 2021.

[115] Candian Solar. *BiHiKu7 Bifacial Mono Perc*. PV Module Product Datasheet V2.1. Available online: www.canadiansolar.com/bihiku/ (accessed on 18 April 2022). ., Feb. 2022.

[116] Global Solar Atlas. *Map and data downloads: Portugal*. GIS data. Available online: globalsolaratlas.info/download/portugal (accessed on 10 April 2022). Solargis, 2021.

[117] European Commission. *EMODnet Digital Bathymetry (DTM)*. Available online: data.europa.eu/data/datasets/ (accessed on 21 May 2022). 2018.

[118] Natural Earth. *Bathymetry*. Available online: www.naturalearthdata.com/downloads/10m-physical-vectors (accessed on 21 May 2022). 2018.

[119] Vestas Wind Systems A/S. *4 MW Platform*. Brochure. Available online: www.vestas.com/en/products/4-mw-platform (accessed on 18 April 2022). Vestas Group, Feb. 2022.

[120] Global Wind Atlas. *Mean Wind Speed: Italy*. GIS data. Available online: globalwindatlas.info/area/Italy (accessed on 10 April 2022). OpenStreetMap, 2021.

[121] Global Wind Atlas. *Mean Wind Speed: Portugal*. GIS data. Available online: globalwindatlas.info/area/Portugal (accessed on 10 April 2022). OpenStreetMap, 2021.

[122] Stuart D.C. Walsh, Laura Easton, Zhehan Weng, Changlong Wang, Joseph Moloney, and Andrew Feitz. "Evaluating the economic fairways for hydrogen production in Australia". In: *International Journal of Hydrogen Energy* (2021). DOI: doi.org/10.1016/j.ijhydene.2021.08.142.

[123] Geoscience Australia. *AusH2 - Australia's Hydrogen Opportunities Tool*. Available online: portal.ga.gov.au/persona/heft (accessed on 03 July 2022). 2021.

[124] Gustavo de Novaes Pires Leite, Franciele Weschenfelder, João Gabriel de Farias, and Muhammad Kamal Ahmad. "Economic and sensitivity analysis on wind farm end-of-life strategies". In: *Renewable and Sustainable Energy Reviews* (2022). DOI: doi.org/10.1016/j.rser.2022.112273.

[125] Trading Economics. *Euro Area Inflation Rate*. Available online: tradingeconomics.com/euro-area/inflation-cpi (accessed on 04 August 2022). 2022.

[126] Bjarne Steffen. "Estimating the cost of capital for renewable energy projects". In: *Energy Economics* (2020). DOI: doi.org/10.1016/j.eneco.2020.104783.

[127] Ludvik Viktorsson, Jukka Taneli Heinonen, Jon Bjorn Skulason, and Runar Unnthorsson. "A Step towards the Hydrogen Economy—A Life Cycle Cost Analysis of A Hydrogen Refueling Station". In: *Energies* (2017). DOI: 10.3390/en10060763.

[128] Tubagus Aryandi Gunawan, Alessandro Singlitico, Paul Blount, James G. Carton, and Rory F.D. Monaghan. "Towards techno-economic evaluation of renewable hydrogen production from wind curtailment and injection into the Irish gas network". In: *Proceedings of ECOS 2019*. The 32nd International Conference on Efficiency, Cost, Optimization, Simulation and Environmental Impact of Energy Systems. Wroclaw, Poland, June 2019.

[129] International Renewable Energy Agency and International Energy Agency Photovoltaic Power Systems. *End-of-Life Management: Solar Photovoltaic Panels*. Technical Report. IRENA and IEA-PVPS, June 2016.

[130] Gabriele Giovannini. "Wind Farm Decommissioning: A Perspective on Regulations and Cost Assessment in Italy and Sweden". MA thesis. Uppsala University, 2014.

[131] Energy Department for Business and Industrial Strategy. *Hydrogen Production Costs 2021*. Technical Guide. UK: BEIS, Aug. 2021.

[132] Franz Lehner and David Hart. "Chapter 1 - The importance of water electrolysis for our future energy system". In: *Electrochemical Power Sources: Fundamentals, Systems, and Applications*. Elsevier, 2022. DOI: doi.org/10.1016/B978-0-12-819424-9.00008-2.

[133] NEL. *PEM Electrolyser Specifications*. Available online: nelhydrogen.com/product/m-series-3/ (accessed on 06 August 2022).

[134] Cummins. *HyLYZER Water Electrolyzers*. Available online: www.cummins.com/sites/default/files/2021-08/cummins-hylyzer-1000-specsheet.pdf (accessed on 06 August 2022). 2022.

[135] Plug Power. *The Plug EX-425D*. Available online: www.plugpower.com/hydrogen/electrolyzer-hydrogen/ (accessed on 06 August 2022).

[136] Siemens Energy. *Silyzer 300*. Available online: www.siemens-energy.com/global/en/offerings/renewable-energy/hydrogen-solutions.html (accessed on 06 August 2022). 2022.

[137] Raymond Byrne, Davide Astolfi, Francesco Castellani, and Neil J. Hewitt. "A Study of Wind Turbine Performance Decline with Age through Operation Data Analysis". In: *Energies* (2020). DOI: 10.3390/en13082086.

[138] Jonathan A. Lesser. *Out To Sea: The Dismal Economics Of Offshore Wind*. Report. Belgium: Manhattan Institute, Aug. 2020.

[139] Javier Pollos Ezquerra. "Analysing the competitiveness of offshore hydrogen-wind production models". Available online: fenix.tecnico.ulisboa.pt/cursos/mege/dissertacao/1972678479054934 (accessed on 05 July 2022). MA thesis. Instituto Superior Técnico, Jan. 2021.

[140] Canadian Solar. *Bifacial High Power Dual Cell PERC Module*. Available online: www.csisolar.com/bihiku7/ (accessed on 09 August 2022). 2022.

[141] Tafara Mahachi and Arnold Rix. "Energy yield analysis and evaluation of solar irradiance models for a utility scale solar PV plant in South Africa". PhD thesis. Stellenbosch University, 2016. DOI: 10.13140/RG.2.2.19638.45127.

[142] Herdian Wibowo, Yohandri Bow, and Carlos Sitompul. "Performance Comparison Analysis of Fixed and Solar-Tracker Installed Panel at PV System". In: *IOP Conference Series: Earth and Environmental Science* (2021). DOI: 10.1088/1755-1315/709/1/012003.

[143] Global Wind Atlas. *(November 2018 Release Note)*. Release Note. Available online: globalwindatlas.info/about/ReleaseNotes (accessed on 13 April 2022). GWA 2.3, 2022.

[144] Dillon Clayton. *Wind Turbine Spacing: How Far Apart Should They Be?* Available online: energyfollower.com/wind-turbine-spacing/ (accessed on 10 August 2022). 2022.

[145] Richard Gaughan. *How Much Land Is Needed for Wind Turbines?* Available online: sciencing.com/much-land-needed-wind-turbines-12304634.html (accessed on 10 August 2022). 2018.

[146] George Duval. *How Many Wind Turbines Can Fit On One Acre?* Available online: www.semprius.com/how-much-space-does-a-wind-turbine-need/ (accessed on 10 August 2022). 2021.

[147] William E Hart, Jean-Paul Watson, and David L Woodruff. "Pyomo: modeling and solving mathematical programs in Python". In: *Mathematical Programming Computation* (2011).

[148] Michael L. Bynum, Gabriel A. Hackebeil, William E. Hart, Carl D. Laird, Bethany L. Nicholson, John D. Siirola, Jean-Paul Watson, and David L. Woodruff. *Pyomo–optimization modeling in python*. Third. Vol. 67. Springer Science & Business Media, 2021.

[149] Thomas Huld, Richard Müller, and Attilio Gambardella. "A new solar radiation database for estimating PV performance in Europe and Africa". In: *Solar Energy* (2012). DOI: doi.org/10.1016/j.solener.2012.03.006.

[150] Stefan Pfenninger and Iain Staffell. "Long-term patterns of European PV output using 30 years of validated hourly reanalysis and satellite data". In: *Energy* (2016). Available online: www.renewables.ninja (accessed on 14 August 2022). DOI: doi.org/10.1016/j.energy.2016.08.060.

[151] Iain Staffell and Stefan Pfenninger. "Using bias-corrected reanalysis to simulate current and future wind power output". In: *Energy* (2016). Available online: www.renewables.ninja (accessed on 14 August 2022). DOI: doi.org/10.1016/j.energy.2016.08.068.

[152] Dalila Khalfa, Abdelouaheb Benretem, Nassir Cheikchouk, and Lazher Herous. "Comparative study of wind speed extrapolation methods for sites with different roughness". In: *International Journal of Power and Energy Conversion* (2018). DOI: 10.1504/IJPEC.2018.092686.

[153] Paul E. Black. *Algorithms and Theory of Computation Handbook*. 5 January 2021. Available online: www.nist.gov/dads/HTML/nphard.html (accessed on 16 August 2022). "NP-hard", in Dictionary of Algorithms and Data Structures: CRC Press LLC, 1999.

[154] Octeract. *Octeract Engine*. Available online: octeract.gg/ (accessed on 16 June 2022). 2022.

[155] C. Moné, A. Smith, B. Maples, and M. Hand. *Cost of Wind Energy 2013 Review*. Technical Report NREL/TP-5000-63267. TN 37831-0062, USA: National Renewable Energy Laboratory, Feb. 2015.

APPENDICES

A Published Articles

Over the past two years, in anticipation of this thesis, an extensive literature review was conducted on various hydrogen–related issues. 'Green Hydrogen', in particular, is a relatively recent hot–topic in the scientific community and thus requires a holistic approach to understanding all of its constituting elements in the value chain. This broad study was compiled and organized into two separate works, from which resulted two independent articles—published in different scientific journals during the past year.
The following is a list that briefly describes the contents of each paper; the DOI links are also provided.

- *Recent Developments on Hydrogen Production Technologies: State–of–the–Art Review with a Focus on Green–Electrolysis*. Published on December, 2021 in MDPI's Applied Sciences. 10.3390/app112311363
  This first paper seeks to compile a series of state–of–the–art articles concerning the new improvements in hydrogen production technologies. It starts by giving a historical overview of the relationship between fossil–fuel consumption, carbon dioxide emissions and global median temperature anomaly, from which bases the need to focus on non–polluting production techniques. An outline of hydrogen's value chain is presented, with a background exposition of some relevant concepts. Finally, an in–depth study of electrolysis is given, addressing and comparing the current leading electrolyser technologies.
  At the time of writing, this article has 16 citations registered in Google Scholar and almost 5000 single–IP, full–text views.

- *A Review of the Impact of Hydrogen Integration in Natural Gas Distribution Networks and Electric Smart Grids* in MDPI's Energies. Published on April, 2022 in MDPI's Energies. 10.3390/en15093160
  The second paper brings together all the research downstream of hydrogen production, i.e. storage technologies, transmission/distribution and end–use. It starts by offering an exhaustive assessment of the prevailing techniques for physically storing hydrogen, moving to a detailed analysis of its integration in present–day gas networks. In the end, there is a focus on examining the implementation of such systems in smart grids, emphasising stand–alone microgrids and grid–tied multi–microgrids.
  Since its publication, this article has gathered 700 single–IP, full–text views.

The next two pages display the first–page cover of both articles, in the same order.

applied sciences

MDPI

Review

Recent Developments on Hydrogen Production Technologies: State-of-the-Art Review with a Focus on Green-Electrolysis

Leonardo Vidas [1] and Rui Castro [2,*]

[1] Instituto Superior Técnico, University of Lisbon, 1049-001 Lisboa, Portugal; leonardo.vidas@tecnico.ulisboa.pt
[2] INESC-ID/IST, University of Lisbon, 1000-029 Lisboa, Portugal
* Correspondence: rcastro@tecnico.ulisboa.pt

Abstract: Growing human activity has led to a critical rise in global energy consumption; since the current main sources of energy production are still fossil fuels, this is an industry linked to the generation of harmful byproducts that contribute to environmental deterioration and climate change. One pivotal element with the potential to take over fossil fuels as a global energy vector is renewable hydrogen; but, for this to happen, reliable solutions must be developed for its carbon-free production. The objective of this study was to perform a comprehensive review on several hydrogen production technologies, mainly focusing on water splitting by green-electrolysis, integrated on hydrogen's value chain. The review further deepened into three leading electrolysis methods, depending on the type of electrolyzer used—alkaline, proton-exchange membrane, and solid oxide—assessing their characteristics, advantages, and disadvantages. Based on the conclusions of this study, further developments in applications like the efficient production of renewable hydrogen will require the consideration of other types of electrolysis (like microbial cells), other sets of materials such as in anion-exchange membrane water electrolysis, and even the use of artificial intelligence and neural networks to help design, plan, and control the operation of these new types of systems.

Keywords: hydrogen value chain; hydrogen storage methods; hydrogen production technologies; water electrolysis technologies; alkaline water electrolysis; proton-exchange membrane electrolysis; solid oxide electrolysis

Citation: Vidas, L.; Castro, R. Recent Developments on Hydrogen Production Technologies: State-of-the-Art Review with Focus on Green-Electrolysis. *Appl. Sci.* **2021**, *11*, 11363. https://doi.org/10.3390/app112311363

Academic Editors: Pooya Davari, Enrico Cagno, Mohsen Soltani and Edris Pouresmaeil

Received: 31 July 2021
Accepted: 19 November 2021
Published: 1 December 2021

1. Introduction

Nowadays, an ever-expanding human population coupled with a growth in anthropogenic activities and general better standards of living have led to a significant surge in overall energy consumption [1,2]. Presently, most of the energy generation comes from fossil fuel sources; Figures 1 and 2 show how the widespread use of coal, oil, and natural gas since the beginning of the 19th century has led to the continued emission of greenhouse gases—such as carbon dioxide, methane, and nitrous oxide—causing a gradual increase in the concentration of these gases in the Earth's atmosphere and contributing to environmental degradation and climate change (it should be noted that the most recent measurement has already peaked at 419 ppm, in May of this year) [3,4].

As is well known, the presence of these gases in the atmosphere traps heat radiating from the Earth toward space, effectively warming it. Figure 3 shows how there is mounting evidence that this global warming is man-made, namely, by observing the rise of world temperatures, the warming of the oceans, shrinking ice sheets, glacial retreats, decreased snow cover, the declining of the Arctic Sea ice, a broad sea level rise, widespread ocean acidification, and more extreme weather events in general [5–7].

energies

MDPI

Review

A Review of the Impact of Hydrogen Integration in Natural Gas Distribution Networks and Electric Smart Grids

Leonardo Vidas [1], Rui Castro [2] and Armando Pires [3,4,*]

[1] Instituto Superior Técnico, University of Lisbon, 1049-001 Lisboa, Portugal; leonardo.vidas@tecnico.ulisboa.pt
[2] INESC-ID/IST, University of Lisbon, 1000-029 Lisboa, Portugal; rcastro@tecnico.ulisboa.pt
[3] SustainRD, EST Setúbal, Polytechnic Institute of Setubal, 2914-508 Setubal, Portugal
[4] Centre of Technology and Systems (CTS-UNINOVA), 2829-516 Caparica, Portugal
* Correspondence: armando.pires@estsetubal.ips.pt

Abstract: Hydrogen technologies have been rapidly developing in the past few decades, pushed by governments' road maps for sustainability and supported by a widespread need to decarbonize the global energy sector. Recent scientific progress has led to better performances and higher efficiencies of hydrogen-related technologies, so much so that their future economic viability is now rarely called into question. This article intends to study the integration of hydrogen systems in both gas and electric distribution networks. A preliminary analysis of hydrogen's physical storage methods is given, considering both the advantages and disadvantages of each one. After examining the preeminent ways of physically storing hydrogen, this paper then contemplates two primary means of using it: integrating it in Power-to-Gas networks and utilizing it in Power-to-Power smart grids. In the former, the primary objective is the total replacement of natural gas with hydrogen through progressive blending procedures, from the transmission pipeline to the domestic burner; in the latter, the set goal is the expansion of the implementation of hydrogen systems—namely storage—in multi-microgrid networks, thus helping to decarbonize the electricity sector and reducing the impact of renewable energy's intermittence through Demand Side Management strategies. The study concludes that hydrogen is assumed to be an energy vector that is inextricable from the necessary transition to a cleaner, more efficient, and sustainable future.

Keywords: hydrogen technologies; hydrogen economy; hydrogen storage methods; natural gas infrastructures; smart grids

Citation: Vidas, L.; Castro, R.; Pires, A. A Review of the Impact of Hydrogen Integration in Natural Gas Distribution Networks and Electric Smart Grids. *Energies* **2022**, *15*, 3160. https://doi.org/10.3390/en15093160

Academic Editor: Wei-Hsin Chen

Received: 28 March 2022
Accepted: 21 April 2022
Published: 26 April 2022

1. Introduction

Hydrogen-related technologies have been through many cycles of expectations over the past few decades. Nowadays, a growing body of evidence finally suggests the soon-to-be end of these cycles, with hydrogen standing as an attractive alternative—some even say, an indispensable option—for the deep decarbonization needed by our global energy system [1]. This scenario is further supported by recent scientific improvements that considerably reduced costs and increased the performance of hydrogen-related technologies, to a point where its economic viability is no longer discussed.

To speak about the development of the hydrogen economy is to first discuss the strategic configurations on its value chain. Nowadays, most hydrogen (H_2) road maps put forward by governments around the world recognize hydrogen as an exceptionally versatile energy vector, with several possible applications in all main sectors of modernized societies—industry, buildings, transportation, and of course, energy [2]. Figure 1 presents a general diagram of the value chain usually associated with hydrogen, showing that to proceed with its implementation, a definition of the possible strategic configurations (from production to end-use) must first be made.

B Chart of Citations

The subjects discussed in this thesis mainly refer to recent, evolving technologies. Thus, an effort was made to mostly use bibliography published in the last five years—and, whenever impracticable, never beyond ten years. The following charts intend to visually display the consulted literature, arranging each reference according to its year of publication, primary subject matter and the number of times cited in this thesis.

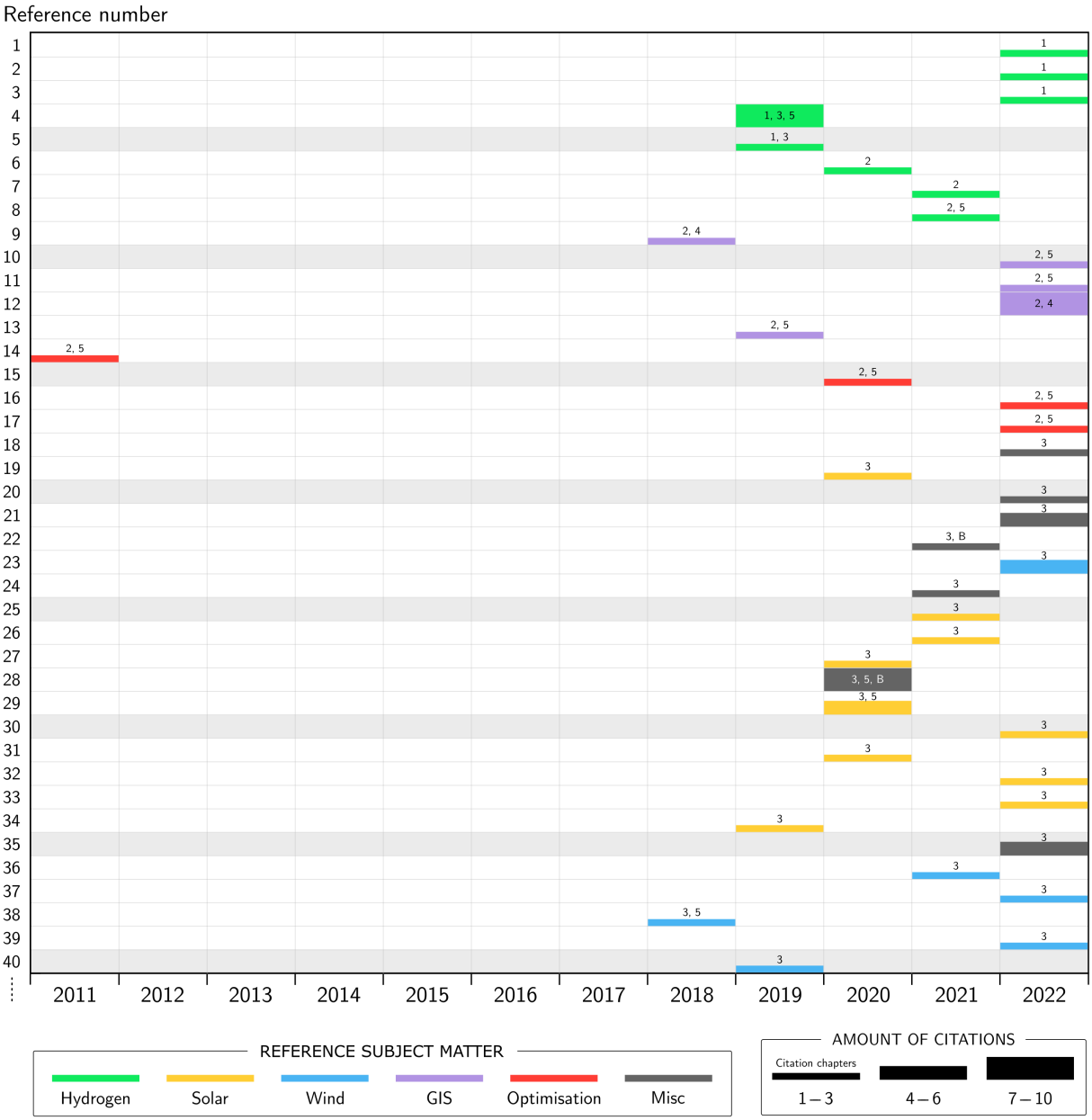

Figure B.1: Citation chart for references [1]–[40]

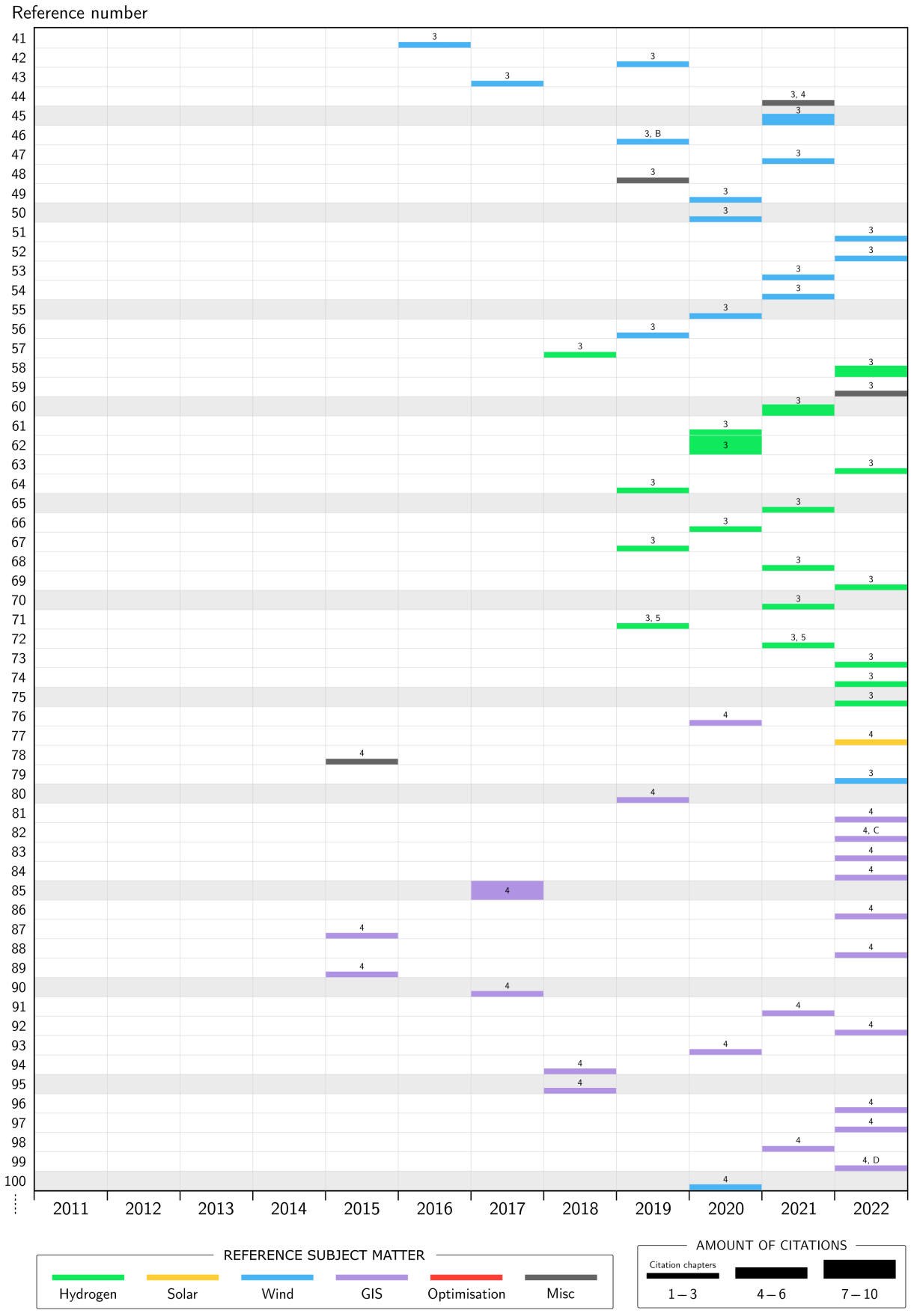

Figure B.2: Citation chart for references [41]–[100]

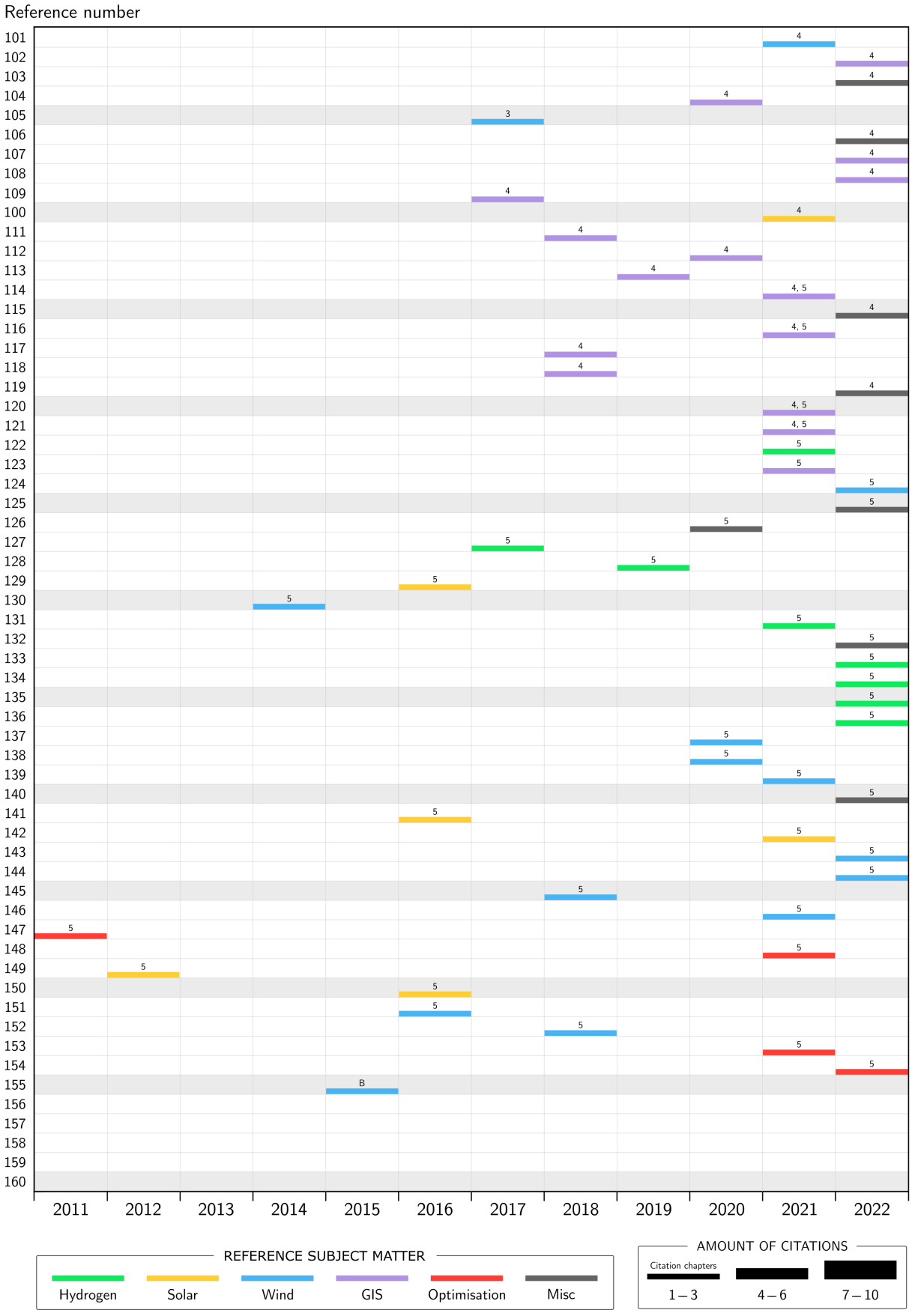

Figure B.3: Citation chart for references [101]–[155]

C RES Systems Cost Breakdown

The cost components of each technology can vary greatly depending on the designer, development and construction company, the country and its laws or the year in which the project takes place. A detailed but non–exhaustive list of the costs of each RES system is presented below, adapted from the respective source. A careful analysis was carried out beforehand since the projects accessed in this work are not yet common and, therefore, present a cost structure not correspondent to that typically given in international market reports.

C.1 Solar Photovoltaic

Table C.1: Solar PV system CapEx categories breakdown structure.

CapEx Category	Description
Non–module hardware	
Cabling and wiring	All DC components (cables, connectors and combiner boxes).
Monitoring and control	Monitoring system, meteorological system (e.g., irradiation and temperature sensors), and supervisory control and data system.
Racking and mounting	Complete mounting system (including ramming profiles, foundations and all the material for assembling), and all material necessary for mounting the combiner boxes.
Safety and security	Fences, cameras, and security systems (including all equipment installed for theft and fire protection).
Installation	
Electrical installation	DC installation (module interconnection and DC cabling), installation of monitoring and control systems, and necessary electrical tests (e.g., DC string measurement).
Inspection	Construction supervision and health and safety inspections.
Mechanical installation	Access and internal roads, preparation for cable routing (e.g., cable trench, cable trunking system), installation of mounting/racking system, solar PV modules' installation, and uploading and transport of components or other equipment.

Table C.1: *Cont.*

CapEx Category	Description
Soft costs	
Financing	All financing costs necessary for the development and construction of the PV system, such as costs for construction finance.
Permitting	Permits necessary for development, construction and operation, and all costs related to environmental regulations.
Project margin	Margin for the EPC company or the project developer for development and construction of the PV system, including profit, wages, finance, customer service, legal, human resources, rent, office supplies, purchased corporate professional services and vehicle fees.
System design	Geological surveys or structural analysis, surveyors, conceptual and detailed design, and preparation of documentation.

Note: For a complete detailed description of these categories, please refer to [22] .

Table C.2: Solar PV system OpEx categories breakdown structure.

OpEx Category	Description
Operations and Maintenance	
Maintenance and repairs	Annual inspection and preventive maintenance, corrective maintenance and spare parts' management, cabling repairs, and exchange of defected PV modules.
Operations and technical management	Continuous performance monitoring and reporting, plant control, interface with off–taker, and warranty and insurance claim management.
Commercial management	Financial management, accounting and tax reporting, and interface with local authorities.
Site management	Vegetation management/green–keeping, module cleaning, snow clearing and security.
Other OpEx	
Land lease	Land preparation work and rent.
Insurance	Insurance on the material property of the project.
Various taxes	Investment, production tax credits, and property taxes.

Note: For a complete detailed description of these categories, please refer to [28] .

C.2 Onshore Wind

Table C.3: Onshore wind system's CapEx categories breakdown structure.

CapEx Category	Description
Turbine	
———————— Rotor module	
Blade	Root structure, sandwich core, spar/spar box, bond, fasteners, laminates, paint and coatings, lightening protection, de–icing system, ballast and aerodynamic accessories.
Pitch assembly	Pitch drive, pitch cabinet, sensors and miscellaneous.
Hub assembly	Hub, nose cone, exit hatch.
———————— Nacelle module	
Structural assembly	Enclosure, drive–train and generator support structures, and coatings.
Drive–train box	Gearbox, low–speed shaft and main bearing system, and high–speed shaft and breaking system.
Electrical components	Generator, frequency stabilizer, power electrical system (including rectifier and filtering capacitors) , control and communication system (supervisory control and data acquisition), and auxiliary nacelle electrical system.
Yaw system	Brake, drives and bearings, hydraulics and yaw sensors.
———————— Tower module	
Tower system	Tower structure, fasteners and coatings, electrical and ancillary assembly, and tower transportation to the staging area.
Balance of system	
Development	Permitting and leasing, professional advisory services, engineering, site characterization, project management during development, and financing and incentives.
Engineering project	Detailed design and construction, procurement and construction management, project certification and health, safety, and environmental. monitoring
Foundation	Excavation, primary structure, batch plant and foundation transportation.
Site access and staging	Facilities, including lay–down area and utilities.
Assembly and installation	Roads, erection, commissioning and foundation.
Electrical infrastructure	Array cable system, ancillary systems and substations (switch–gear, shunt reactors, DC converter and filtering system, among others).
Soft costs	
Financing	Carrying charges of expenditures on equipment and services incurred for the development and construction of the system.
Reserve accounts	Maintenance reserve accounts, debt service and decommissioning reserve account.
Insurance	Insurance policies held by the owner during the construction period.
Contingency fund	Provides a liquid financial instrument set up to respond to 'known unknown' costs that arise during construction.

Note: For a complete detailed description of these categories, please refer to [155].

Table C.4: Onshore wind system's OpEx categories breakdown structure.

OpEx Category	Description
Operations and Maintenance	
Maintenance and repairs	Bi–annual inspection and testing of safety–related equipment, preventive and corrective maintenance (especially replacement of wear and tear parts, repair of component's defects, replacement of gearbox), spare parts' management, and tower motion survey.
Operations and technical management	Continuous performance monitoring and reporting, plant control, interface with off–taker, warranty and insurance claim management.
Commercial management	Financial management, accounting and tax reporting, and interface with local authorities.
Site management	Maintenance of access roads, and environmental compensation measures.
Other OpEx	
Land lease	Land preparation work and rent.
Insurance	Insurance on the material property of the project and taxes.
Administration	Management and administration including audits, management activities, forecasting services and remote–control measures.

Note: For a complete detailed description of these categories, please refer to [28] .

C.3 Fixed Offshore Wind

Table C.5: Fixed offshore wind system's CapEx categories breakdown structure.

CapEx Category	Description
Turbine	
—————— Rotor module	
Blade	Root structure, sandwich core, spar/spar box, bond, fasteners, laminates, paint and coatings, lightening protection, de–icing system, ballast and aerodynamic accessories.
Pitch segment	Hydraulic/electric pitch system, pitch drive, pitch cabinet, sensors and miscellaneous.
Hub assembly	Hub, nose cone, exit hatch.
Auxiliary systems	Automatic lubrication system, blade load measurement and maintenance support features.

Table C.5: *Cont.*

CapEx Category	Description
Turbine	
———————— Nacelle module	
Structural assembly	Condition monitoring system, nacelle enclosure, drive–train and generator support structures, coatings and auxiliary systems.
Drive–train box	Bedplate, main bearing system, gearbox, low–speed and high–speed shafts, and breaking system.
Electrical components	Generator, frequency stabilizer, power take–off electrical system (including rectifier and filtering capacitors) , control system, and auxiliary nacelle electrical system.
Yaw system	Brake, drives and bearings, hydraulics and yaw sensors.
———————— Tower module	
Tower system	Tower structure, fasteners and coatings, electrical and ancillary assembly, and tower transportation to the staging area.
Balance of system	
Array cables	Loops of cable or individual strings connecting wind turbines to the offshore substation, including cable protection and accessories.
Engineering project	Detailed design and construction, procurement and construction management, project certification and health, safety, and environmental. monitoring
Substructure and foundation	Excavation, monopile primary structure (including transportation), jacket, transition pieces, corrosion protection and scour protection.
Project development	Permitting and leasing, professional advisory services, engineering, site characterization, project management during development, and financing and incentives.
Assembly and installation	Offshore substation, including electrical conversion systems, auxiliary facilities, safety and protection equipment, and steel structures.
Electrical infrastructure	Ancillary systems and stations (including rectifiers, DC converter and filtering system).
Soft costs	
Financing	Charges of expenditure on equipment and services incurred for the development and construction of the system.
Plant commissioning	Offshore logistics, consisting of sea–based support, marine coordination and weather forecasting and metaocean data, among others.
Project insurance	Insurance policies held by the owner during the construction period.
Contingency fund	Provision of a liquid financial instrument set up to respond to 'known unknown' costs that may arise during construction.

Note: For a complete detailed description of these categories, please refer to [46] .

Table C.6: Fixed offshore wind system's OpEx categories breakdown structure.

OpEx Category	Description
Operations	
Offshore logistics	Crew transfer and service operation vessels, turbine access systems, helicopters, marine planning software, communications equipment and safety planning.
Health and safety inspections	Inventory tracking, namely first aid and advanced medical kit, gloves and safety boots, ear defenders and safety eye–wear, fire extinguishers, personal locator beacon, life–vests and float devices, among others.
Personnel training	Training courses, examinations and certification.
Maintenance and services	
Turbine maintenance and service	Blade inspection and repair, nacelle component refurbishment, replacement and repair, and electrical transmission system maintenance.
Balance of plant service and maintenance	Foundation and cable inspection and repair, scour monitoring and management, and substation maintenance and service.

Note: For a complete detailed description of these categories, please refer to [46] .

C.4 Floating Offshore Wind

Table C.7: Floating offshore wind system's CapEx categories breakdown structure.

CapEx Category	Description
Turbine	
———————— Rotor module	
Blade	Root structure, laminates, paint and coatings, lightening protection, de–icing system, ballast and aerodynamic accessories.
Pitch segment	Hydraulic/electric pitch system, pitch drive, pitch cabinet and sensors.
Hub assembly	Hub, nose cone, and exit hatch.
Auxiliary systems	Automatic lubrication system and blade load measurement system.
———————— Nacelle module	
Structural assembly	Condition monitoring system, nacelle enclosure, drive–train and generator support structures, coatings and auxiliary systems.
Drive–train box	Bedplate, main bearing system, gearbox, low–speed and high–speed shafts, and breaking system.
Electrical components	Generator, frequency stabilizer, power take–off electrical system (including rectifier and filtering capacitors) , control system, and auxiliary nacelle electrical system.
Yaw system	Brake, drives and bearings, hydraulics and yaw sensors.
———————— Tower module	
Tower system	Tower structure, fasteners and coatings, electrical and ancillary assembly, and tower transportation to the staging area.

Table C.7: *Cont.*

CapEx Category	Description
Balance of system	
Array cables	Loops of cable or individual strings connecting wind turbines to the offshore substation, including cable protection and accessories.
Engineering project	Detailed design and construction, procurement and construction management, project certification and health, safety, and environmental. monitoring
Floating substructure	Excavation, anchorage primary structure, buoyancy modules, seabed protection mats and ducting system.
Project development	Permitting and leasing, professional advisory services, engineering, site characterization, project management during development, and financing and incentives.
Assembly and installation	Offshore substation, including electrical conversion systems, auxiliary facilities, safety and protection equipment, and steel structures.
Electrical infrastructure	Ancillary systems and stations (including rectifiers and DC converter).
Soft costs	
Financing	Charges of expenditure on equipment and services incurred for the development and construction of the system.
Plant commissioning	Offshore logistics, consisting of sea–based support, marine coordination and weather forecasting and metaocean data, among others.
Project insurance	Insurance policies held by the owner during the construction period.
Contingency fund	Provision of a liquid financial instrument set up to respond to 'known unknown' costs that may arise during construction.

Note: For a complete detailed description of these categories, please refer to [155] .

Table C.8: Floating offshore wind system's OpEx categories breakdown structure.

OpEx Category	Description
Operations	
Offshore logistics	Crew transfer and service operation vessels, turbine access systems, helicopters, marine planning software, communications equipment and safety planning.
Health and safety inspections	Inventory tracking, namely first aid and advanced medical kit, gloves and safety boots, ear defenders and safety eye–wear, fire extinguishers, personal locator beacon, life–vests and float devices, among others.
Personnel training	Training courses, examinations and certification.
Maintenance and services	
Turbine maintenance and service	Blade inspection and repair, nacelle component refurbishment, replacement and repair, and electrical transmission system maintenance.
Balance of plant service and maintenance	Foundation and cable inspection and repair, scour monitoring and management, and substation maintenance and service.

Note: For a complete detailed description of these categories, please refer to [46] .

D QGIS Functions Summary

QGIS allows the use of a vast set of functions provided by core features and plugins, enabling multiple actions of geospatial data manipulation. A short overview of general categories of features is presented below, followed by the respective definition.

Table D.1: Summary description of QGIS functions.

Feature	Definition
Vector general	
`Reproject layer`	Reprojects a vector layer in a different coordinate reference system.
`Merge vector layers`	Combines multiple vector layers of the same geometry type into a single one.
`Create spatial index`	Creates an index to speed up access to the features in a layer based on their spatial location.
Vector geometry	
`Add geometry attributes`	Computes geometric properties of the features in a vector layer based on a selected coordinate reference system.
`Delete holes`	Takes a polygon layer and removes holes which are smaller than a specified area threshold.
`Dissolve`	Takes a vector layer and combines its features into new features, erasing common boundaries of adjacent polygons.
`Buffer`	Computes a buffer area for the features of a layer, using a fixed distance.
`Simplify`	Simplifies the geometries in a line/polygon layer, creating a new layer with the same features but with geometries containing a lower number of vertices; simplification methods include distance–based ('Douglas–Peucker' algorithm), area–based ('Visvalingam' algorithm) and snapping–to–grid.
`Fix geometry`	Attempts to create a valid representation of a given invalid geometry without losing any of the input vertices.
Vector selection	
`Select by expression`	Creates a feature selection in a vector layer based on criteria written on a QGIS expression.
Vector overlay	
`Clip`	Clips a vector layer using the features of an additional polygon layer.
`Difference`	Extracts features from the input layer that don't fall within the boundaries of the overlay layer.

Table D.1: *Cont.*

Feature	Definition
Vector table	
`Refactor fields`	Allows editing the structure of the attribute table of a vector layer.
Raster Analysis	
`Reclassify by table`	Reclassifies a raster band by assigning new class values based on the ranges specified in a fixed table.
`Sample raster values`	Extracts raster values at the point locations.
GDAL[1] Raster extraction	
`Clip raster by mask layer`	Clips any GDAL–supported raster by a vector mask layer.
GDAL Raster conversion	
`Polygonize (raster to vector)`	Creates vector polygons for all connected regions of pixels in the raster that share a common pixel value.
`Rasterize (vector to raster)`	Converts vector geometries (points, lines and polygons) into a raster image, with the option to burn–in a field value to each pixel.

[1] Geospatial Data Abstraction Library: a translator library for raster and vector geospatial data formats.

Note: For a complete detailed description of these features, please refer to [82].

Figure D.1 provides the process–flowchart of the procedure to obtain a new buffered layer from a typical vector layer, using some of the functions described in the table above.

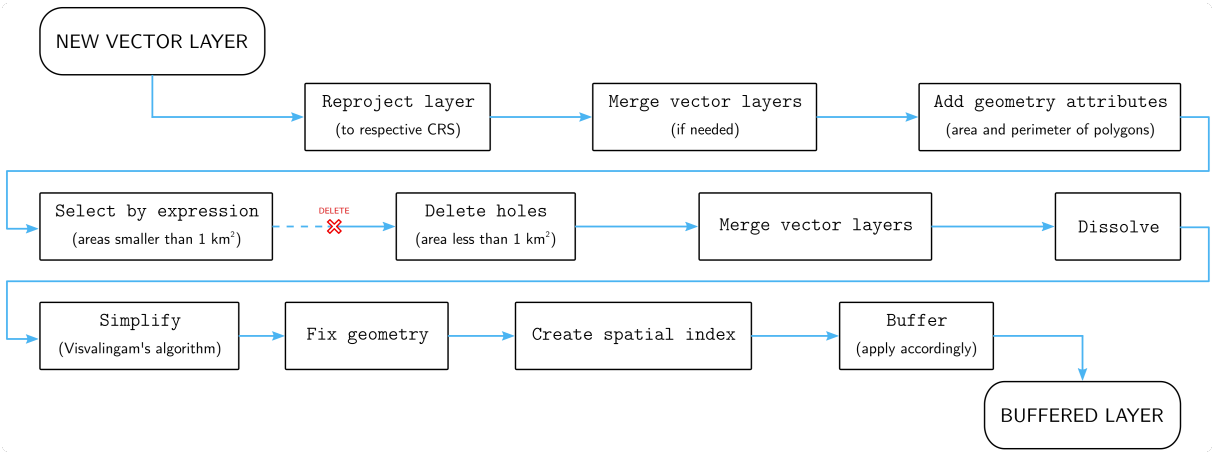

Figure D.1: GIS procedure flowchart: from new vector layer to buffered layer.

E Density of Shipping Routes

One of the essential criteria for offshore land–eligibility analysis is the distance between the wind turbine installation site and the predominant maritime routes. These routes are mapped out and produced by the European Maritime Safety Agency in the form of 'Route Density Maps' that are further prepared, organized in years and months, and distributed via the EMODnet portal [99].

Figure E.1 shows the total route density of both countries during 2021. This density is measured in the number of routes per square kilometre per year and evaluated considering four categories: cargo, tanker, fishing and passenger. Figures E.2 and E.3 show the route densities of such categories for Portugal and Italy, respectively, during last year.

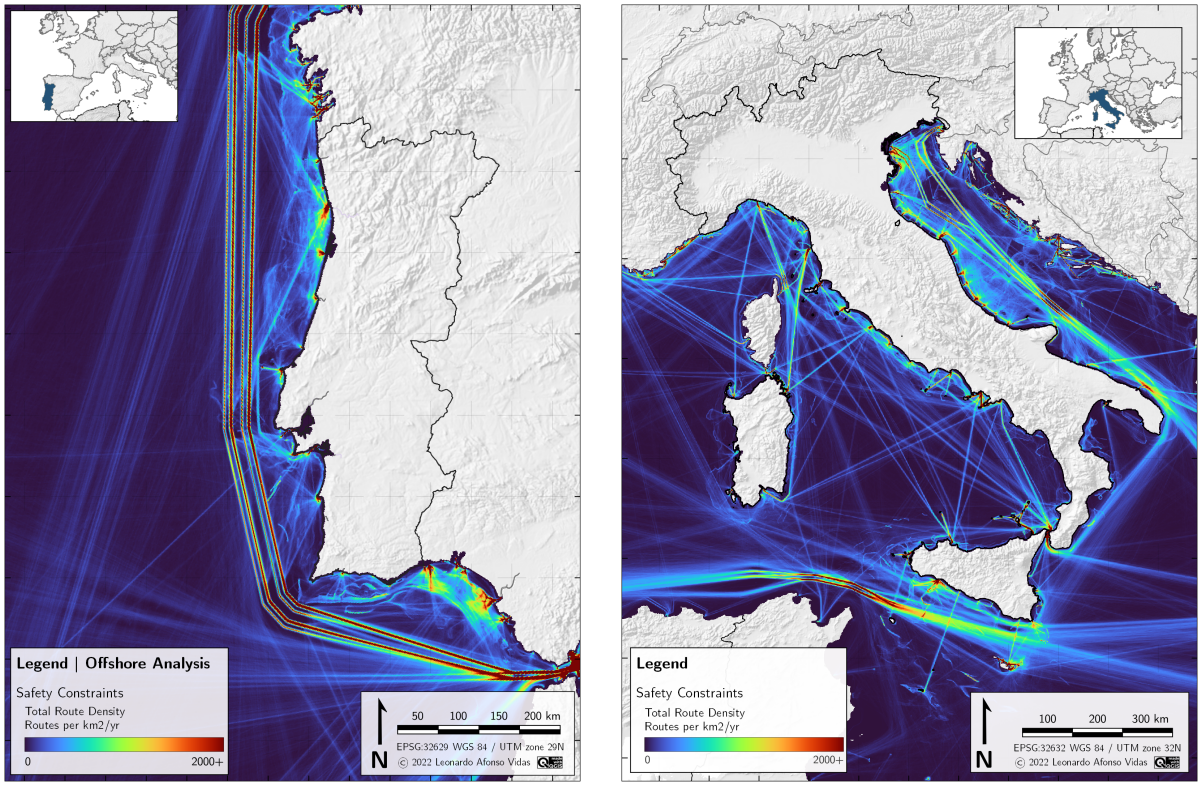

(a) Portugal (b) Italy

Figure E.1: Density of total shipping routes in 2021.

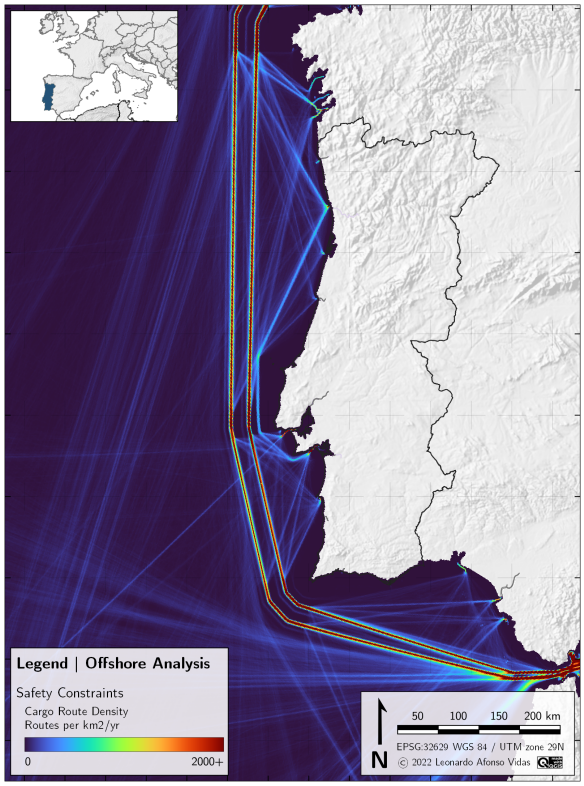

(a) Cargo.

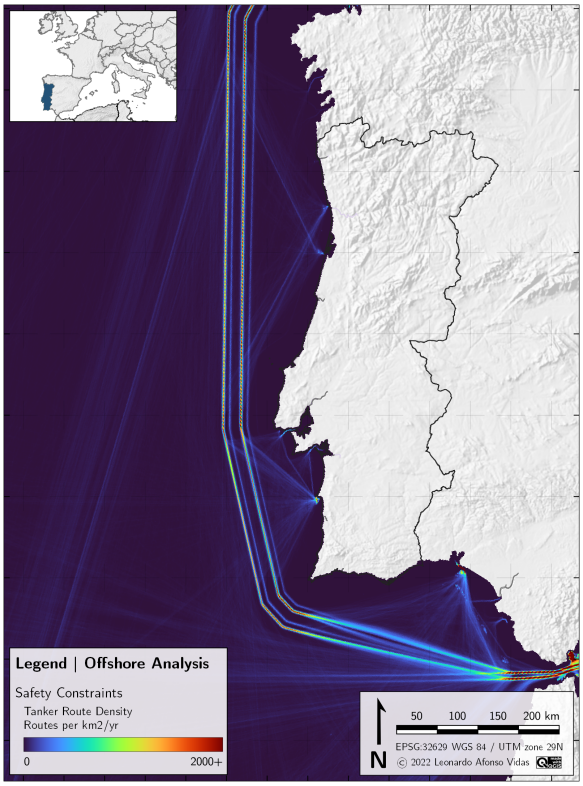

(b) Tanker.

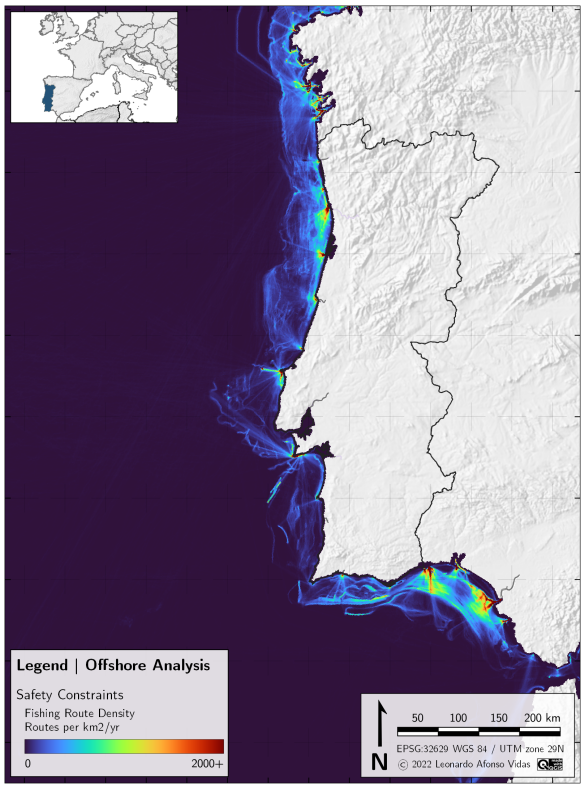

(c) Fishing.

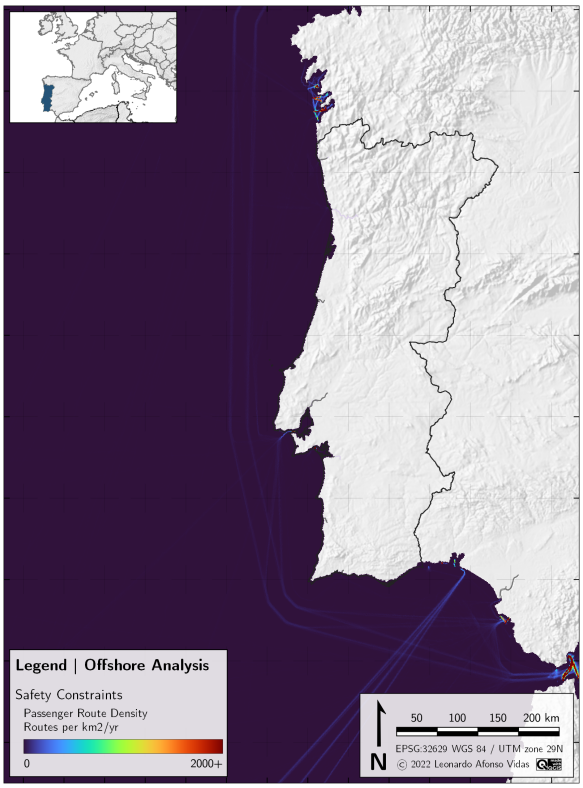

(d) Passenger.

Figure E.2: Density of shipping routes around Portugal, in 2021.

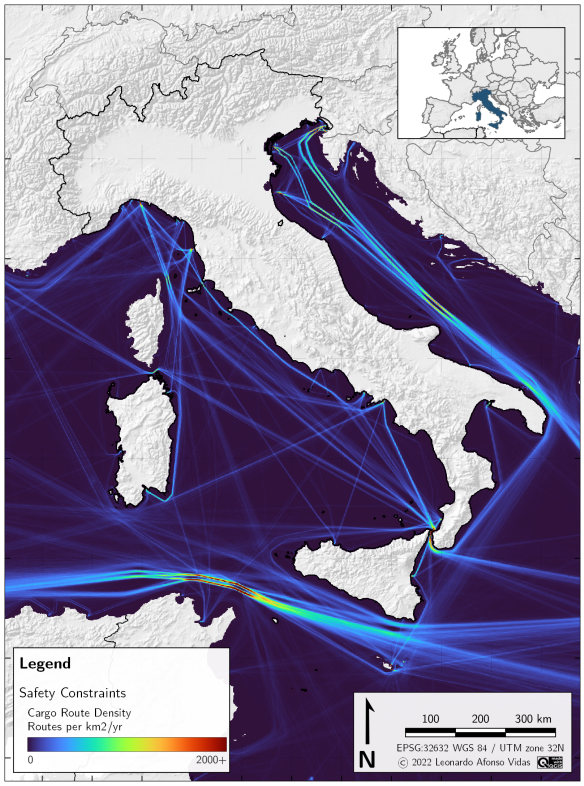

(a) Cargo

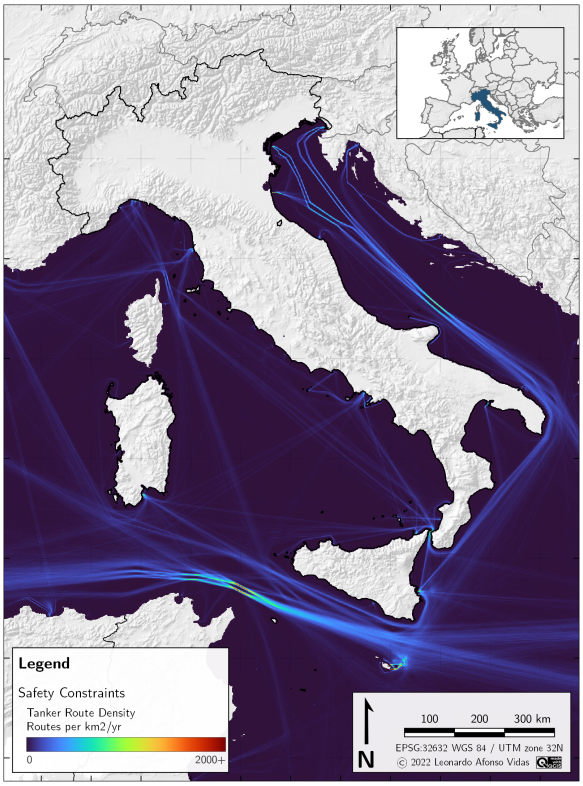

(b) Tanker

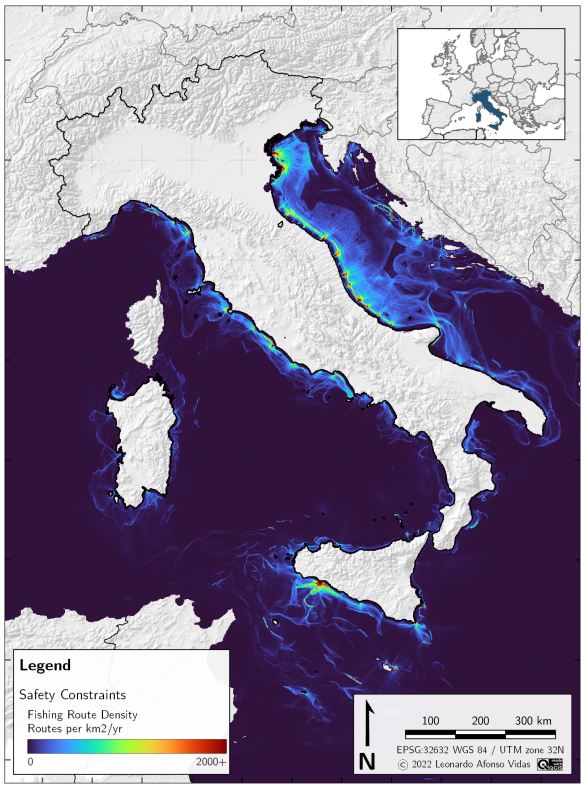

(c) Fishing

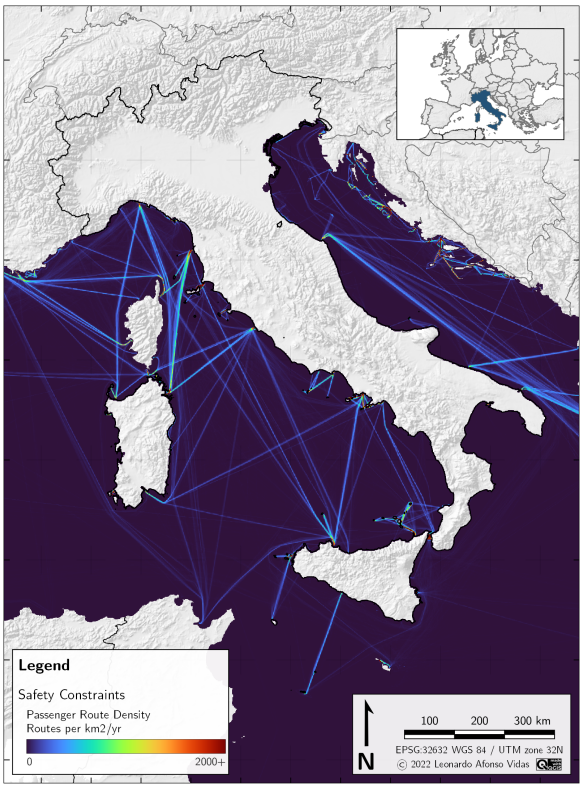

(d) Passenger

Figure E.3: Density of shipping routes around Italy, in 2021.

— END MATTER —